## Supporting Information

# Ammonia Synthesis by the Reductive N-N Bond Cleavage of Hydrazine Using an Air-Stable, Phosphine-Free Ruthenium Catalyst

Aisa Mohanty,[a] Smruti Rekha Rout,[b] Rambabu Dandela[b] and Prosenjit Daw*[a]

[a]Department of Chemical Sciences, Indian Institute of Science Education and Research Berhampur, Transit Campus, (Govt. ITI Building), Engg. School Junction, Berhampur 760010, Odisha, India

[b]Department of Industrial and Engineering Chemistry, Institute of Chemical Technology, Indian Oil Odisha Campus, Samantpuri, Bhubaneswar 751013 Odisha, India

Corresponding Author

Email: pdaw@iiserbpr.ac.in

## Contents

## 1. General Experimental details

All the experiments were performed under a nitrogen-filled glovebox or by standard Schlenk technique unless otherwise stated. All chemicals were purchased from commercial suppliers and used without further purification unless otherwise stated. $RuCl_3.3H_2O$ was purchased from Arora-Matthey. $SmI_2(thf)_2$ (0.1M in THF), contains samarium chips as a stabilizer, $CoCp_2$ and $CoCp^*_2$ were purchased from Sigma-Aldrich. All the solvents were pre-dried following the literature processes. THF and diethyl ether were dried by distillation in the presence of benzophenone and sodium metal. Dichloromethane was distilled from calcium hydride and stored under a 4 Å molecularsieve. Methanol was dried by distillation from magnesium turning and iodine cake. $^1H$ and $^{13}C$ spectra were recorded on 400 MHz FT-NMR Bruker AVANCE NEO ascend 400 spectrometers.The chemical shifts (δ) for $^1H$ NMR are given in parts per million (ppm) referenced to the residual proton signal of the deuterated solvent ($CHCl_3$ at δ 7.26 ppm, DMSO at 2.50 ppm and $H_2O$ in DMSO at 3.33 ppm); coupling constants are expressed in hertz (Hz). $^{13}C$ NMR spectra were referenced to the carbon signal of $CDCl_3$ (77.0 ppm). The following abbreviations are used to describe NMR signals: s = singlet, d = doublet, t = triplet, m = multiplet, dd = doublet of doublets, q = quartet. High-resolution mass spectrometry (HRMS)-ESI was performed on Xevo G2-XS QT of quadrupole time of flight mass spectrometer from Waters India Pvt. Ltd. Elemental analysis was done using the UNICUBE CHNSO element analyzer. IR spectra were recorded on Bruker TENSOR II FT-IR Spectrometer. The abbreviation br = broad in IR spectral data. The evolved hydrogen gas was analyzed by gas chromatography (SHIM$^1$ADZU GC-2030, thermal conductivity detector (TCD, 4 Å Molecular sieve 5 Å porous layer open tubular capillary column, Ar carrier gas flow). UV-visible absorption spectra of the synthesized samples were taken at room temperature employing a Shimadzu UV-1800 spectrophotometer. The GCMS analysis of the crude reaction mixture was analyzed by GCMS-FID (TRACE 1610, TG-5MS column). Cyclic voltammetry was measured by an Electrochemical workstation (CH instrument, Model 600E series). 2,2':6',2''-terpyridine[1] and 6,6''-dibromo-2,2':6',2''-terpyridine[2] were prepared using a literature procedure.

## 2. Ligand Synthesis

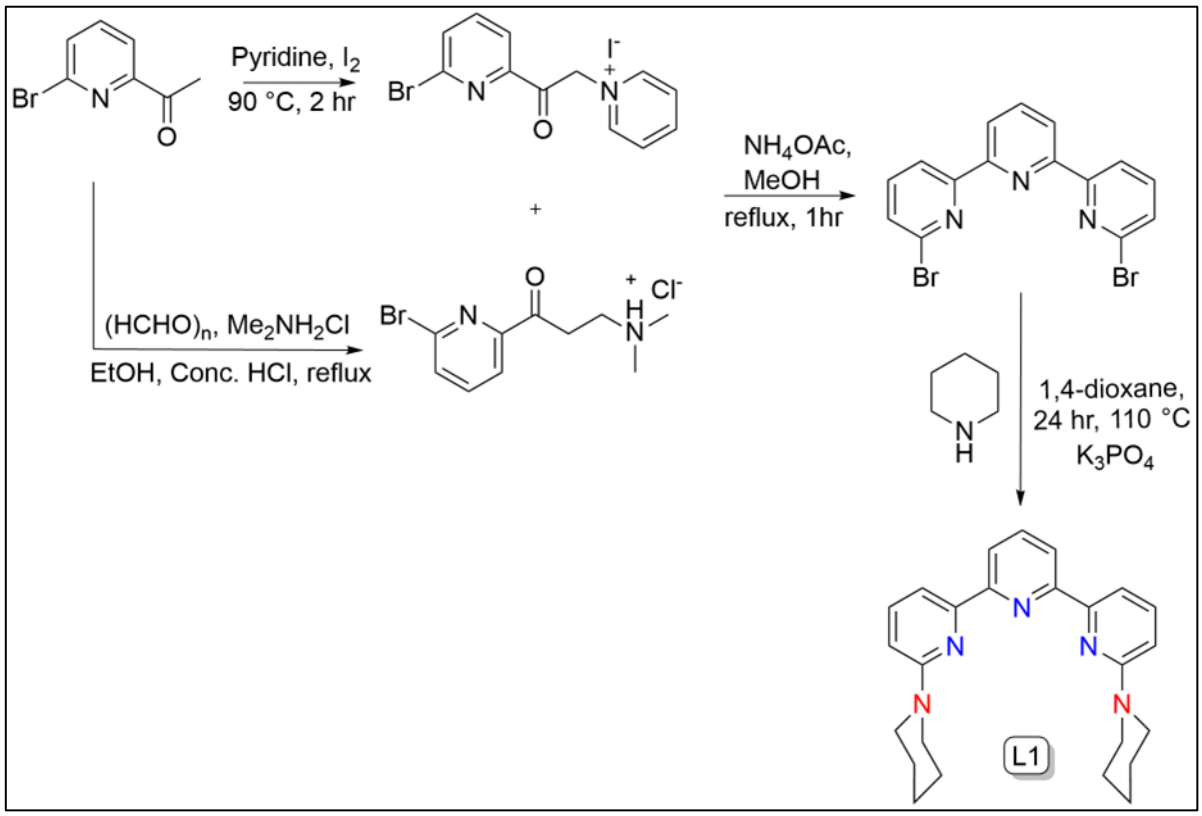


**Scheme S1**. Reaction scheme of Ligand **L1** synthesis

### 2.1. Synthesis of 6,6''-di(piperidin-1-yl)-2,2':6',2''-terpyridine (L1)

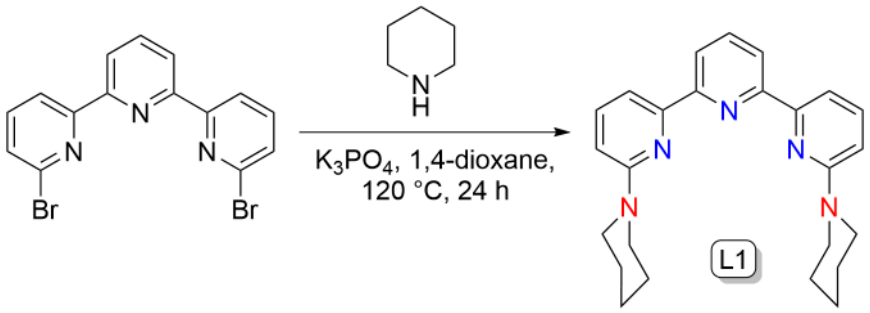


In a sealed tube, 6,6''-dibromo-2,2':6',2''-terpyridine (1.278 mmol), piperidine (8.946 mmol, 7 equiv.), potassium phosphate (8.946 mmol, 7 equiv.), and 1,4-dioxane (5 ml) were added and flushed with $N_2$. The reaction mixture was kept at 120 °C for 24 h. After completion of the reaction, the crude reaction mixture was completely evaporated and diluted with distilled water (15 ml). The aqueous layer was extracted three times with dichloromethane (3 x 20 ml). The combined organic layer was washed with brine solution, dried over $Na_2SO_4$, and evaporated to

dryness to get a yellow solid product 6,6"-di(piperidin-1-yl)-2,2':6',2"-terpyridine (**L1**) (0.951 mmol, 74.50% yield).

$^{1}$H NMR (400 MHz, $CDCl_3$) δ (ppm) = 8.37 (d, *J* = 7.7 Hz, 2H), 7.95 (d, *J* = 7.3 Hz, 2H), 7.86 (t, *J* = 8.2 Hz, 1H), 7.62 (t, *J* = 7.7 Hz, 2H), 6.70 (d, *J* = 8.4 Hz, 2H), 3.65 (s, 8H), 1.68 (s, 12H).

$^{13}$C NMR (101 MHz, $CDCl_3$) δ (ppm) = δ 159.16, 155.87, 154.28, 138.15, 137.13, 120.33, 109.93, 107.25, 77.34, 77.02, 76.70, 46.45, 25.57, 24.85.

HRMS (m/z) = 400.3039 ($M+H^+$)

Elemental analysis for $C_{25}H_{29}N_5$ Analy calc: C:75.15 H:7.32 N:17.43, Found: C:74.89 H:7.78 N:15.58

IR (ATR) $\bar{\upsilon}$ ($cm^{-1}$) = 2925 (s), 2849 (s), 1590, 1564, 1435, 1379, 1248, 1127, 1099, 1066, 125, 979, 942, 855, 780,723, 632.

## 3. Synthesis of metal complexes

### 3.1. Synthesis of Complex 1

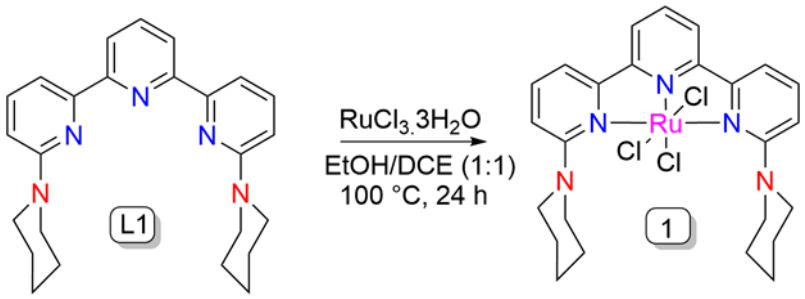


In a 25 ml Schlenk tube, Ligand **L1** (0.5 mmol, 1 equiv.) and metal salt ($RuCl_3.3H_2O$) (0.5 mmol, 1 equiv.) were introduced in 10 ml of dry EtOH/DCE (1:1). The reaction mixture was kept at 100 °C for 24 h where the dark red colour solution changed to dark green colour solution gradually with the course of the reaction. After 24 h, the solution was evaporated to result in a dark green coloured precipitate, washed with dry diethyl ether (3 x 10 ml) and dried under reduced pressure to afford green solid (complex **1**) with a yield of 75% (0.378 mmol). The resulting complex was recrystallized in DCM/$Et_2O$ to get the purified compound for further spectral characterization.

HRMS (m/z) = 571.0822 $[1\text{-}Cl^-]^+$

IR (ATR) $\bar{\upsilon}$ ($cm^{-1}$) = 2947, 2806, 2732, 2525, 1962, 1591, 1454, 1383, 1340, 1238, 1089, 1027, 947, 860, 782, 750, 641, 555, 507

Elemental analysis for $C_{25}H_{29}Cl_3N_5Ru.2CH_2Cl_2$ Analy calc: C: 41.75 H: 4.28 N: 9.02, Found: C: 39.92 H: 4.87 N: 8.35

### 3.2. Synthesis of Complex 2

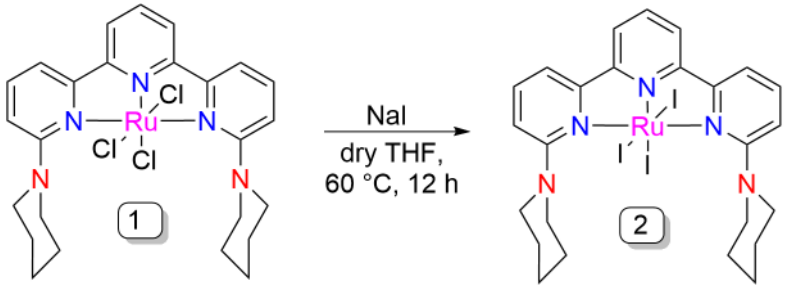


In an oven-dried 25 ml Schlenk tube, complex **1** (0.136 mmol, 1 equiv.) and sodium iodide (2.734 mmol, 20 equiv.) was taken with the addition of 20 ml dry THF and kept for heating at 60 °C for 12 h under an inert atmosphere. After completion of the reaction, the colour of the reaction changed from a dark green-coloured solution to a dark blue-coloured solution. The solution was evaporated completely and diluted with 20 ml of dry DCM. The white precipitate resulting from the solution was filtered off through a pad of celite under a dinitrogen atmosphere. The blue-coloured solution was concentrated and washed with dry diethyl ether (3 x 10 ml) to afford the product as complex **2** (0.068 mmol, 49.75% yield).

HRMS (m/z) = 754.9576 $[2\text{-}I^-]^+$ , 126.8810 $[I]^-$

IR (ATR) $\bar{\upsilon}$ ($cm^{-1}$) = 2929, 2818, 1969, 1594, 1555, 1448, 1382, 1346, 1238, 1103, 1058, 1025, 928, 860, 781, 743, 636, 542, 508

Elemental analysis for $C_{25}H_{29}I_3N_5Ru$ Analy calc: C:34.02 H:3.32 N:7.95 Found: C:32.63 H:3.44 N:7.02

### 3.3. Synthesis of Complex 3

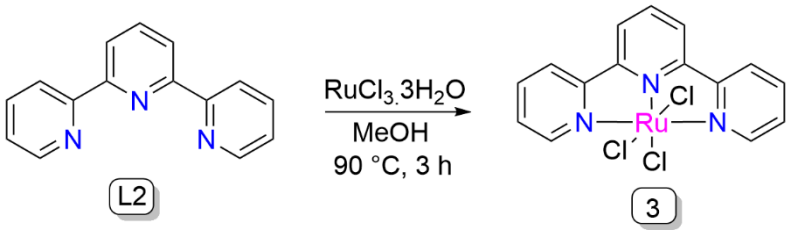


Complex **3** was synthesized by following the literature procedure.[3] In a 25 ml Schlenk tube, Ligand **L2** (2,2':6',2"-terpyridine) (0.27 mmol, 1 equiv.) and metal salt ($(RuCl_3.3H_2O)$ (0.27

mmol, 1 equiv.) were added in 7 ml of dry MeOH. The reaction mixture was heated to reflux at 90 °C for 3 h under the flow of dinitrogen. The colour of the solution become dark brown in colour. After 3 h, methanol was decanted and the resulting dark brown precipitate was washed with methanol (3 x 5 ml) and diethyl ether (3 x 5 ml) to afford brown solid (complex **3**) with a yield of 67% (0.18 mmol). The HRMS analysis of complex **3** showed m/z peak at 404.93 which corresponds to the $[3\text{-}Cl^-]^+$ along with the major intensity of ligand **L2** peak might be due to the limited solubility of complex **3** in acetonitrile.

HRMS (m/z) = 404.9301 $[3\text{-}Cl^-]^+$

Elemental analysis for $C_{15}H_{11}Cl_3N_3Ru.H_2O$ Analy calc: C: 37.79 H: 3.17 N: 8.81, Found: C: 36.06 H: 3.18 N: 8.30

## 4. Cyclic Voltammetry

The electrochemical measurements were carried out under an inert atmosphere using a three-electrode electrochemical cell with glassy carbon as the working electrode, Pt wire as the counter electrode, and Ag/AgCl (sat. KCl) as a reference electrode. By using cyclic voltammetry with a potential sweeping between 2 V to -2 V at a scan rate of 100 $mVs^{-1}$, the electrochemical signal of the ligand **L1** and complex **2** were recorded in 10 mL of dry THF solvent containing 0.1 M of tetrabutylammonium hexafluorophosphate $(Bu)_4NPF_6$ as the supporting electrolyte. Ferrocene was added as an internal standard independently with $E_0$ value vs $Ag^{+/0}$ = 0.56 V, followed by all potentials referred to as the $Fc^+/Fc$ couple.

### 4.1. Cyclic Voltammetry of L1

Cyclic voltammetry of **L1** (0.1 mmol) was measured in dry THF with 0.1 M of $(Bu)_4NPF_6$ in the potential window of +2 V to -2 V (**Figure S1**).

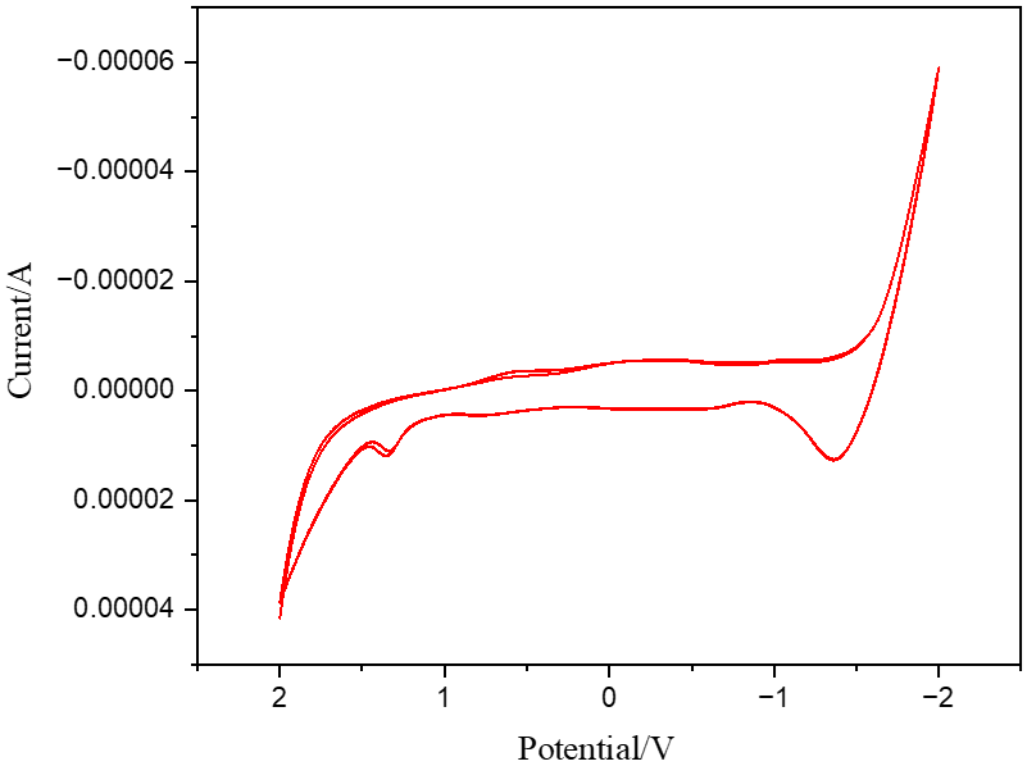


**Figure S1:** Cyclic voltammetry of **L1**

### 4.2. Cyclic voltammetry of 1

Complex **1** (0.1 mmol) was bearing the partial solubility in dry THF and dry Acetonitrile, subjected to cyclic voltammetry measurements in dry acetonitrile with 0.1M of $(Bu)_4NPF_6$ in the potential range of +2 V to -2 V (**Figure S2**).

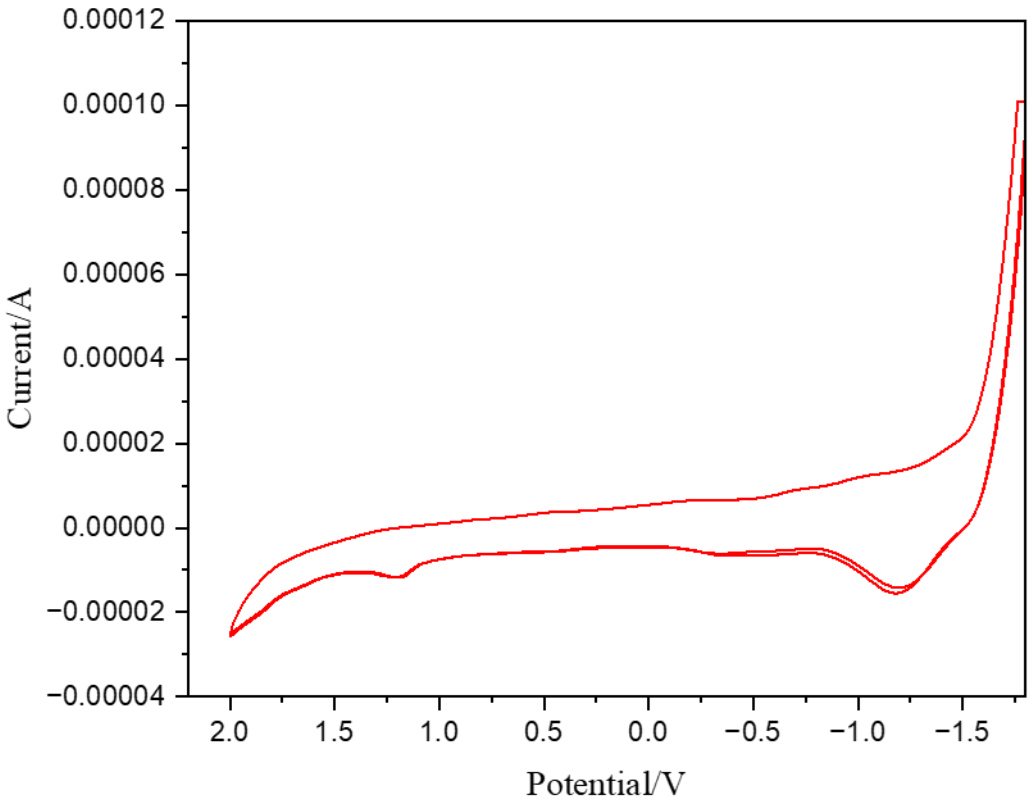


**Figure S2:** Cyclic voltammetry of **1**

### 4.3. Cyclic voltammetry of 2

Cyclic voltammetry of complex **2** (0.01 mmol) was measured in dry THF with 0.1 M of $(Bu)_4NPF_6$. In the potential window of +2 V to -2 V, it shows four reduction and two oxidation waves.[4] The oxidation waves at $E_{pa}$ at 0.498V and 0.878V can be attributed to the two consecutive oxidation movements from Ru(III) to Ru(V). Whereas the reduction waves at $E_{pc}$ at 0.629 V and -0.254V can be assigned to subsequent reversible peaks that is Ru(V) to Ru(III). Further undergoing two irreversible reductions at -0.753V and -1.18V witnessing the Ru(III)→Ru(II) and Ru(II)→Ru(I) respectively (**Figure S3A, S3B**).[5]

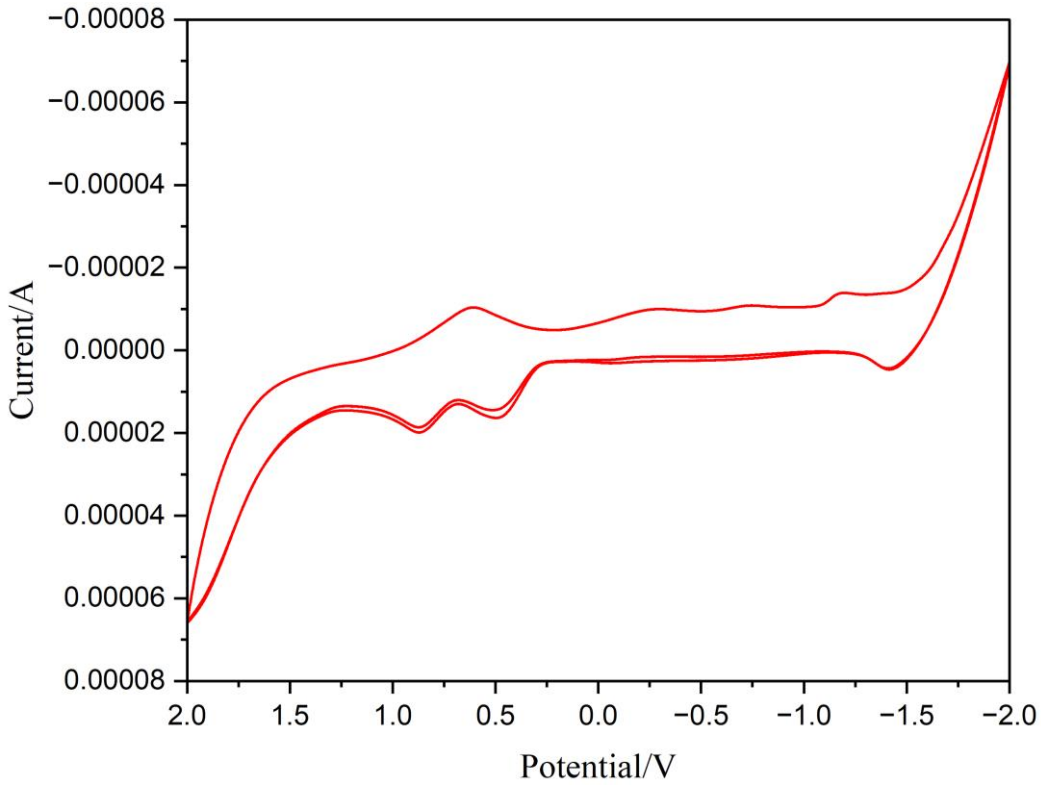


**Figure S3A:** Cyclic voltammetry of complex **2** from 2 to -2V potential window

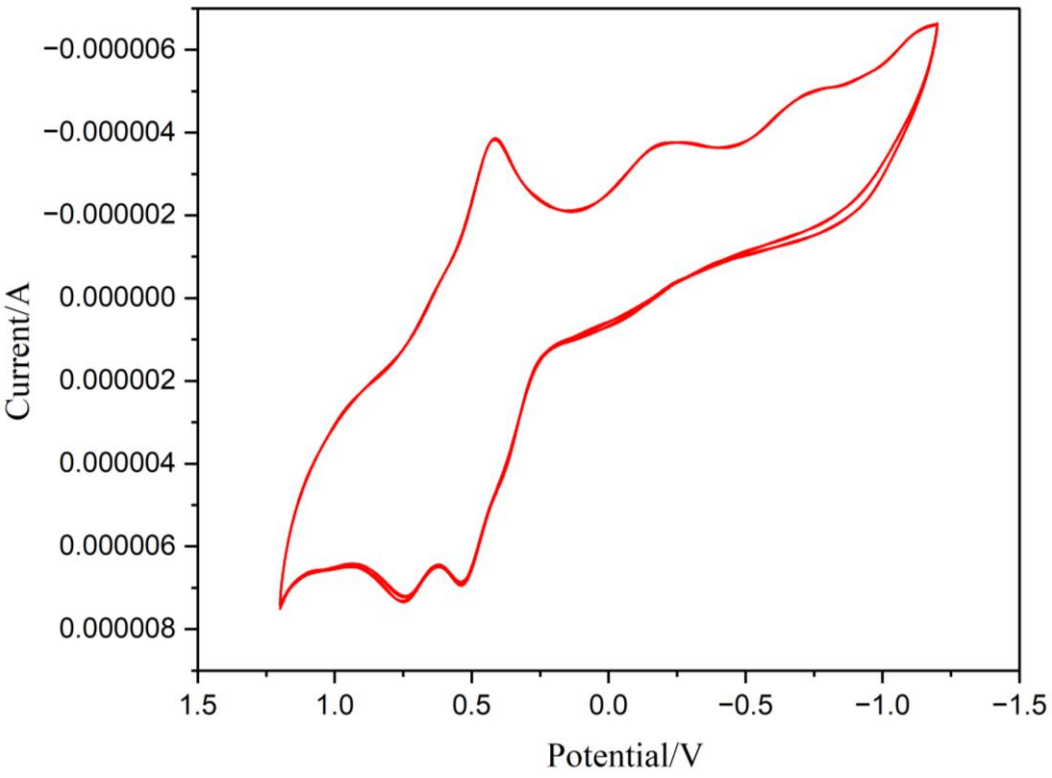


**Figure S3B:** Cyclic voltammetry of complex **2** from 1.5 to -1.5V potential window

## 5. General procedure for hydrazine hydrate disproportionation reaction to ammonia

All the catalytic reactions were set up in the nitrogen-filled glove box. In a 25 ml round-bottom flask, catalyst (0.003 mmol, 3.3 mol%) and hydrazine hydrate (0.09 mmol, 30 equiv. w.r.t catalyst) were added, along with 2 ml of dry THF. The flask was sealed properly taken out of the glove box and heated at 55 °C for 4 h. After cooling to room temperature, all the volatiles in the reaction mixture were frozen and 5 ml of HCl (2M in $Et_2O$) was added instantly. The acidified reaction mixture was stirred for 30 min and volatile components were removed under reduced pressure to give a sticky solid product. It was diluted with 1 ml of DMSO followed by the addition of the internal standard as mesitylene [0.015 mmol, 6.77 ppm (s, 3H)]. An aliquot from the reaction mixture was taken and $^1$H NMR was recorded with DMSO-$d_6$, where the amount of $NH_4^+$ quantified clearly as the main component with a distinct triplet in 1:1:1 ratio with the J value corresponding to 51-53 Hz (7.12 ppm -7.40 ppm region).

Yields were calculated using the equation mentioned in Table **S1**.

$n(NH_4^+)$ (in mmol) = [mmol of internal standard / 4] * $\int NH_4^+$ ($^1$H NMR)

$NH_4^+$ (% yield) = [experimental value $n(NH_4^+)$ (in mmol) / theoretical value $n(NH_4^+)$ (in mmol)] * 100

**Table S1. Catalytic runs of disproportionation reaction**[a]

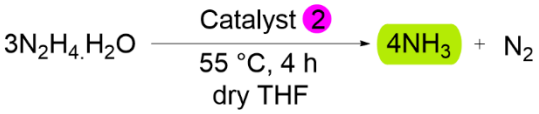


| Entry | Cat loading (mmol) | Hydrazine loading (mmol) | $n(NH_4^+)$ (in mmol) | | $NH_4^+$ (%Yield) |
|---|---|---|---|---|---|
| 1 | 0.003 | 0.09 | Run1 | 0.0082 | 6.83 |
| | | | Run2 | 0.0076 | 6.33 |
| 2[b] | 0.003 | 0.09 | Run1 | 0.0070 | 5.83 |
| 3 | - | 0.09 | Run1 | 0 | - |
| | | | Run2 | 0.0006 | 0.5 |
| 4[c] | 0.003 | 0.09 | Run1 | 0.0165 | 13.75 |
| | | | Run2 | 0.0198 | 16.50 |
| 5[d] | 0.003 | 0.09 | Run1 | 0.0055 | 4.59 |

[a]Reaction Conditions: [Catalyst **2** (0.003 mmol, 3.3 mol%), $N_2H_4.H_2O$ (0.09 mmol, 30 equiv. w.r.t catalyst), THF (2 ml), 55 °C, 4 h], [b]$N_2H_4$ (1M in THF) was used, [c]**1** as the catalyst, [d]$RuCl_3.3H_2O$ used as the catalyst**.**

## 6. General procedure for catalytic hydrazine hydrate reduction to ammonia

All the catalytic reactions were set up in the nitrogen-filled glove box. In a 25 ml round-bottom flask, catalyst (0.003 mmol, 3.3 mol%) and $SmI_2(thf)_2$ (0.1 M in THF, 0.18 mmol) and hydrazine hydrate (0.09 mmol, 30 equiv. w.r.t catalyst) and water (0.18 mmol) were introduced. The flask was sealed properly taken out of the glove box and heated at 55 °C for 4 h. After cooling to room temperature, all the volatiles in the reaction mixture were frozen and 5 ml of HCl (2M in $Et_2O$) was added instantly. The acidified reaction mixture was stirred for 30 min and volatile components were removed under reduced pressure to give a sticky solid product. It was diluted with 1 ml of DMSO followed by the addition of the internal standard as mesitylene [0.015 mmol, 6.77 ppm (s, 3H)]. An aliquot from the reaction mixture was taken and $^1$H NMR was recorded with DMSO-$d_6$, where the amount of $NH_4^+$ quantified clearly as the main component with a distinct triplet in 1:1:1 ratio with the J value corresponding to 51-53 Hz (7.12 ppm -7.40 ppm region).

Yields were calculated using the equation mentioned in Table **S2**.

$n(NH_4^+)$ (in mmol) = [mmol of internal standard / 4] * $\int NH_4^+$ ($^1$H NMR)

$NH_4^+$ (% yield) = [experimental value $n(NH_4^+)$ (in mmol) / theoretical value $n(NH_4^+)$ (in mmol)] * 100

**Table S2: Catalytic runs of reduction reaction**[a]

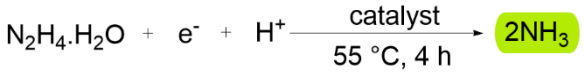


| Entry | Catalyst | Reductant | Proton source | $n(NH_4^+)$ (in mmol) | | $NH_4^+$(%Yield)[i] |
|---|---|---|---|---|---|---|
| 1[b] | **2** | $SmI_2$ | $H_2O$ | Run 1 | 0.030 | 17.1 |
| 2 | **2** | $SmI_2$ | $H_2O$ | Run 1 | 0.092 | 51.3 |
| | | | | Run 2 | 0.090 | 50.5 |
| 3[c] | **2** | $SmI_2$ | $H_2O$ | Run 1 | 0.102 | 57 |

| | | | | | | |
|---|---|---|---|---|---|---|
| 4 | **2** | $SmI_2$ | - | Run 1 | 0.041 | 23.2 |
| | | | | Run 2 | 0.038 | 21.1 |
| 5 | - | $SmI_2$ | $H_2O$ | Run 1 | 0.054 | 30 |
| | | | | Run 2 | 0.053 | 29.5 |
| 6[b] | - | $SmI_2$ | $H_2O$ | Run 1 | 0.011 | 6.3 |
| 7 | **1** | $SmI_2$ | $H_2O$ | Run 1 | 0.058 | 32.4 |
| | | | | Run 2 | 0.049 | 27.3 |
| 8 | **3** | $SmI_2$ | $H_2O$ | Run 1 | 0.057 | 31.6 |
| | | | | Run 2 | 0.056 | 31.1 |
| 9 | $RuCl_3.3H_2O$ | $SmI_2$ | $H_2O$ | Run 1 | 0.047 | 26.1 |
| | | | | Run 2 | 0.039 | 22 |
| 10[d] | **2** | $SmI_2$ | $H_2O$ | Run 1 | 0.038 | 21.1 |
| 11[#] | **2** | - | $H_2O$ | Run 1 | 0.010 | 9 |
| | | | | Run 2 | 0.009 | 7.8 |
| 12 | **2** | $CoCp_2$ | [LutH]OTf | Run 1 | 0.085 | 47.6 |
| | | | | *Run 2 | 0.067 | 37.2 |
| 13 | **2** | $CoCp_2$* | [LutH]OTf | Run 1 | 0.014 | 8.1 |
| | | | | *Run 2 | 0.011 | 6.1 |
| 14[e] | **2** | $SmI_2$ | $H_2O$ | Run 1 | - | - |
| 15[f] | **2** | $SmI_2$ | $H_2O$ | Run 1 | 0.075 | 42 |
| 16[g] | **2** | $SmI_2$ | $H_2O$ | Run 1 | 0.113 | 62.7 |
| 17[h] | **2** | $SmI_2$ | $H_2O$ | Run 1 | 0.171 | 95.1 |
| | | | | Run 2 | 0.170 | 94.7 |
| | | | | Run 3 | 0.158 | 87.7 |

[a]Reaction conditions: Catalyst (0.003 mmol, 3.3 mol%), $N_2H_4.H_2O$ (0.09 mmol, 30 equiv. w.r.t catalyst), $SmI_2(thf)_2$ (0.18 mmol), $H_2O$ (0.18 mmol). Catalytic runs are performed at 55 °C for 4 h unless otherwise mentioned. [b]Reaction performed at rt. [c]Reaction performed for 12 h. [d]$N_2H_4$(1M in THF) was used. [e]Reaction performed without hydrazine. [f]Reaction performed with 1.5 mol% (0.0015 mmol) catalyst loading. [g]Reaction performed with 5.5 mol% (0.0054 mmol) catalyst loading. [h]Reaction performed with 13 mol% (0.012 mmol) catalyst loading. [i]The generated $NH_3$ was treated with $HCl{\cdot}Et_2O$ to converted it into $NH_4Cl$. By integrating the

$NH_4^+$ resonance with regard to internal reference (mesitylene) in $^1H$ NMR, the yields of $NH_4Cl$ were measured. #The %yield of $NH_4^+$ was calculated using equation mentioned for Table **S1**. *0.020 mmol of mesitylene was used.

## 7. Reaction mixture gas phase analysis by GC-TCD

GC analysis was carried out using the following procedure on an (SHIMADZU GC-2030, thermal conductivity detector [TCD, Argon (Ar) as a carrier gas flow, Agilent]. GC-TCD was analysed by taking 100 µL of gas from the headspace of the crude reaction mixture. All the reactions were performed under an N2-filled glove box, resulting in the appearance of a peak corresponding to nitrogen ($N_2$) with a retention time of 7.5 min. The oxygen ($O_2$) peak appears with a retention time of 5.03 min, during the manual sample injection. The hydrogen ($H_2$) peak with a retention time of 3.78 min, is entirely due to the $H_2$ gas produced from the reaction mixture.

**Determination of %yield of $H_2$: -**

The area under the curve of $H_2$ for the pure $H_2$ gas = 28958148

100 µL of gas syringe contains 4.46 µmole of gas

For example:-

Let the area under the curve of $H_2$ for any sample = x

x area of the sample contains = (4.46 * x)/28958148 = y µmole of $H_2$ gas

100 µL of gas syringe contains = y * $10^{-3}$ mmol of $H_2$ gas

10000 µL (10 ml) of reaction flask contains = y * $10^{-3}$ * 100 = z mmol of $H_2$ gas

%yield = [z mmol of $H_2$ gas/theoretical yield of $H_2$ (in mmol) based on $SmI_2$] * 100

## GC profile for pure $H_2$ gas[a]

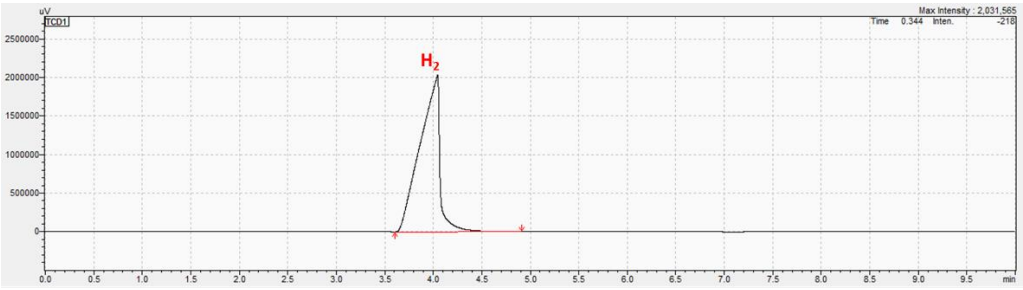


**Figure S4:** GC analysis for pure $H_2$ gas

**Table S3. Quantification of $H_2$ gas with various control experiments**

| Entry | Catalyst 2 (in mmol) | $SmI_2$ (in mmol) | $H_2O$ (in mmol) | Area of the $H_2$ | Volume of the reaction flask (in ml) | mmol of $H_2$ gas obtained | $H_2$ (%yield) |
|---|---|---|---|---|---|---|---|
| **Figure S5** | 0.003 | - | - | - | 10 | - | - |
| **Figure S6** | 0.003 | 0.18 | 0.18 | 2115087 | 10 | 0.032575 | 36.19 |
| **Figure S7** | - | 0.18 | 0.18 | 638880 | 10 | 0.00983 | 10.92 |
| **Figure S8** | 0.012 | 0.18 | 0.18 | (a) 656064 | 10 | 0.0101 | 11.22 |
| | | | | (b) 1360080 | 10 | 0.020 | 23.27 |
| | | | | (c) 555247 | 25 | 0.021 | 23.75 |
| **Figure S9** | 0.003 | 0.18 | 0.18 | 338448 | 25 | 0.01303 | 14.47 |
| **Figure S10** | 0.003 | 0.18 | 0.18 | 1450688 | 25 | 0.05585 | 62.06 |
| **Figure S11** | 0.003 | 0.18 | 0.18 | 2344343 | 10 | 0.03610 | 40.11 |

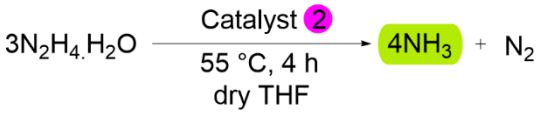


## GC profile for disproportionation reaction[a]

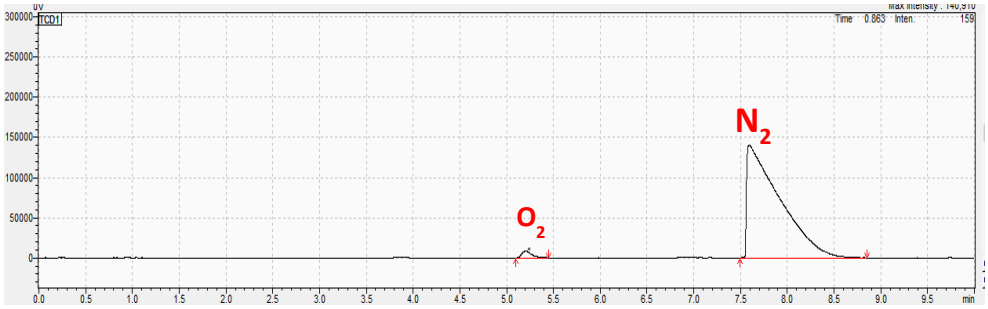


**Figure S5:** Reaction condition[a]: catalyst **2** (0.003 mmol, 3.3 mol%), $N_2H_4.H_2O$ (0.09 mmol), dry THF (2 ml) at 55 °C in 4 h.

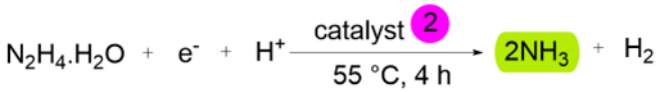


## GC profile for Reduction reaction[a] [With catalyst 2 (3.3 mol%, 0.003 mmol)]

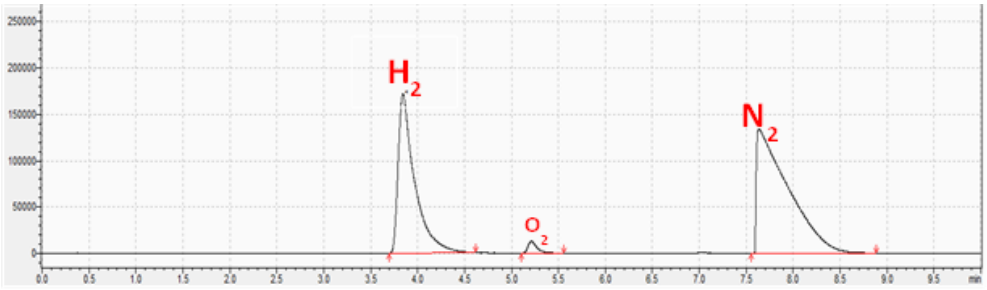


**Figure S6:** Reaction condition[a]: catalyst **2**(0.003 mmol, 3.3 mol%), $N_2H_4.H_2O$ (0.09 mmol), $SmI_2(thf)_2$ (0.1M in THF, 1.8 ml), $H_2O$ (0.18 mmol) at 55 °C in 4 h.

## GC profile for Reduction reaction[a] (Without catalyst 2)

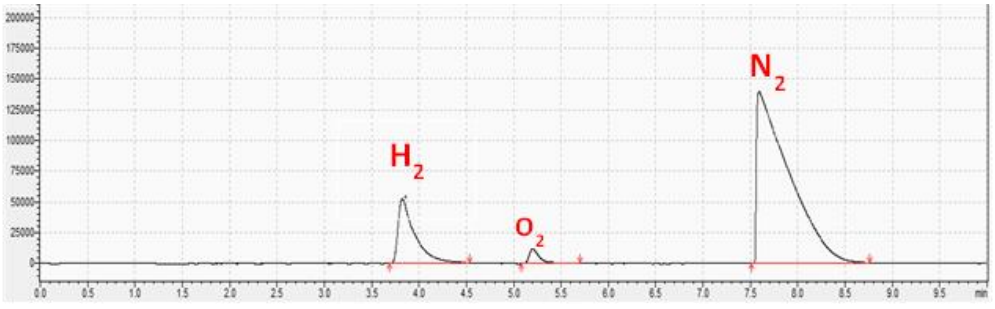


**Figure S7:** Reaction condition[a]: $N_2H_4.H_2O$ (0.09 mmol), $SmI_2(thf)_2$ (0.1M in THF, 1.8 ml), $H_2O$ (0.18 mmol) at 55 °C in 4 h.

## GC profile for Reduction reaction[a] [With catalyst 2 (13 mol%, 0.012 mmol)]

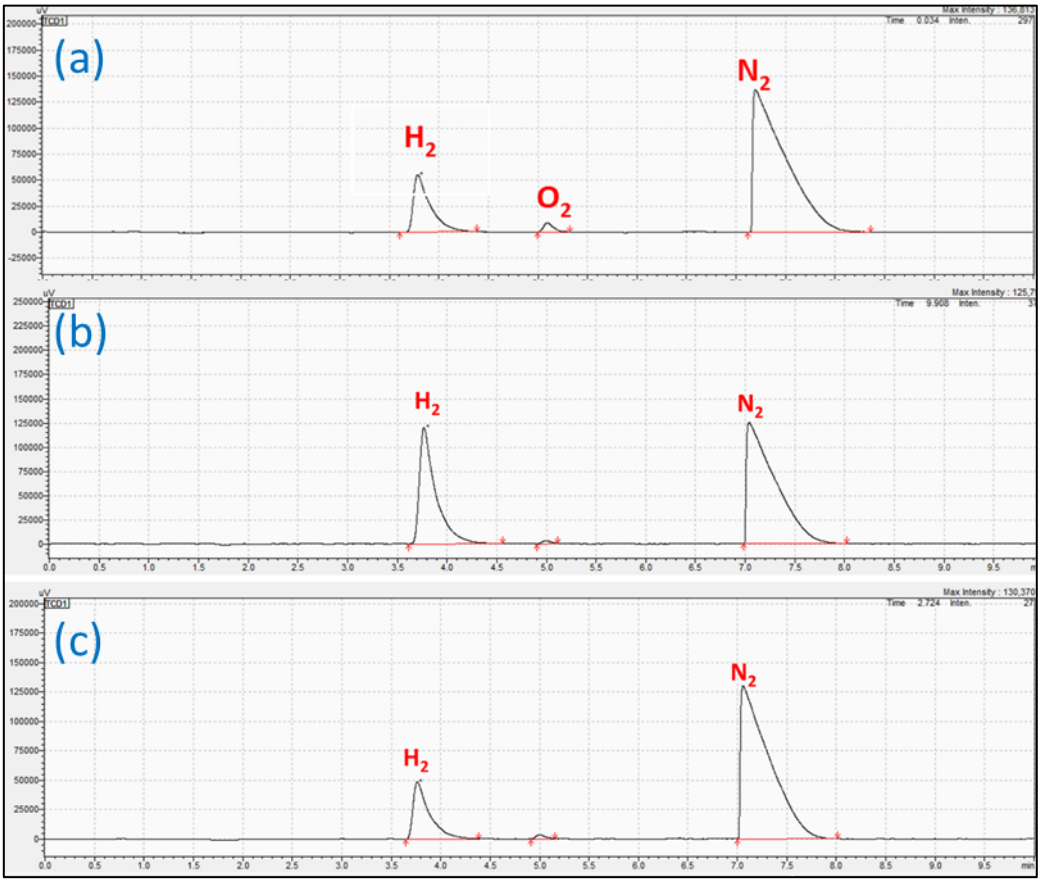


**Figure S8:** There different runs were taken under the same reaction condition[a]: catalyst **2** (0.012 mmol, 13 mol%), $N_2H_4.H_2O$ (0.09 mmol), $SmI_2(thf)_2$ (0.1M in THF, 1.8 ml), $H_2O$ (0.18 mmol) at 55 °C in 4 h.

## GC profile for Reduction reaction[a] [With $CoCp_2$ & (LutH)OTf]

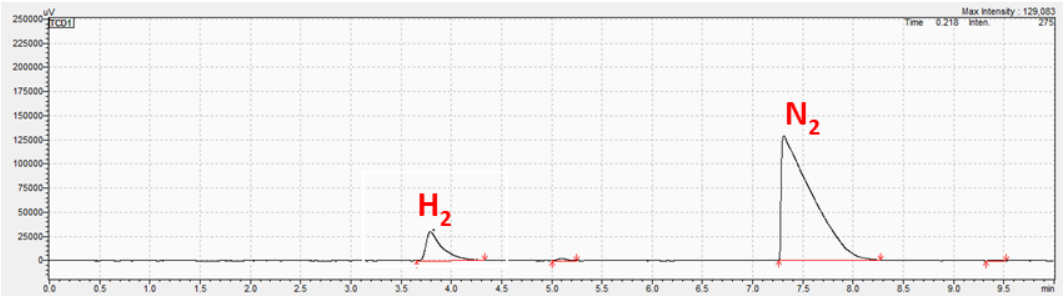


**Figure S9:** Reaction condition[a]: catalyst **2**(0.003 mmol, 3.3 mol%), $N_2H_4.H_2O$ (0.09 mmol), $CoCp_2$ (0.18 mmol), [LutH]OTf (0.18 mmol) at 55 °C in 4 h.

## GC profile for Reduction reaction[a] [With $CoCp_2$* & (LutH)OTf]

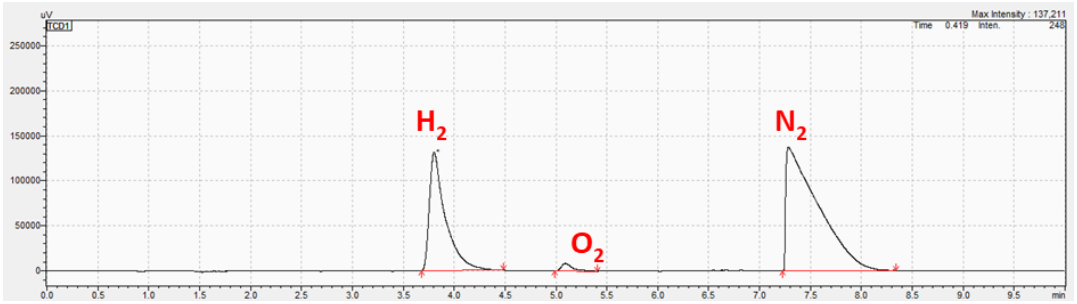


**Figure S10:** Reaction condition[a]: catalyst **2**(0.003 mmol, 3.3 mol%), $N_2H_4.H_2O$ (0.09 mmol), $CoCp_2$* (0.18 mmol), [LutH]OTf (0.18 mmol) at 55 °C in 4 h

## GC profile for Catalyst 2 with $SmI_2$ and $H_2O$[a]

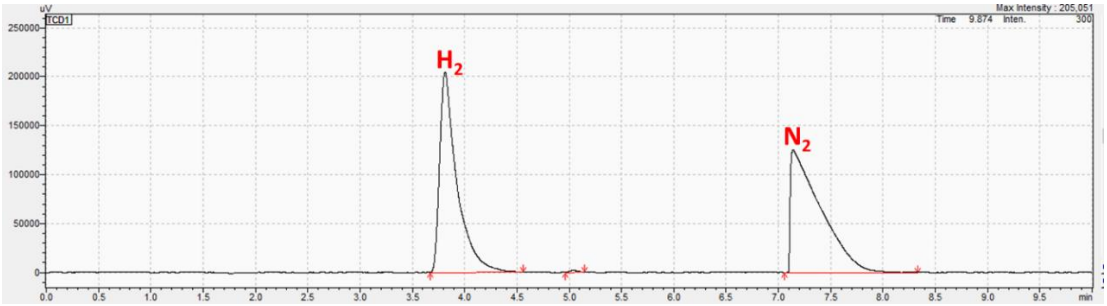


**Figure S11:** Reaction condition[a]: catalyst **2** (0.003 mmol, 3.3 mol%), $SmI_2(thf)_2$ (0.1M in THF, 1.8 ml), $H_2O$ (0.18 mmol) at 55 °C in 4 h.

## 8. UV-visible spectrometry for detection of remaining hydrazine concentration

The concentration of hydrazine in the reaction mixture was detected by using the *p*-(dimethylamino)benzaldehyde (*p*-DMAB) method.[6]

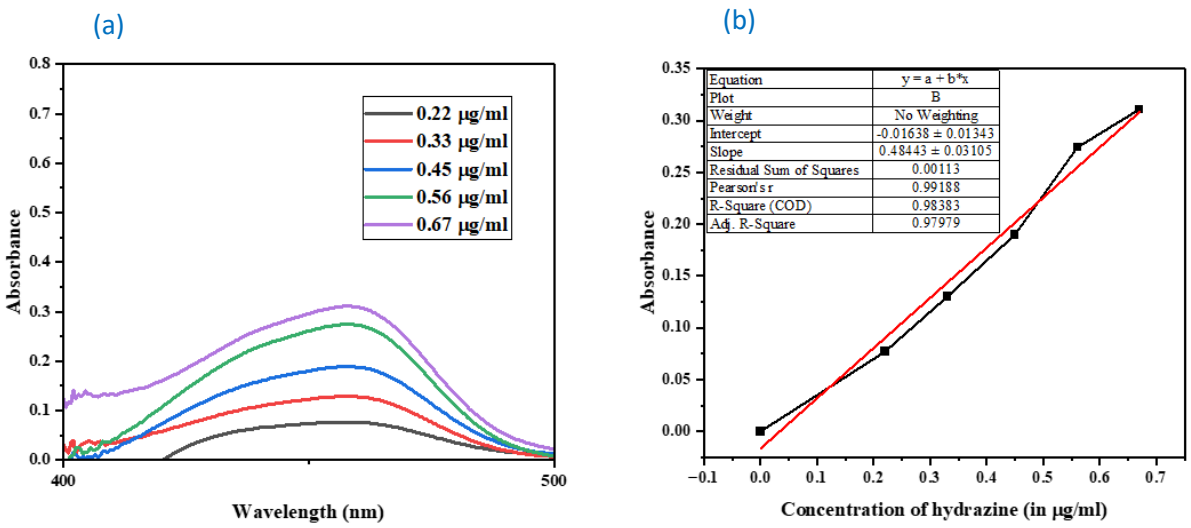


**Figure S12:** (a) UV-visible absorption spectra of different $N_2H_4.H_2O$ concentrations varying from 0.22 to 0.67 µg/ml of 0.045 M $N_2H_4.H_2O$ in 2 ml of dry THF. (b) Calibration curve used for the calculation of $N_2H_4$ concentration at absorbance 458 nm.

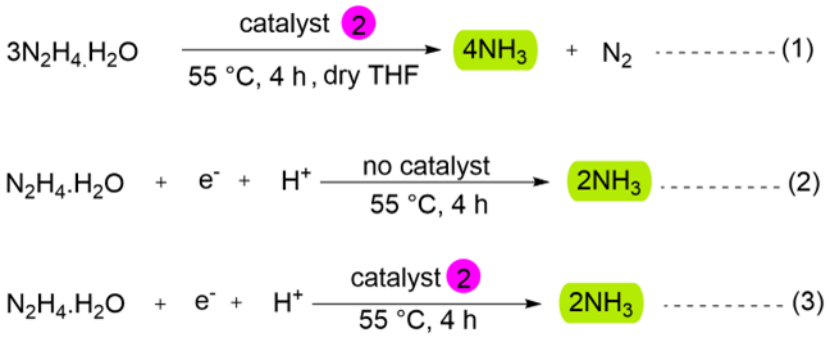


Reaction condition: [Reaction 1 :- catalyst **2** (0.003 mmol, 3.3 mol%), $N_2H_4.H_2O$ (0.09 mmol), dry THF (2ml)], [Reaction 2 :- $N_2H_4.H_2O$ (0.09 mmol), $SmI_2(thf)_2$ (0.1M in THF, 1.8 ml), $H_2O$ (0.18 mmol)] [Reaction 3 :- catalyst **2** (0.003 mmol, 3.3 mol%), $N_2H_4.H_2O$ (0.09 mmol), $SmI_2(thf)_2$ (0.1M in THF, 1.8 ml), $H_2O$ (0.18 mmol)] at 55 °C in 4 h. The volume of the reduction reaction is up to 2 ml with dry THF. The absorption at 458 nm was recorded by diluting, 2 µl of reaction mixture aliquot with standard *p*-DMAB solution followed by 2M HCl treatment **(Figure S13)**.[6]

**Table S4:**

| Entry | Absorbance (458 nm) | Remaining $N_2H_4$ (% ) |
|---|---|---|
| Reaction 1 | 0.151 | 69 |
| Reaction 2 | 0.142 | 65 |
| Reaction 3 | 0.045 | 20 |

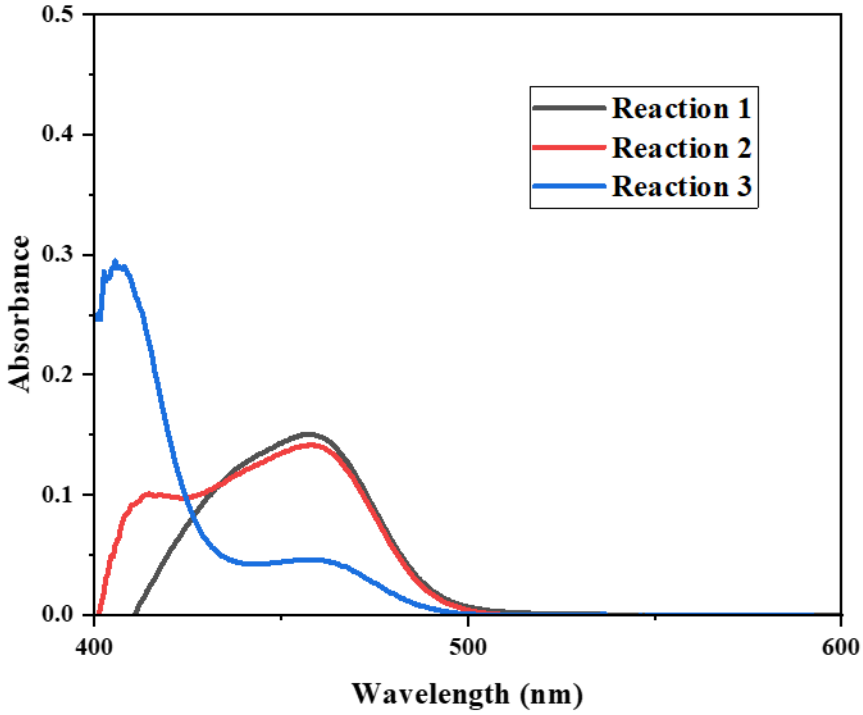


**Figure S13:** UV-visible absorption spectrum of hydrazine detection from the crude mixture of the reaction 1, 2 and 3.

## 9. Kinetics studies

### 9.1 Amount of ammonia produced with time[a]

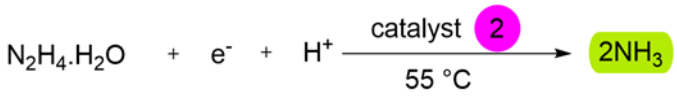


To determine the rate order dependency, the kinetics investigations were conducted with complex **2**. A six different set of reactions were performed using the standard reaction conditions varying with different time intervals (catalyst **2** loading = 0.003 mmol (3.3 mol%), $SmI_2(thf)_2$ = 1.8 mmol, $H_2O$ = 1.8 mmol, $N_2H_4$. $H_2O$ = 0.09 mmol, 55 °C, 4 h). As shown in **Figure S14**, the concentration of ammonia formed was plotted against the time. The reaction time was varied from 0.5 h to 12 h and ammonia yield was measured. Although the reaction was run for 24 h following the standard reaction condition, resulted decrease in yield to 43.5%, which might be due to the catalyst degradation or some unknown decomposition process for

the longer period of time under the optimized conditions. At different time interval, the reaction mixture was subjected to acid quench followed by quantification of $NH_4^+$ from the $^1H$ NMR spectroscopy (**Figure S14**).

**Table S5:**

| Entry | Time (h) | n($NH_4^+$) (in mmol) | $NH_4^+$ (%Yield) |
|---|---|---|---|
| 1 | 0.5 | 0.062 | 34.4 |
| 2 | 1 | 0.067 | 37.2 |
| 3 | 2 | 0.072 | 40 |
| 4 | 4 | 0.085 | 47.2 |
| 5 | 6 | 0.09 | 50 |
| 6 | 12 | 0.102 | 57 |

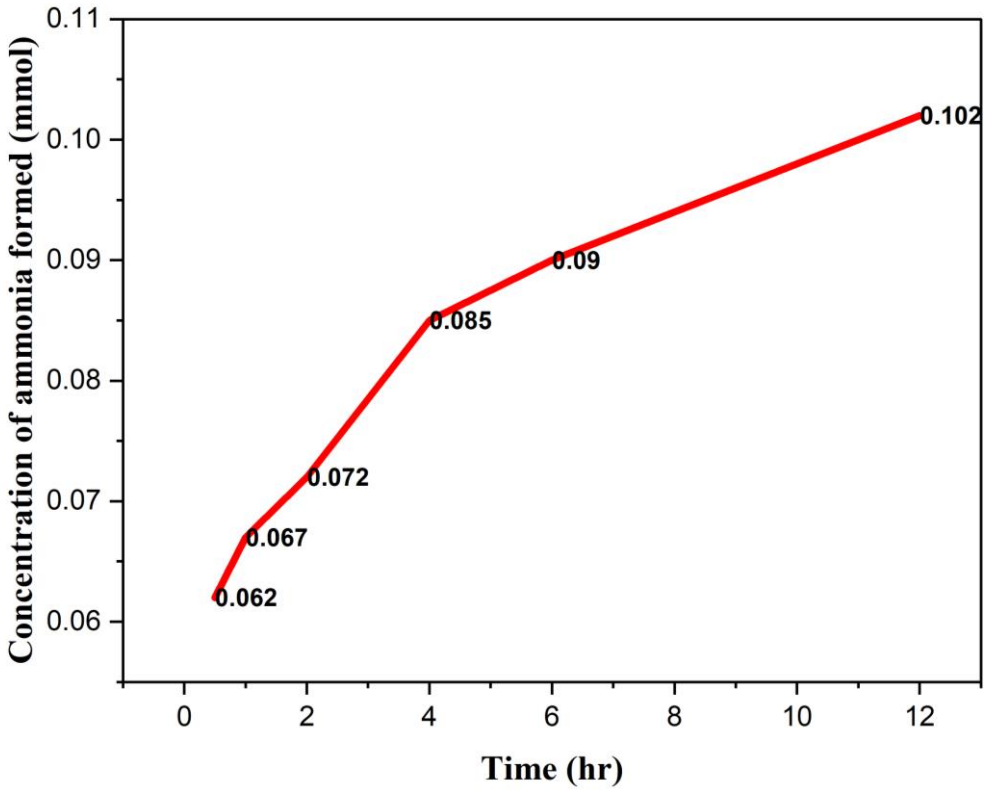


**Figure S14:** Reaction condition[a]: catalyst **2**(0.003 mmol, 3.3 mol%), $N_2H_4.H_2O$ (0.09 mmol), $SmI_2(thf)_2$ (0.1M in THF, 1.8 ml), $H_2O$ (1.8 mmol) at 55 °C.

### 9.2. Rate of formation of $NH_4^+$ with catalyst loading concentration[a]

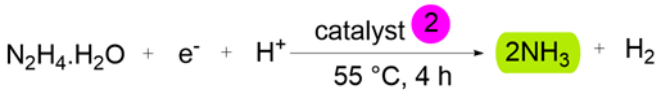

The rate of formation of $NH_4^+$ at time 4 h was plotted against varying catalyst **2** loading, which is indicative of a first-order dependence on the concentration of the catalyst using the first-order rate law equation (**Figure S15**).

Rate of the reaction = $n[NH_4^+]/t$

Rate equation = $[\ln(n[NH_4^+]/t) = \ln K + n \ln(\text{catalyst})]$, n = order of the reaction

**Table S6:**

| Entry | Catalyst **2** Loading (in mmol) | $n(NH_4^+)$ (in mmol) | **$NH_4^+$ (%Yield))** | ln(catalyst | $\ln([NH_4^+]/t)$ |
|---|---|---|---|---|---|
| 1 | 0 | 0.054 | 30 | - | -4.30507 |
| 2 | 0.0015 | 0.075 | 41.6 | -6.50229017 | -3.97656 |
| 3 | 0.003 | 0.093 | 51.6 | -5.80914299 | -3.76145 |
| 4 | 0.0054 | 0.113 | 62.7 | -5.22135633 | -3.56666 |
| 5 | 0.012 | 0.173 | 96.1 | -4.42284863 | -3.14076 |

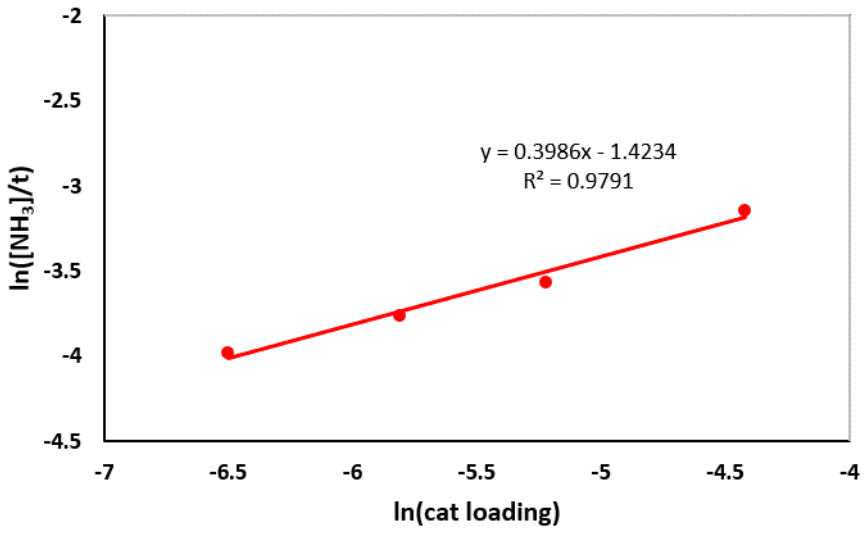


**Figure S15:** Reaction condition[a]: $N_2H_4.H_2O$ (0.09 mmol), $SmI_2(thf)_2$ (0.1M in THF, 1.8 ml), $H_2O$ (0.18 mmol) at 55 °C in 4 h.

### 9.3. Rate of formation of $NH_4^+$ with reductant loading concentration[a]

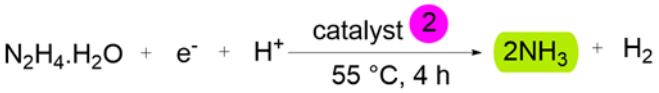

The rate of formation of $NH_4^+$ at time 4 h was plotted against different concentrations of reductant loading, which is indicative of a first-order dependence on the concentration of the reductant using the first-order rate law equation (**Figure S16**).

Rate of the reaction = $[NH_4^+]/t$

Rate equation = $[\ln([NH_4^+]/t) = \ln K + n \ln(SmI_2)]$, n= order of the reaction

**Table S7:**

| Entry | $SmI_2$ loading (in mmol) | $n(NH_4^+)$ (in mmol) | $\ln(SmI_2)$ | $NH_4^+$ (%Yield)) | $\ln([NH_4^+]/t)$ |
|---|---|---|---|---|---|
| 1 | 0 | 0.0107 | - | 6 | -5.923 |
| 2 | 0.045 | 0.0275 | -3.101 | 15.2 | -4.979 |
| 3 | 0.09 | 0.0382 | -2.407 | 21.2 | -4.651 |
| 4 | 0.18 | 0.098 | -1.714 | 54.4 | -3.709 |
| 5 | 0.36 | 0.12 | -1.021 | 66.6 | -3.506 |

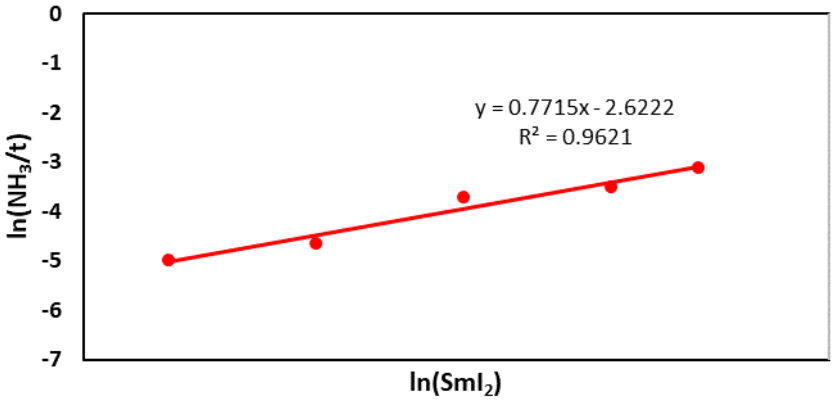


**Figure S16:** Reaction condition[a]: Catalyst **2** (0.003 mmol, 3.3 mol%), $N_2H_4.H_2O$ (0.09 mmol), $H_2O$ (0.18 mmol) at 55 °C in 4 h. The volume of each reaction makes up to 2 ml with dry THF.

### 9.4. Optimization of $H_2O$ loading while using Hydrazine (1M in THF)[a]:

Hydrous hydrazine was utilized in all catalytic reduction and disproportionation processes. In the reduction process, $SmI_2$ was chosen as the reductant, and water served as a proton source. Therefore, transitioning from anhydrous to hydrous hydrazine might not significantly impact ammonia production. To better understand the reactivity with anhydrous hydrazine (1M in

THF), a series of experiments were conducted to highlight the specific concentration of water needed in catalytic reactions.

**Table S8:**

| Entry | $H_2O$ concentration in mmol | Mmol of Ammonia formed | $NH_4^+$ (%Yield) |
|---|---|---|---|
| 1 | 0 | 0.017 | 9.4 |
| 2 | 0.18 | 0.038 | 21.1 |
| 3 | 0.36 | 0.077 | 42.7 |
| 4 | 0.90 | 0.091 | 50.5 |
| 5 | 1.8 | 0.089 | 50 |

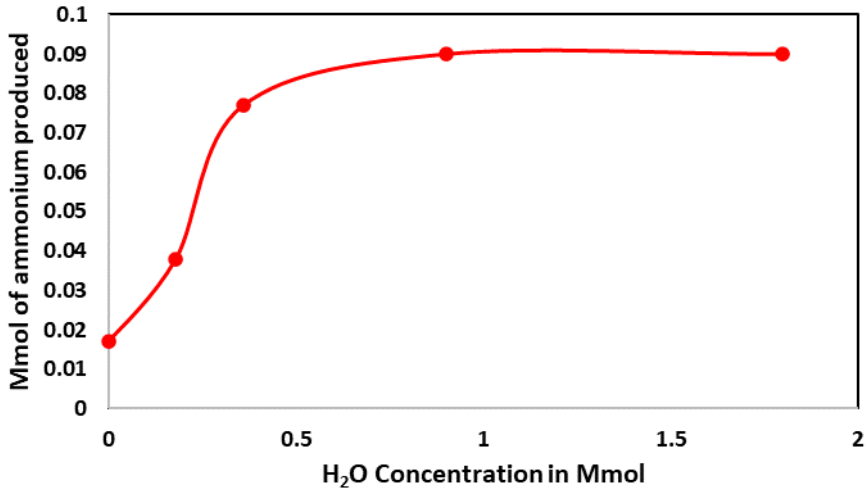


**Figure S17:** Reaction condition[a]: Catalyst **2** (0.003 mmol), $N_2H_4$ (0.09 mmol, 1M in THF), $SmI_2(thf)_2$ (0.1M in THF, 1.8 ml) at 55 °C in 4 hour.

At first, without any addition of water resulted 9.4% ammonium yield demanding the necessity of a proton source in the catalysis reaction. Then an equimolar ratio of $SmI_2$:$H_2O$ (1:1) was taken with anhydrous hydrazine (0.09 mmol) keeping all the standard reaction conditions intact which resulted 21.1% of ammonium production (entry 2, **Table S8**). Further increasing the ratio of $SmI_2$:$H_2O$ to 1:2, produced 42.7% of ammonia. In 1:5 ratio of $SmI_2$:$H_2O$, it was found to be increased to 50.5% of ammonia production and remain almost constant with 1:10 ratio (**Table S8, Figure S17**). The resulting ammonium produced was found to similar with the single catalytic run ammonia production where hydrous hydrazine was used.

## 10. Control Experiments

### 10.1. Stochiometric reaction of Complex 1 with Hydrazine hydrate

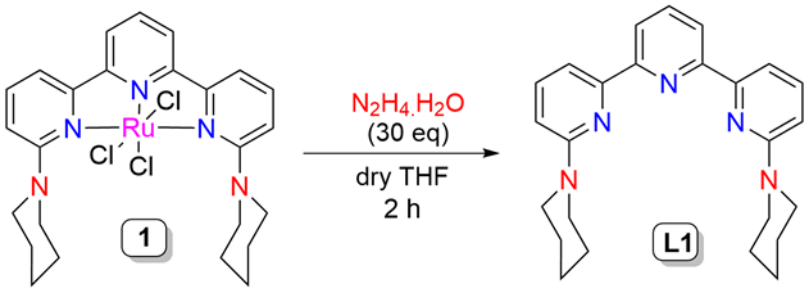


Complex **1** was treated with 5 equiv. of hydrazine hydrate in 2 ml of dry THF. It was kept at stirring, developed a green-coloured solution with black precipitate at the bottom of the Schlenk tube. After 2 h, the aliquot of the reaction mixture was checked for mass spectrometry, which indicated the decomposition of complex **1** to show only the presence of free ligand (**Figure S18**).

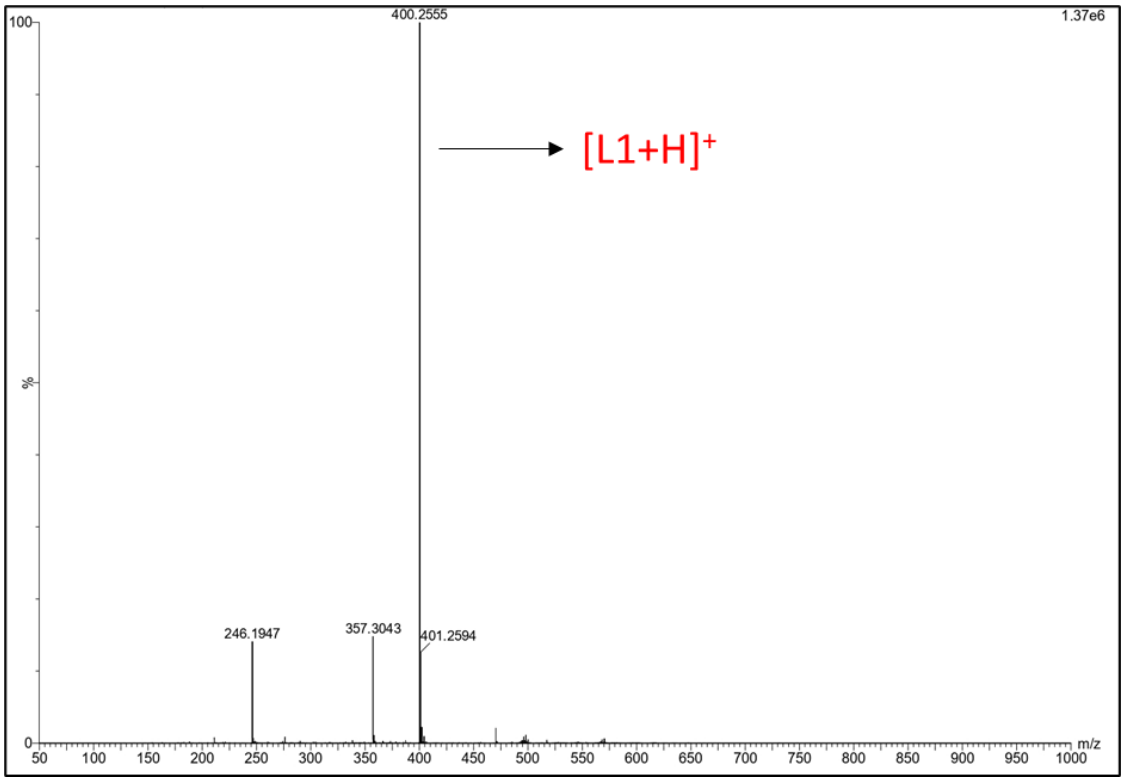


**Figure S18:** Mass analysis of complex **1** treated with hydrazine

### 10.2. Stochiometric reaction of Complex 1 with Ammonia

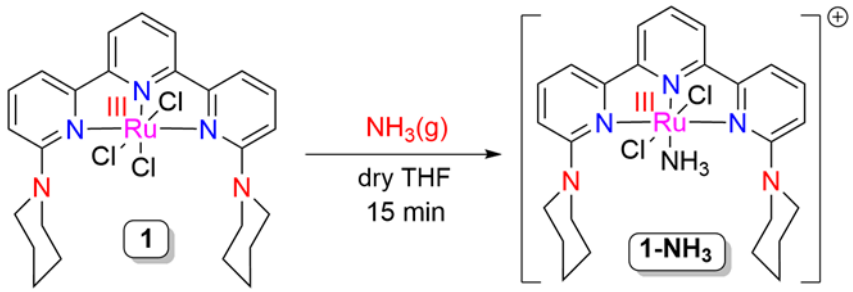


To investigate the reactivity of complex **1** with ammonia, $NH_3$(g) was purged through the reaction mixture containing complex **1** with dry THF. The partial soluble green coloured solution became a homogenous dark green coloured solution. It was stirred for 15 min and the aliquot of the reaction mixture was checked for mass analysis. In the mass spectroscopy, along with the free ligands and other unidentified peaks, a peak at m/z= 588.11 (representing $[1\text{-}NH_3]^+$) was observed which corresponds to the formation of the intermediate **1-NH$_3$**, where ammonia was proposed to bound with the ruthenium centre (**Figure S19**).

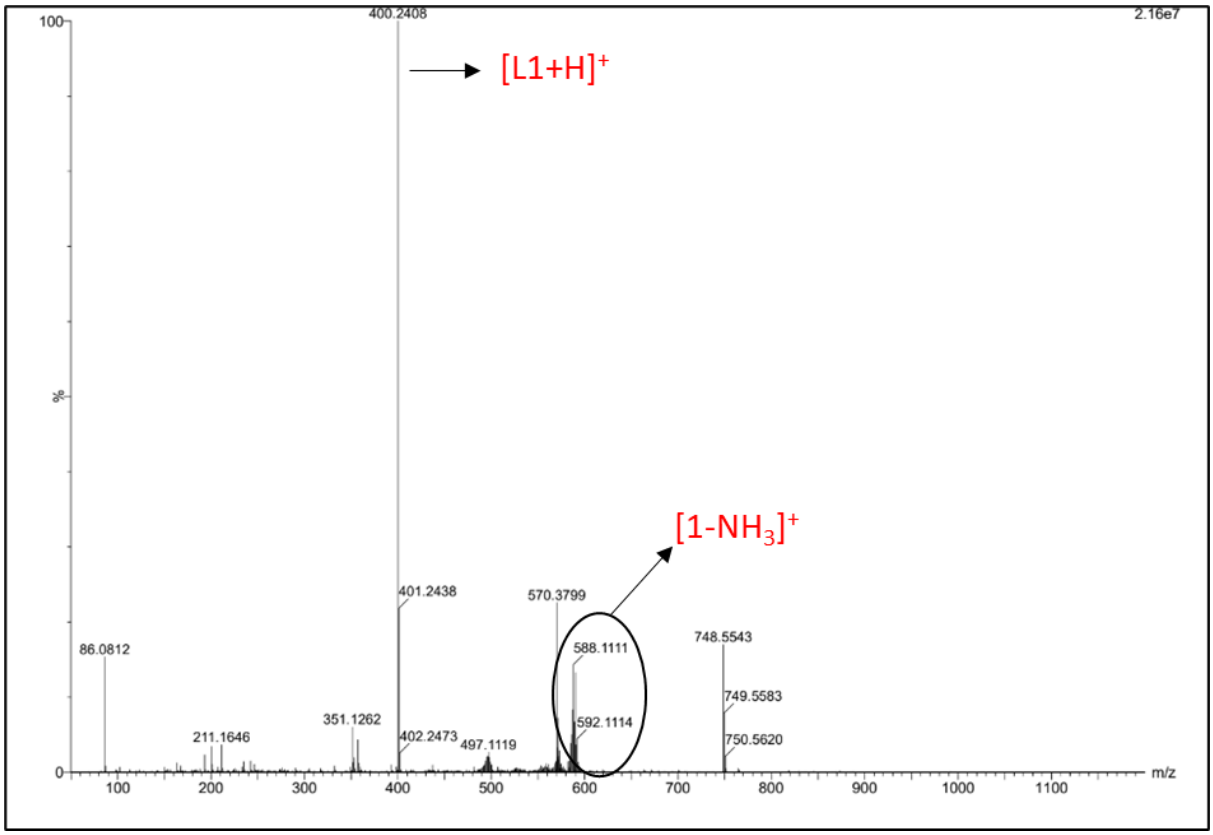

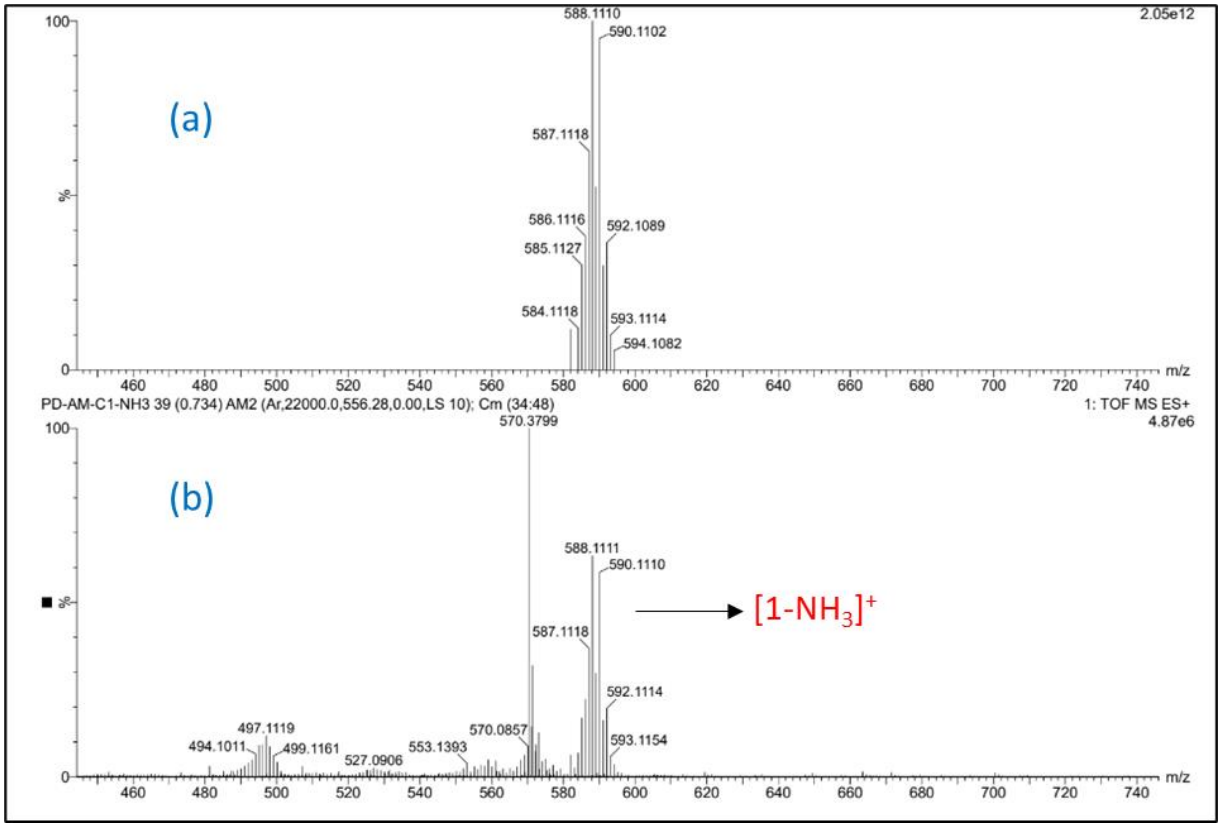


**Figure S19.** HRMS & Isotopic mass distribution analysis of intermediate **1-NH3**. Simulated (a) and Experimental (b).

### 10.3. Stochiometric reaction of Complex 2 with Hydrazine

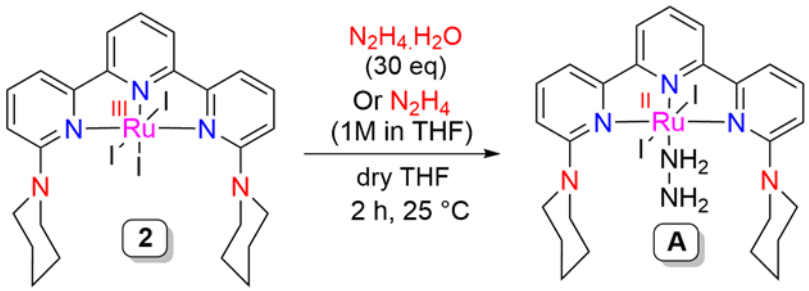


Complex **2** was treated with 30 equiv. of hydrazine hydrate or hydrazine (1M in THF) separately in 2 ml of dry THF. It was kept at stirring for 2 h at room temperature showing the change of solution colour from deep blue to deep purple. After that, the aliquot of the reaction mixture was taken and subjected to mass analysis. From mass spectrometry, one electron-reduced hydrazine bound peak with Ru centre was observed peak at m/z=660.11 (representing $[A\text{-}I]^+$) which corresponds to the formation intermediate **A** (**Figure S20**). It was predicted that iodide being a strong one electron-reducing agent that has a negative charge, can readily reduce the Ru centre to generate $I_2$.[7,8] Under this condition, hydrazine acts as a good coordinating ligand to bind with the Ru centre. Along with the intermediate **A**, another peak at m/z= 692.12

[(A-I+$N_2H_4$)$^+$] was generated which attributed to another hydrazine molecule addition to the ruthenium centre, which might be predicted that one of the pyridine rings can dissociate from the ruthenium centre.

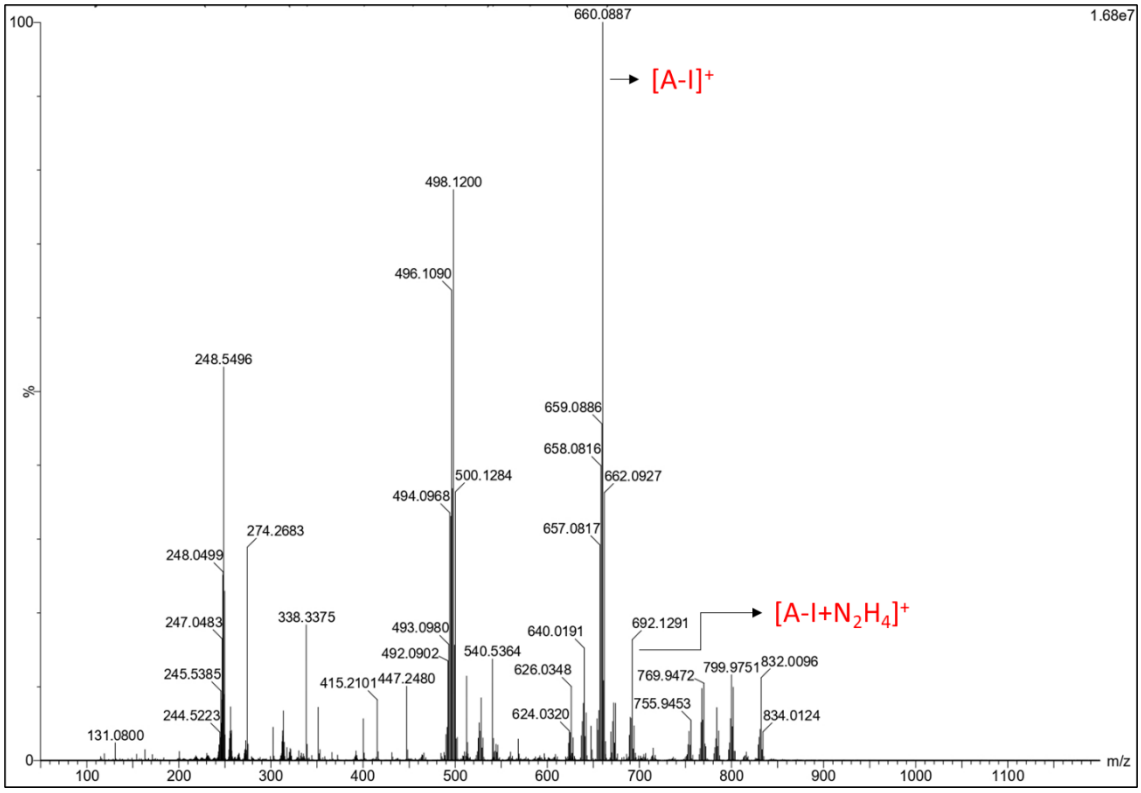


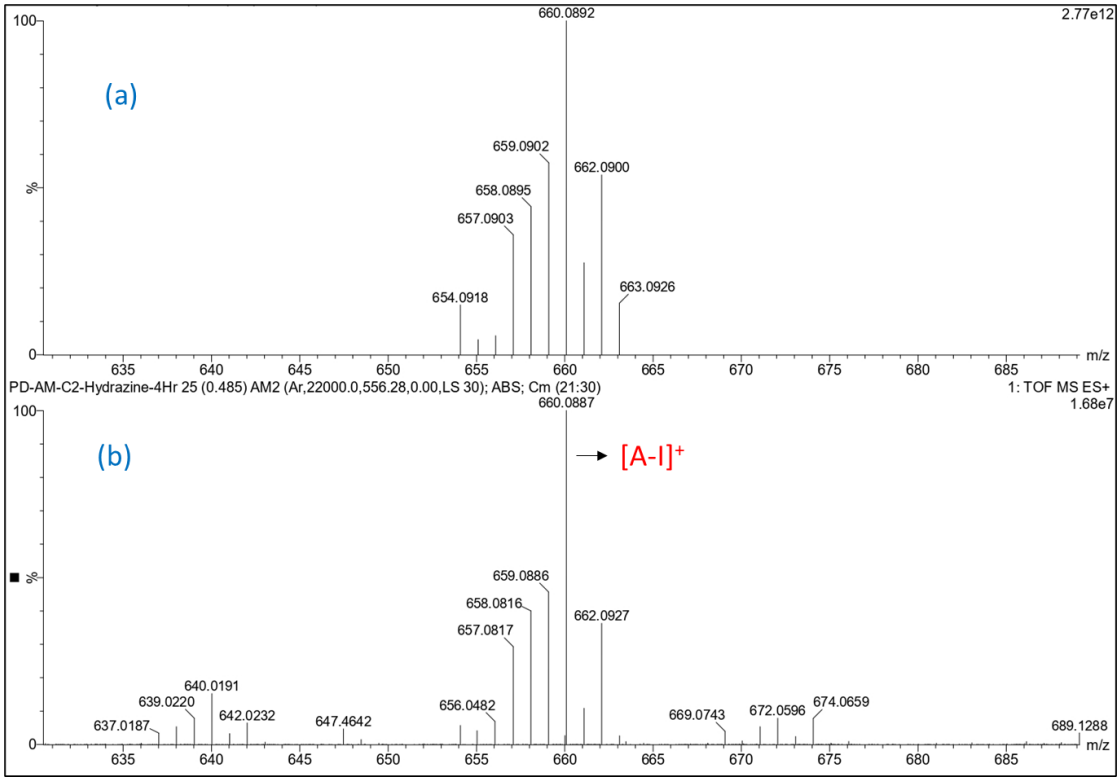

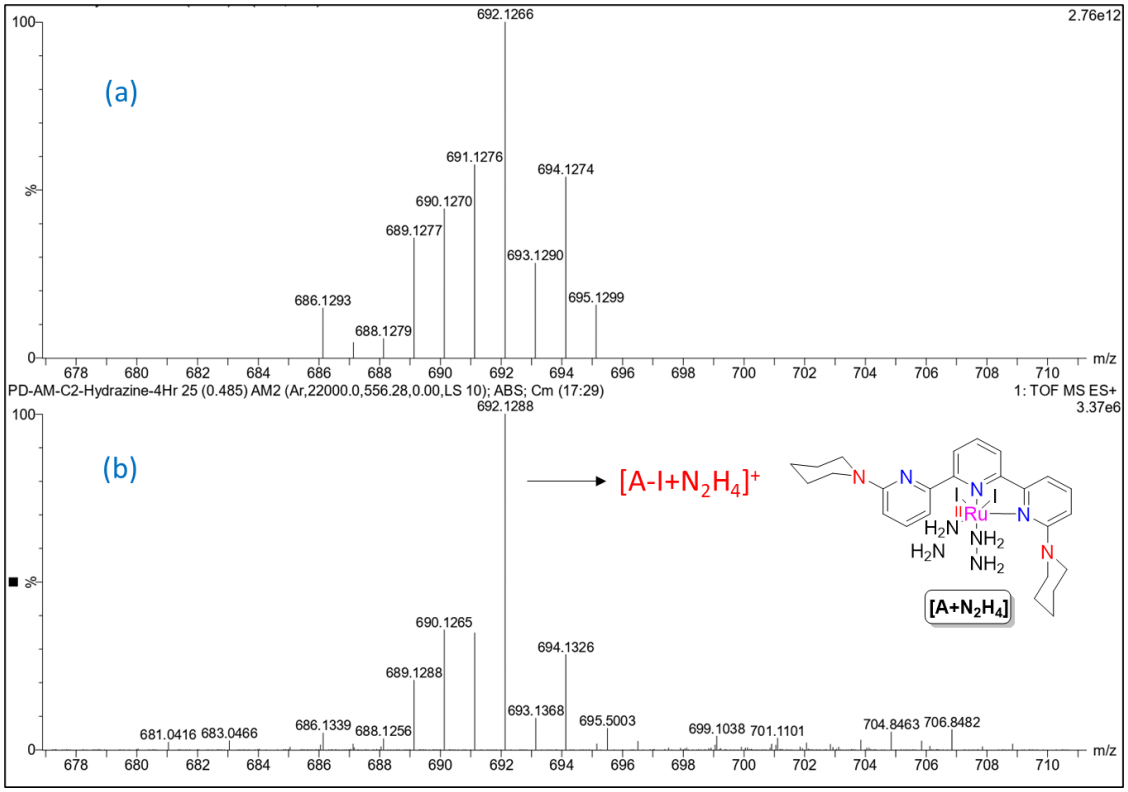


**Figure S20.** HRMS & Isotopic mass distribution analysis of intermediate **A**. Simulated (a) and Experimental (b) Isotopic mass distribution analysis of intermediate **A+$N_2H_4$** Simulated (a) and Experimental (b)

### 10.4. Stochiometric reaction of Complex 2 with Ammonia

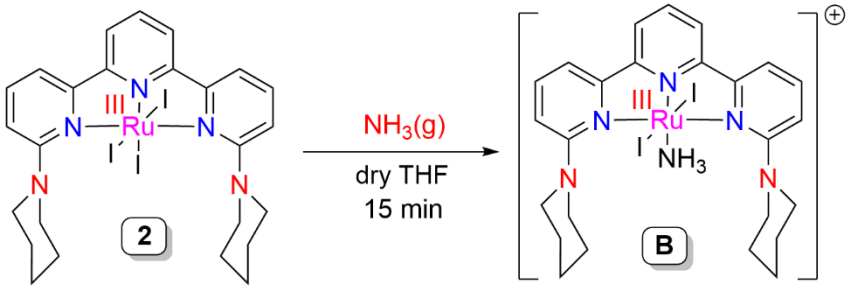


To check the reactivity of complex **2** with ammonia, a reaction was performed where complex **2** was bubbled with the $NH_3$(g) for 15 min and immediately changed the reaction colour from deep blue to deep green. The aliquot of the mixture was taken and checked for mass analysis. From the mass spectroscopy, the complex **2** peak at m/z=754.56 tends to disappear with the appearance of a new peak at m/z=771.98 (representing $[B]^+$) which corresponds to the generation of intermediate **B**, where ammonia was proposed to bound with the ruthenium centre (**Figure S21**).

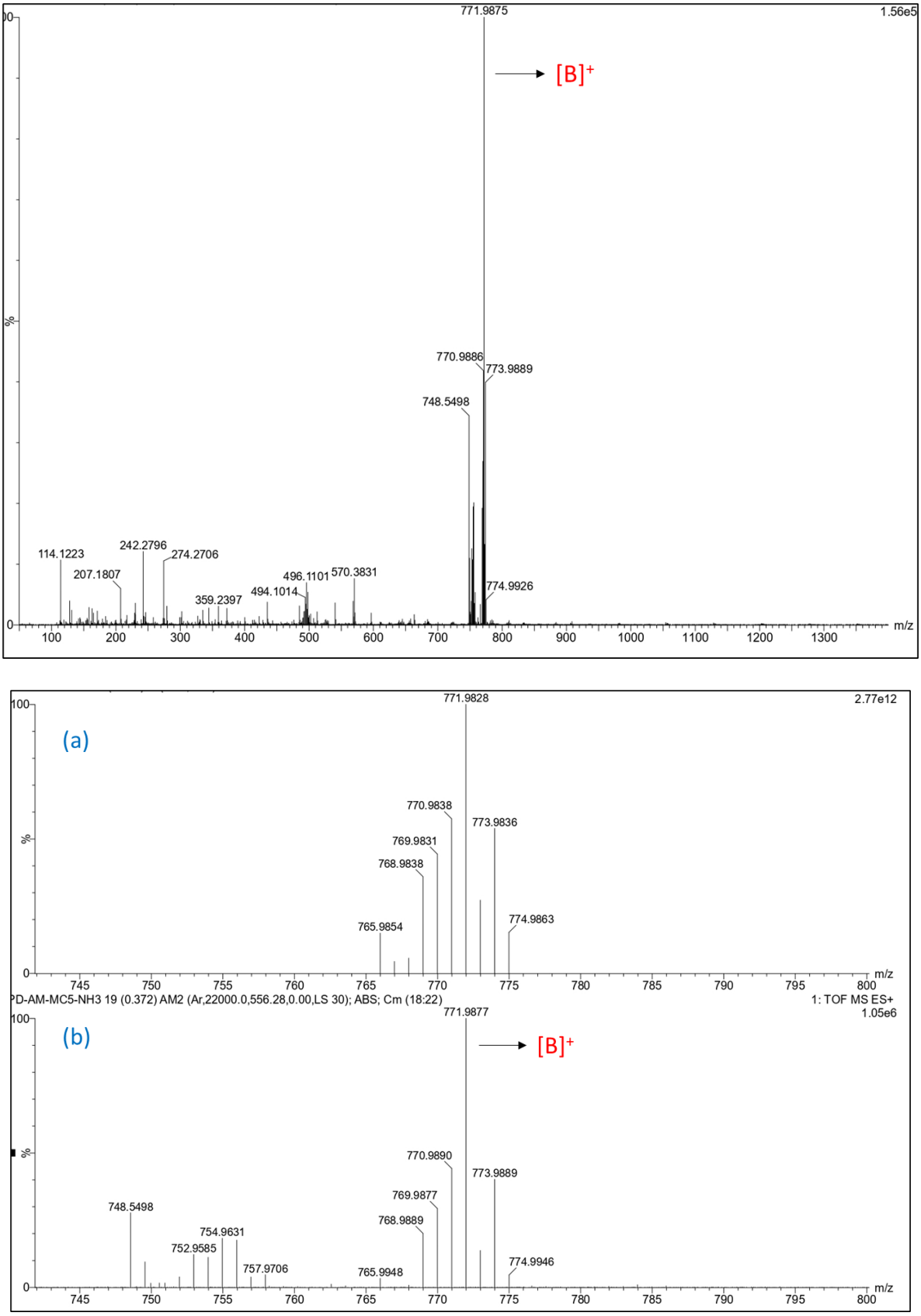


**Figure S21.** HRMS & Isotopic mass distribution analysis of intermediate **B**. Simulated (a) and Experimental (b).

### 10.5. Crossover experiments between intermediate A and intermediate B

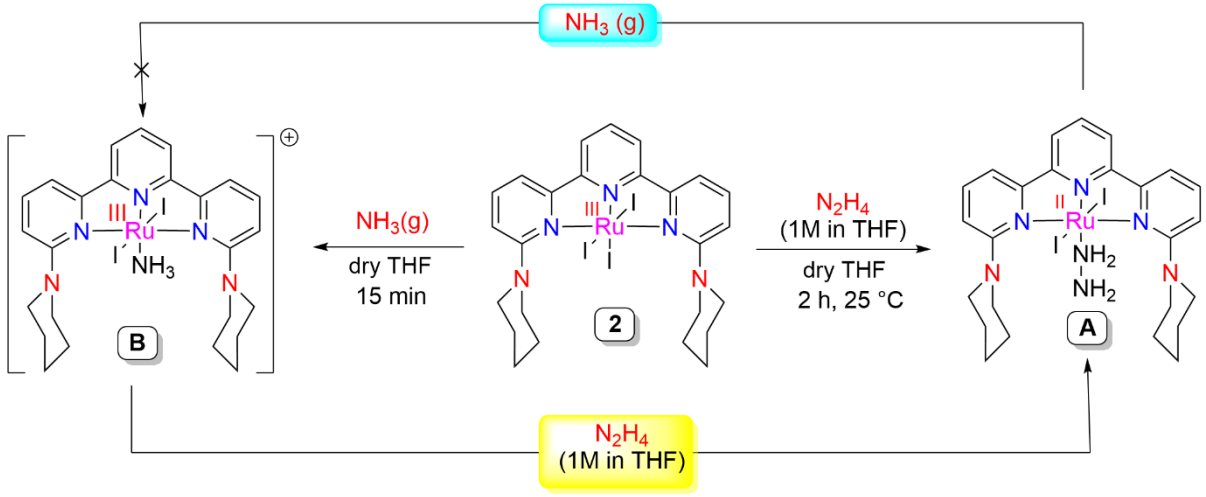


(a) The in-situ generated intermediate **A** (under treatment of complex **2** (0.017 mmol) with $N_2H_4$ (0.170 mmol)) was treated with the addition of excess ammonia(g), which did not resulted any change of colour from dark blue coloured solution. The resulting solution was checked for the mass analysis, which resulted in no change of peak for intermediate **A** other than the major peak at m/z = 660.09 which might indicate that for the hydrazine to be successively reduced, the catalytically active species **A** needs external electrons and protons for substantial N-N bond cleavage (**Figure S22).**

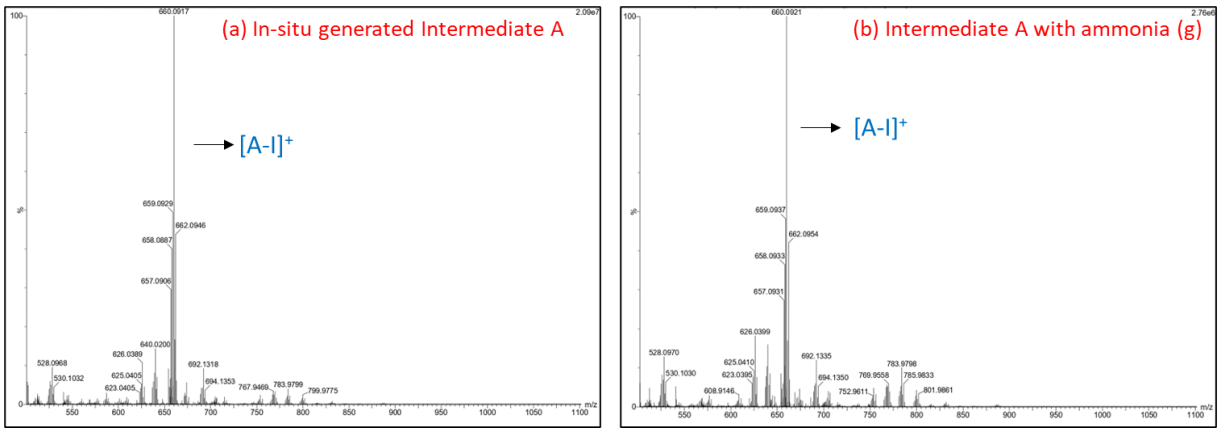


**Figure S22.** HRMS analysis of intermediate **A** (a) and intermediate **A** with ammonia(g) (b).

(b) Simultaneously, intermediate **B** was generated in-situ (under treatment of complex **2** (0.017 mmol) with $NH_3$(g)) and treated with hydrazine (0.85 mmol), immediately the colour of the solution was changed from dark green to dark blue colour and intermediate **A** was generated with the shift of peak from m/z = 771.98 (intermediate **B**) to m/z = 660.09 (intermediate **A**). This indicated that intermediate **B** is not stable enough in the presence of

hydrazine and supports its presence in the proposed catalytic cycle as an intermediate **(Figure S23).**

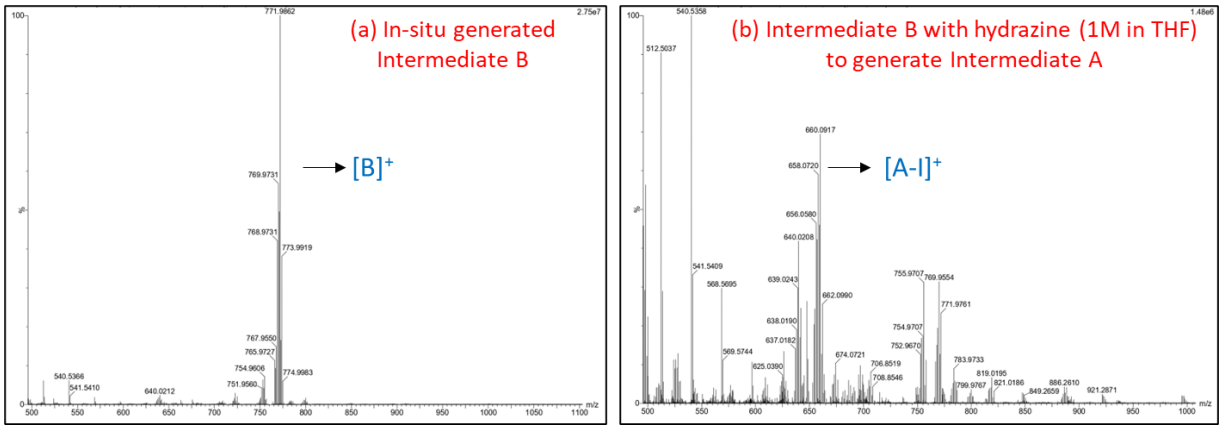


**Figure S23.** HRMS analysis of intermediate **B** (a) and Intermediate **B** with hydrazine to generate intermediate **A** (b).

### 10.6. Catalysis reaction with insitu generated intermediate A

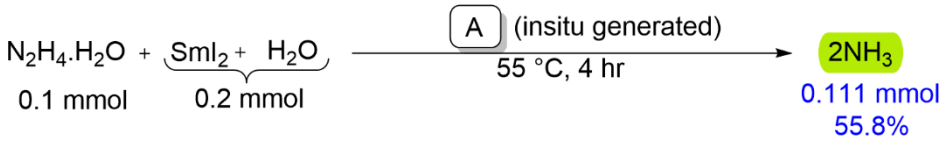


Intermediate **A** was generated by reacting complex **2** with hydrazine hydrate, detected from mass spectroscopy. Intermediate **A** proposed to act as an active intermediate in the catalytic cycle involved in the hydrazine reduction to ammonia. To check the reactivity of intermediate **A**, a reaction was carried out where 0.1 mmol of hydrazine was taken along with 3.3 mol% of catalyst **2** intakes stirred at room temperature in 1 ml of dry THF. After stirring for 1 h, $SmI_2(thf)_2$ and $H_2O$ were added and kept at 55 °C for 4 h. After completion of the reaction, all the volatiles in the reaction mixture were frozen and 5 ml of HCl (2M in $Et_2O$) was added instantly. The acidified reaction mixture was stirred for 30 min and volatile components were removed under reduced pressure to give a sticky solid product. It was diluted with 1 ml of DMSO followed by the addition of the internal standard as mesitylene (0.01 mmol). An aliquot from the reaction mixture was taken and $^1H$ NMR was recorded with DMSO-$d_6$. Up to 55.8% of ammonia was generated depicting the role of intermediate **A** as an active intermediate during the catalysis reaction (**Figure S79**).

### 10.7. Catalysis reaction with insitu generated intermediate B

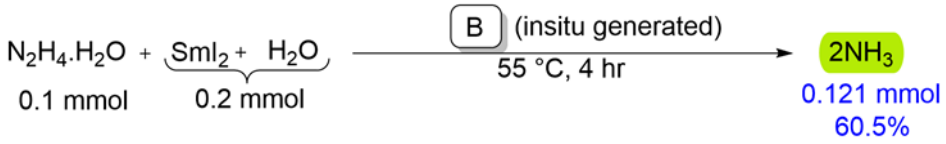


Intermediate **B** was proposed to act as an active intermediate in the catalytic cycle involved in the hydrazine reduction to ammonia. To check the reactivity, intermediate **B** was generated in-situ by treating complex **2** (0.0033 mmol, 3.3 mol%) with $NH_3$(g) (0.0033 mmol) in 1:1 ratio in 1 ml of dry THF. The resulting green coloured solution was added to a 25 ml RB containing 0.1 mmol of hydrazine, $SmI_2(thf)_2$ and $H_2O$ (0.2 mmol) and kept at 55 °C for 4 h. After completion of the reaction, all the volatiles in the reaction mixture were frozen and 5 ml of HCl (2M in $Et_2O$) was added instantly. The acidified reaction mixture was stirred for 30 min and volatile components were removed under reduced pressure to give a sticky solid product. It was diluted with 1 ml of DMSO followed by the addition of the internal standard as mesitylene (0.015 mmol). An aliquot from the reaction mixture was taken and $^1$H NMR was recorded with DMSO-$d_6$. Up to 60.5% of ammonia was generated depicting the role of intermediate **B** as an active intermediate during the catalysis reaction (**Figure S80**).

### 10.8. UV-visible spectrometry of complex 2 with the addition of hydrazine

Complex **2** was converted to intermediate **A** when treated with hydrazine (1M in THF) with liberation of molecular iodine. To verify the liberation of iodine and the shifting of absorption peak during this transformation, UV-visible spectrometry was carried out. Complex **2** developed a distinct absorption peak at 365 nm, later multiple absorption peaks resulted when hydrazine was added to complex **2** with the disappearance of peak at 365 nm. With the increase in time a peak at 332 nm was developed which was assigned to the liberation of $I_2$ peak **(Figure S24)**.[9]

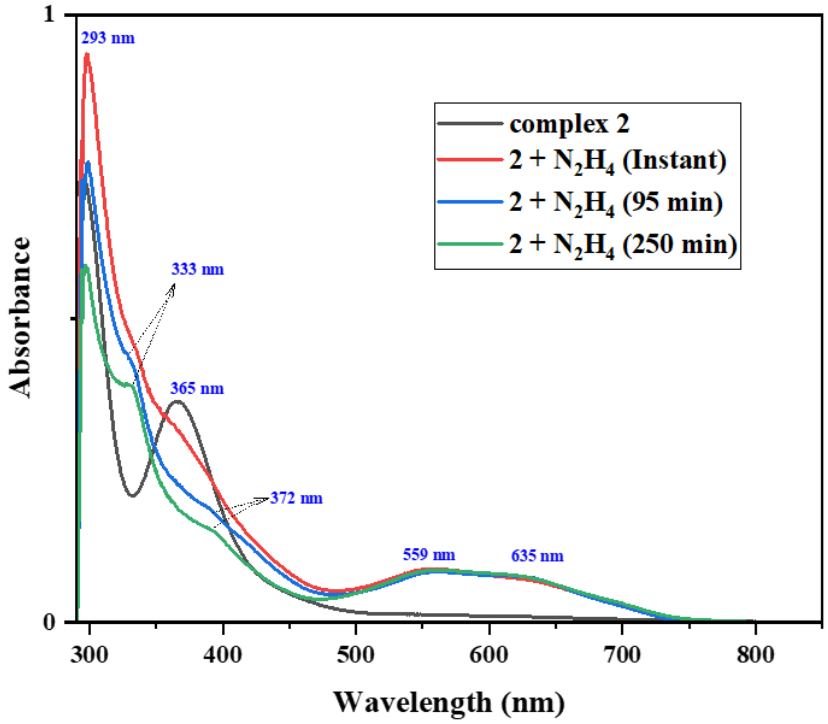


**Figure S24.** UV-visible absorption studies for complex **2** treatment with hydrazine (1M in THF).

### 10.9. UV-visible spectrometry of complex 2 with the addition of $NH_3$(g) followed by hydrazine treatment

Complex **2** was treated with $NH_3$(g) for 5 min, resulting in the change of UV-vis spectrometry from compound **2** with generation of two new peak at 559 nm and 634 nm. After 120 min of the reaction time the peak was remain unchanged (blue). Followed to the ammonia addition, hydrazine was added led to the generation of new species with libearation of $I_2$ peak (333 nm) which was assigned to the generation of intermediate **A** *via* intermediate **B** (**Figure S25**). The generation of intermediate **A** was confirmed from the independent treatment of complex **2** with hydrazine (see section 10.8).

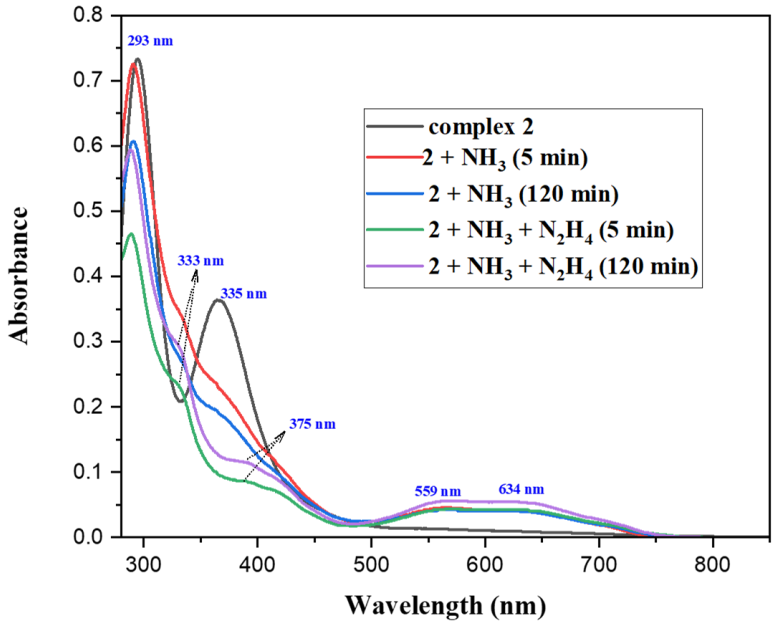


**Figure S25.** UV-visible absorption studies for complex **2** treatment with $NH_3$(g) followed by hydrazine (1M in THF).

### 10.10. Reactivity of ligand L1 under acid treatment:

The ligand **L1** bearing two nitrogen donating arm, basic aliphatic piperidine sites at the C2 position of the terpyridine ring. The ligand **L1** shows a [M+H]= 400.24 in HRMS spectroscopy (see **Figure S32**). To check the protonating sites at the piperidine ring, 3 equiv. of formic acid (0.111 mmol) was added with the ligand **L1** (0.037 mmol) in 1 ml of dry THF. The yellowish solution suddenly changed the colour to reddish solution under acid treatment. In HRMS spectroscopy it showed an m/z value of 200.61 with a charge state of +2 along with the peak at 400.24, indicating that the generation of double protonation at the ligand sites **(Figure S26a)**. The $^1$H NMR analysis was carried out with addition of **L1** with the treatment of formic acid in $CDCl_3$. This experiment showed at 3 equiv. of formic acid addition, one of the aromatic ring was protonating causes the shift towards downfield along with the 0.05 ppm of shifting towards downfield for the piperidine protons indicating the free N-arm protonation **(Figure S26b)**. Both HRMS and $^1$H NMR analysis suggests that the piperidine 'N' sites may undergo protonation under acidic conditions, potentially in the same way it may facilitate the proton transfer process during catalysis reactions.

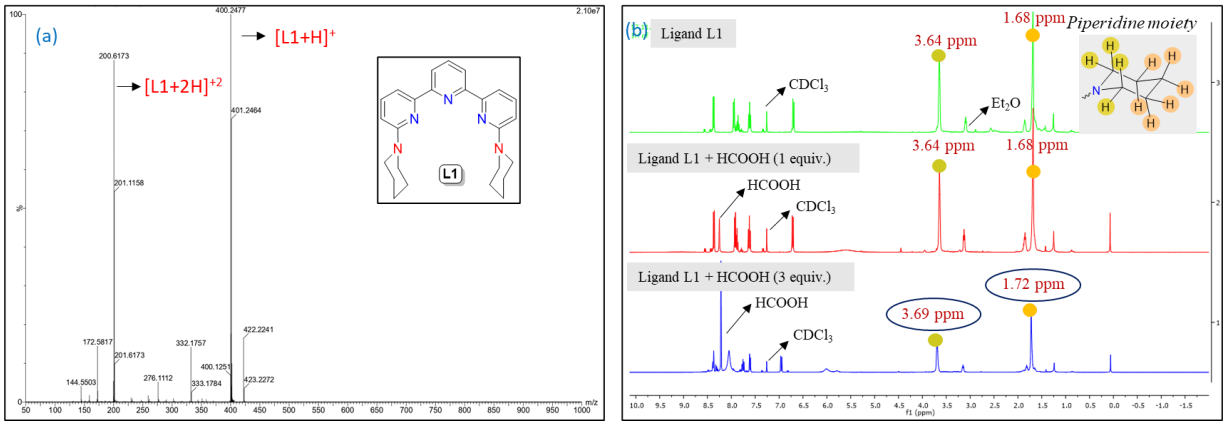


**Figure S26.** (a) HRMS spectra of ligand **L1** under formic acid treatment (b) $^{1}$HNMR spectra of ligand **L1** under formic acid treatment.

### 10.11. Reactivity studies of insitu generated intermediate A:

Complex **2** (0.017 mmol, 1 equiv.) was treated with $N_2H_4$ (1M in THF, 0.17 mmol, 10 equiv.) to generate intermediate **A**, detected from the generation of mass peak at m/z= 660.09, where no peaks at the higher mass range was observed. To check the possibility of redox reactivity at the terpyridine centre, the resulting solution of intermediate **A** was evaporated and refluxed in the presence of dry acetonitrile to check the possibility of C-C coupling at the 4-position of the terpyridine ring. But no such observation was found except for the exclusion of free ligand from HRMS spectroscopy. This result suggests the ligand **L1** might not involve in any kind of redox behaviour when coordinating with the Ru centre (**Figure S27**).

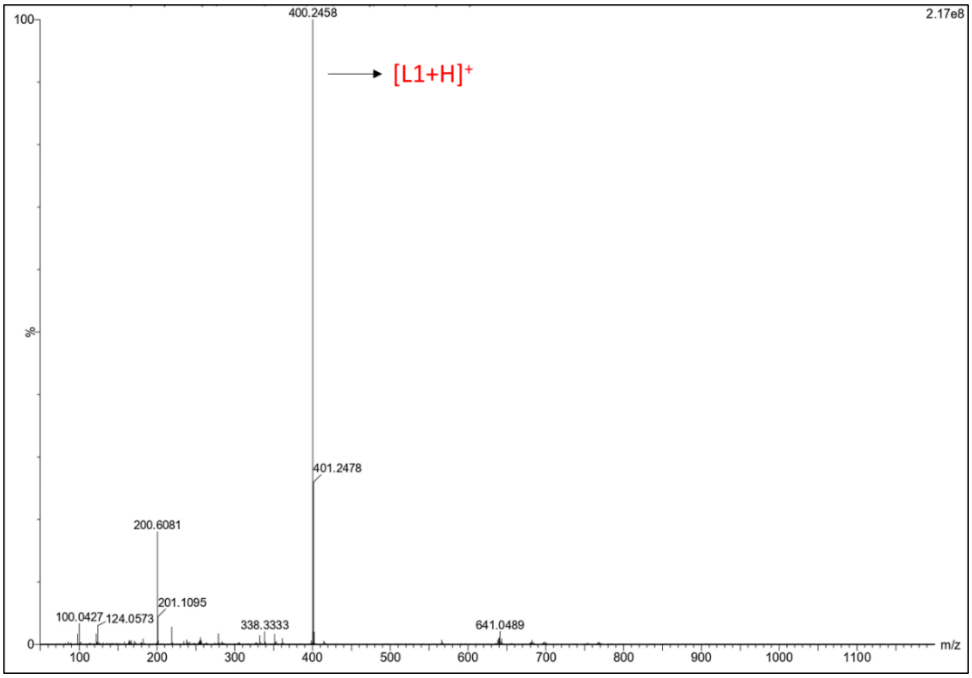


**Figure S27.** HRMS spectra of reactivity of insitu generated intermediate **A**

## 11. Other N-N bond activation

### 11.1. Phenyl hydrazine reduction reaction

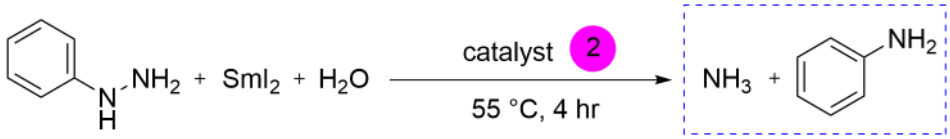


Phenyl hydrazine being a suitable substitute for hydrazine was taken for the study to check the reactivity as the N-C bond in phenyl hydrazine will be kinetically persistent and lead to generate aniline and ammonia as two products. In the presence of catalyst **2,** phenyl hydrazine reduction was checked in the presence of $SmI_2/H_2O$ which yielded 83% and 74% of ammonia and aniline respectively. Without any catalyst keeping the standard reaction condition the same, only 19% of ammonia and 43% of aniline resulted **(Figure S81, S82)** (**Table S9**).

**Table S9: Catalytic runs for phenyl hydrazine reduction**[a]

| Entry | Catalyst | TON | $NH_4^+$ (%Yield)[b] | $PhNH_3^+$ (%Yield)[b] |
|---|---|---|---|---|
| 1 | **2** | 25 | 83 | 74 |
| 2 | - | - | 19 | 43 |

[a]Reaction conditions: Catalyst **2** (0.003 mmol, 3.3 mol%), $PhNHNH_2$ (0.09 mmol), $SmI_2(thf)_2$ (0.18 mmol), $H_2O$ (0.18 mmol). Catalytic runs are performed at 55 °C for 4 h unless otherwise mentioned. [b]The generated $NH_3$ and aniline were converted into their respective chloride salt with immediate treatment of $HCl{\cdot}Et_2O$. Mesitylene was used as an internal standard [0.015 mmol, 6.77 ppm (s, 3H)] in $^1H$ NMR, by integrating the phenyl group of anilinium hydrochloride and $NH_4^+$ resonance, the yields of $NH_4Cl$ and $PhNH_3^+Cl^-$ were measured in DMSO-*d6*.

$^1H$ NMR of $NH_4Cl$ (400 MHz, DMSO-*d6*) δ (ppm) = 7.19 ppm, 7.31 ppm, 7.43 ppm (1:1:1)

$^1H$ NMR of $PhNH_3^+Cl^-$ (400 MHz, DMSO-*d6*) δ (ppm) = 7.50 (t, $J$ = 8 Hz, 3H), 7.39(d, $J$ = 8.1 Hz, 2H)

### 11.2. 1,2-diphenyl hydrazine reduction reaction

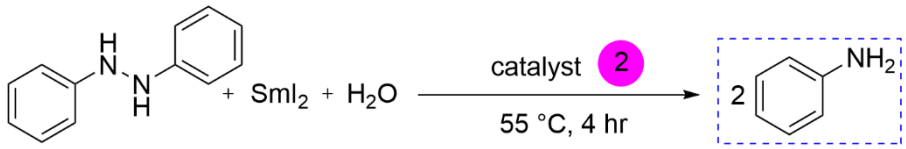


1,2-diphenyl hydrazine bearing two ends of the nitrogen atom substituted with the phenyl group was utilized for the reduction reaction using optimized reaction conditions. When 0.1 mmol of 1,2-diphenyl hydrazine was treated with 0.2 mmol of reductant ($SmI_2$) and proton source ($H_2O$) with 3.3 mol% catalyst loading, 0.172 mmol (86.25%) of aniline was resulted. After completion of the reaction, Mesitylene as an internal standard [0.1 mmol, 6.77 ppm (s, 3H)]) was added and the crude reaction mixture was checked for $^1$H NMR analysis in DMSO-$d_6$, which indicated the peak corresponding to aniline along with the internal standard peak (**Figure S83**).

$^1$H NMR of Aniline (400 MHz, DMSO-*d6*) δ (ppm) = δ 6.99 (t, $J$ = 7.6 Hz, 2H), 6.54 (d, $J$ = 7.6 Hz, 2H), 6.47 (s, 1H), 4.97 (s, 2H).

## 12. Transfer hydrogenation with complex 2

### 12.1 Transfer hydrogenation of Benzophenone

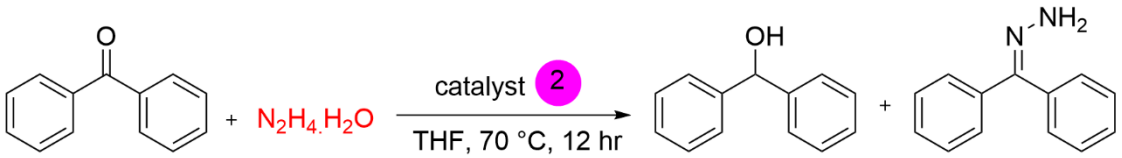


Catalyst **2** was further utilised for the transfer hydrogenation in the presence of hydrazine hydrate as a hydrogenating source for benzophenone to benzhydrol formation. When benzophenone (0.09 mmol) was reacted with $N_2H_4.H_2O$ (0.45 mmol, 5 equiv. w.r.t substrate) in the presence of 3.3 mol% of catalyst loading in THF for 12 h at 70 °C, resulted in 14% of diphenylmethanol with 13% of benzophenone-hydrazone formation. Along with the minimal amount of diphenylmethanol, coupling adducts such as benzophenone-hydrazone were detected along with the unreacted benzophenone in the GC-MS spectrum **(Figure S85A, S85B).**

$^1$H NMR was taken from the crude reaction mixture in $CDCl_3$ with the addition of mesitylene as an internal standard [0.09 mmol, 6.77 ppm (s, 3H)] **(Figure S84).**

### 12.2 Transfer hydrogenation of Nitrobenzene

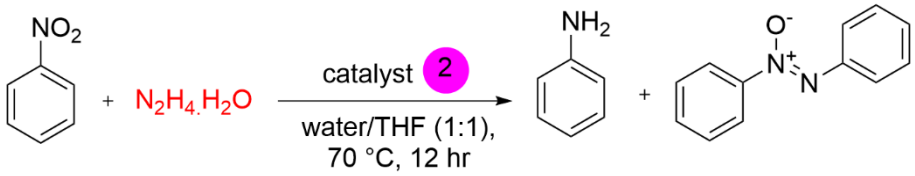


Catalyst **2** was checked with the transfer hydrogenation with a promising substrate such as nitrobenzene in the presence of hydrazine hydrate as a hydrogenating source. When nitrobenzene (0.09 mmol) was treated with $N_2H_4.H_2O$ (0.45 mmol, 5 equiv. w.r.t substrate) in the presence of 3.3 mol% of catalyst loading in water/THF mixture (1:1) for 12 h at 70 °C, resulted 16% of aniline formation detected from $^1$H NMR, with other undistinguishable products such as azoxybenzene and unreacted nitrobenzene which were confirmed from GC-MS spectrum with retention time of 13.87 min and 7.06 min respectively **(Figure 87A, S87B).**

$^1$H NMR was taken from the crude reaction mixture in $CDCl_3$ with the addition of mesitylene as an internal standard [0.015 mmol, 6.77 ppm (s, 3H)] **(Figure S86).**

## 13. X-Ray Crystallographic data

### 13.1. Crystal data of Ligand L1

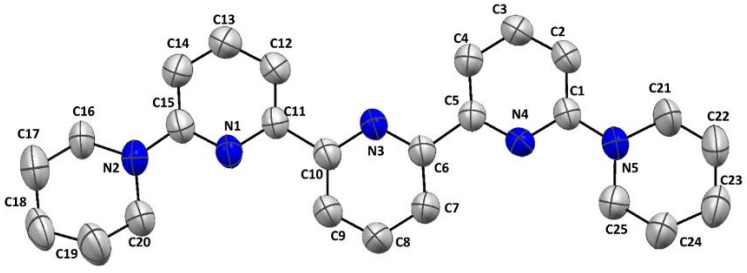


**Figure S28.** Molecular structure of Ligand L1

**Table S10.** Crystal data and structure refinement for Ligand L1

| Name | **L1** |
|---|---|
| CCDC Number | **2290962** |
| Empirical formula | $C_{25.5}H_{31}ClN_5$ |
| Formula weight | 443.00 |
| Temperature/K | 298(2) |
| Crystal system | monoclinic |
| Space group | C2/c |
| a/Å | 29.863(3) |
| b/Å | 9.4396(9) |
| c/Å | 17.2974(16) |
| α/° | 90 |
| β/° | 101.266(3) |
| γ/° | 90 |
| Volume/Å$^3$ | 4782.1(8) |
| Z | 8 |
| $\rho_{calc}$g/cm$^3$ | 1.231 |
| μ/mm$^{-1}$ | 0.182 |
| F(000) | 1888.0 |
| Crystal size/mm$^3$ | 0.24 × 0.2 × 0.16 |
| Radiation | MoKα (λ = 0.71073) |
| 2Θ range for data collection/° | 4.534 to 50.214 |
| Index ranges | -35 ≤ h ≤ 35, -11 ≤ k ≤ 11, -20 ≤ l ≤ 20 |
| Reflections collected | 28059 |
| Independent reflections | 4252 [$R_{int}$ = 0.1135, $R_{sigma}$ = 0.0636] |
| Data/restraints/parameters | 4252/123/382 |
| Goodness-of-fit on F$^2$ | 1.029 |
| Final R indexes [I>=2σ (I)] | $R_1$ = 0.0648, w$R_2$ = 0.1555 |
| Final R indexes [all data] | $R_1$ = 0.1514, w$R_2$ = 0.2061 |
| Largest diff. peak/hole / e Å$^{-3}$ | 0.13/-0.32 |

## 14. Spectroscopic Data

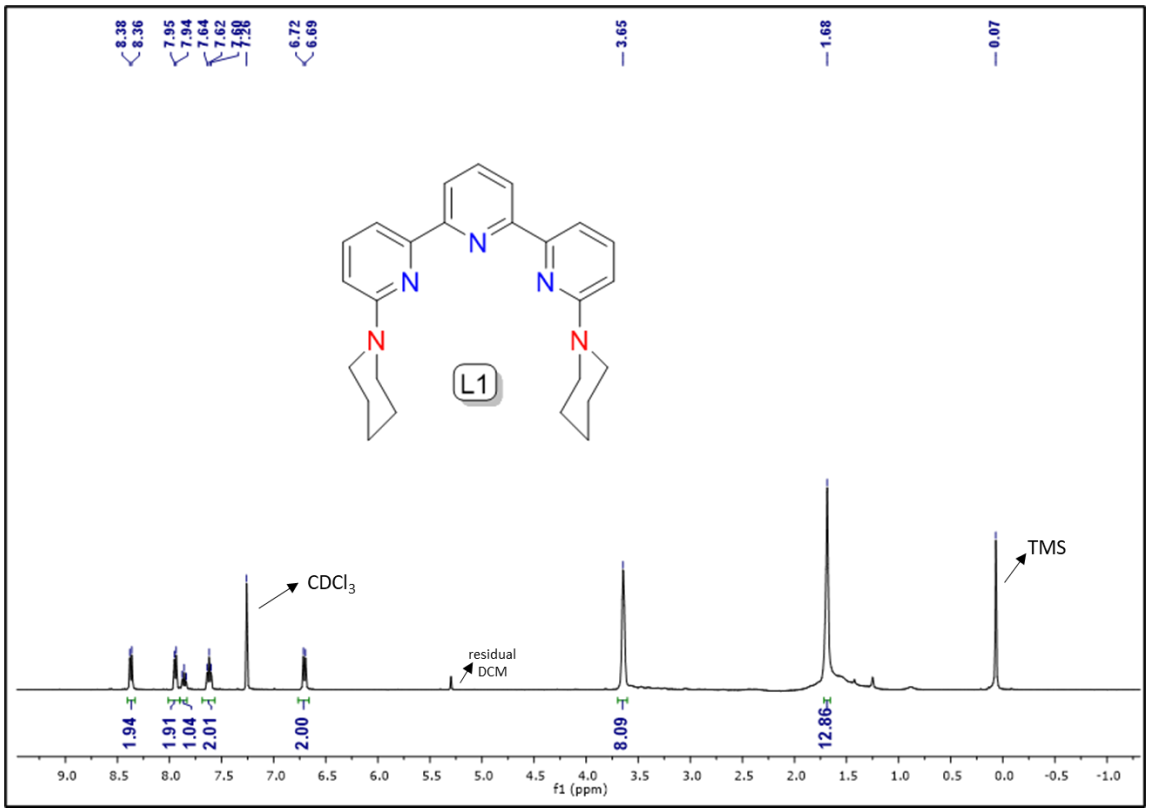


**Figure S29.** $^{1}$H NMR spectrum of 6,6"-di(piperidin-1-yl)-2,2':6',2"-terpyridine **(L1)**

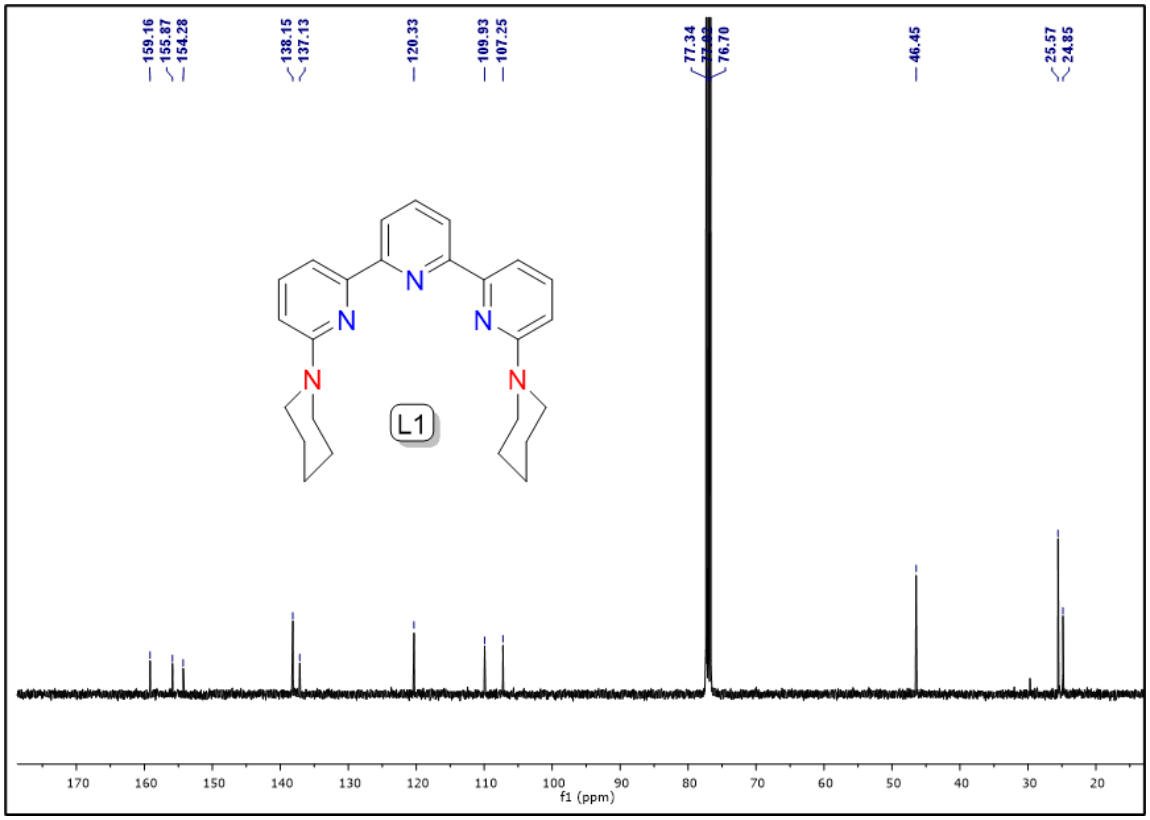


**Figure S30.** $^{13}$C NMR spectrum of 6,6"-di(piperidin-1-yl)-2,2':6',2"-terpyridine **(L1)**

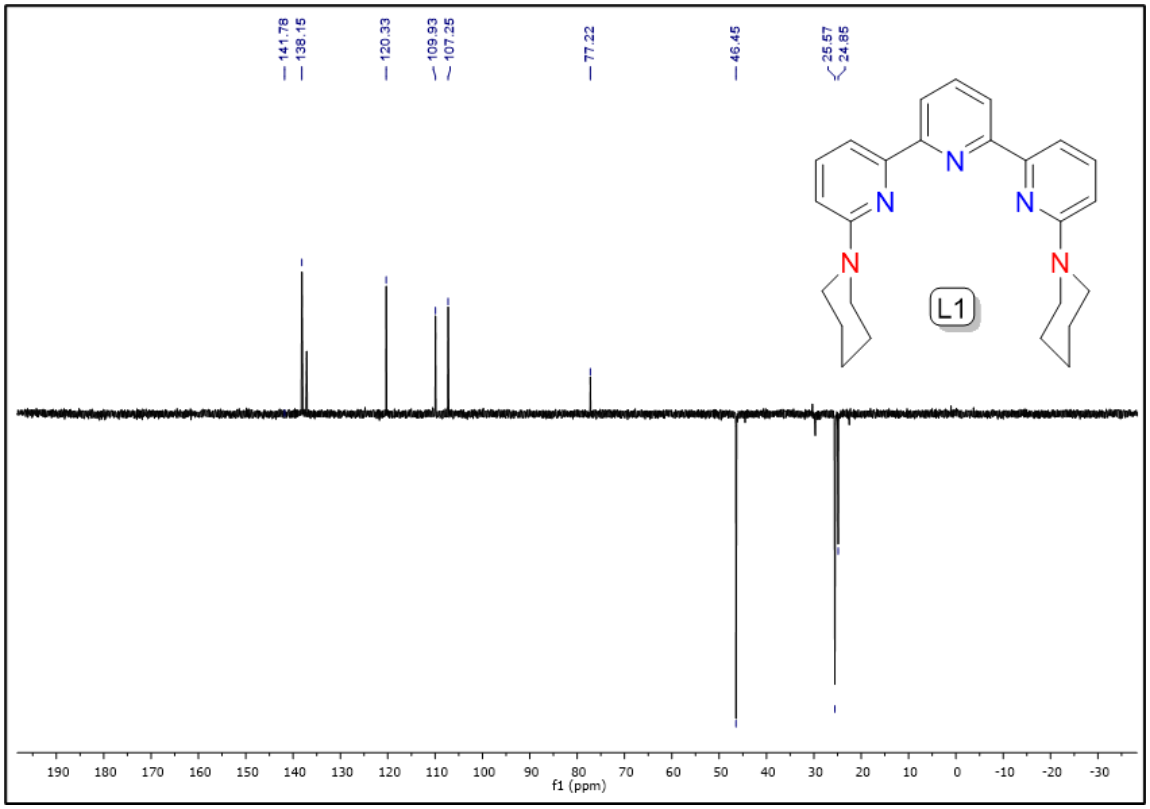


**Figure S31.** DEPT-135 of 6,6''-di(piperidin-1-yl)-2,2':6',2''-terpyridine **L1**

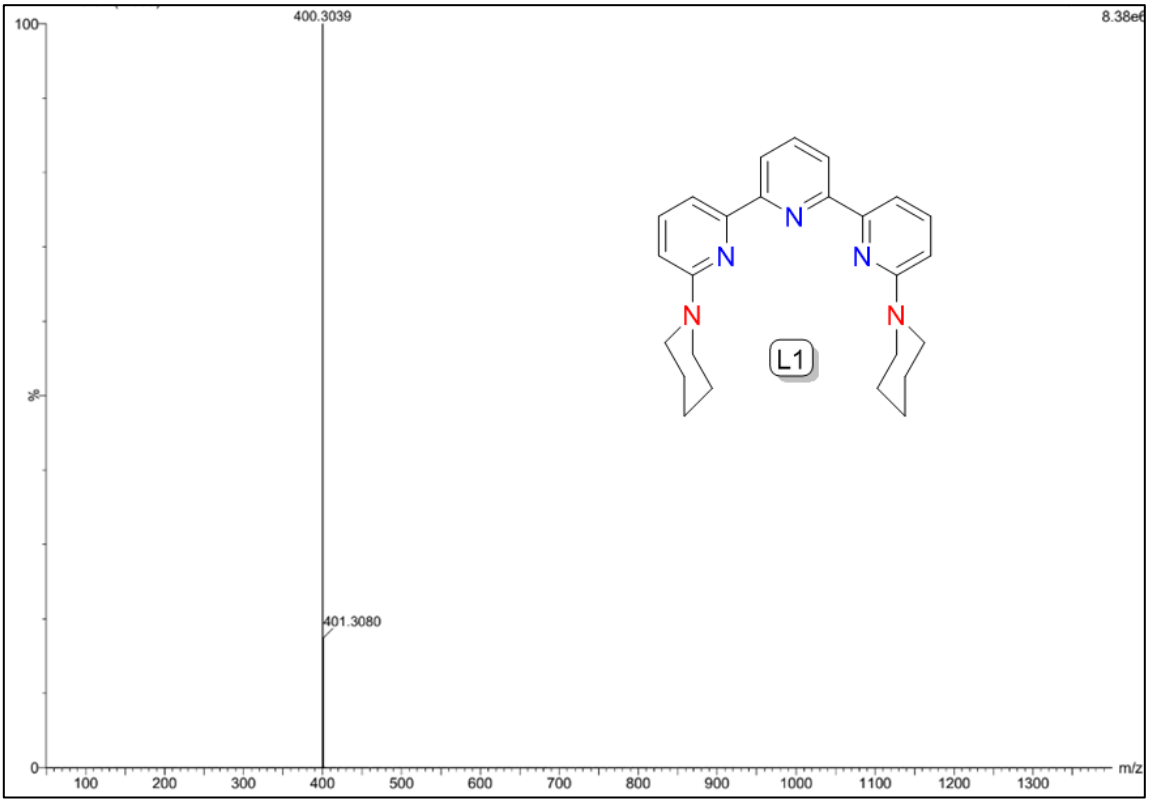


**Figure S32.** HRMS of 6,6''-di(piperidin-1-yl)-2,2':6',2''-terpyridine **L1**

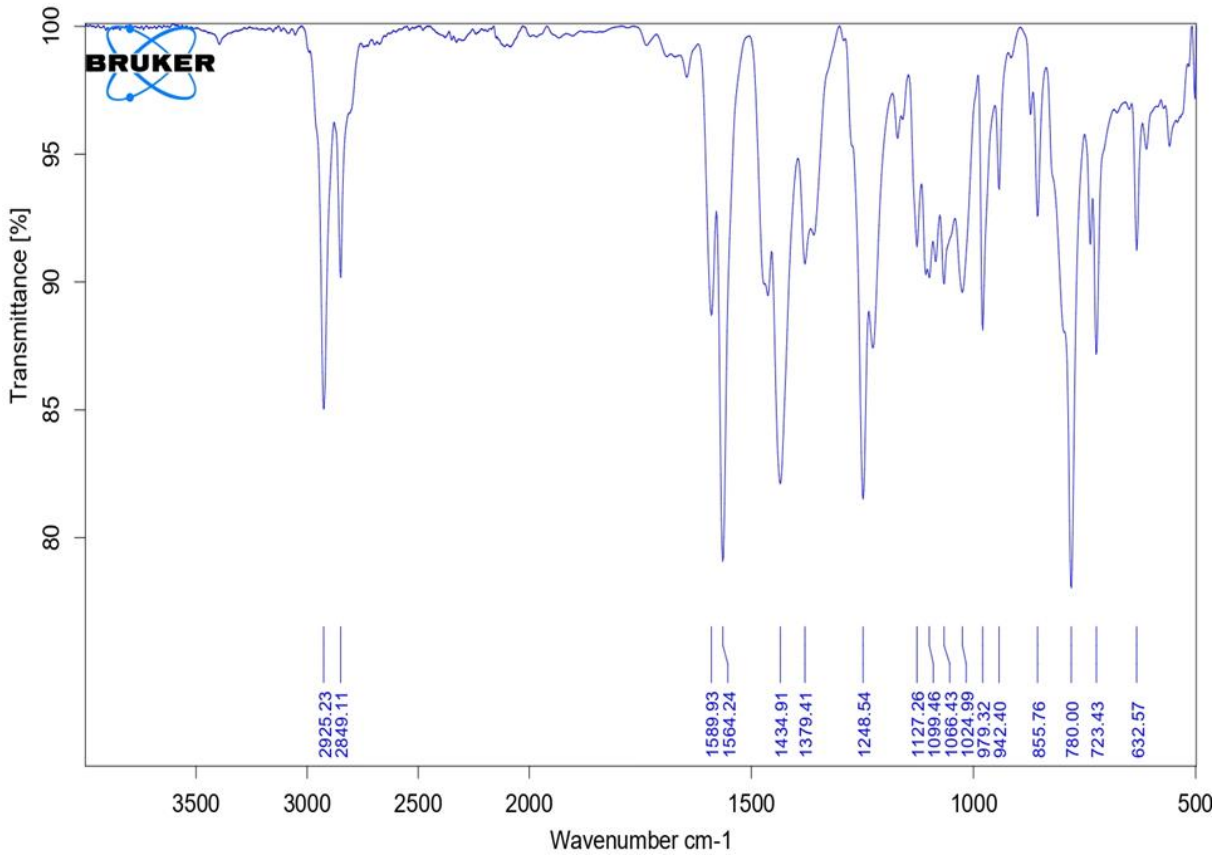


**Figure S33.** FTIR Spectrum of 6,6"-di(piperidin-1-yl)-2,2':6',2"-terpyridine **L1**

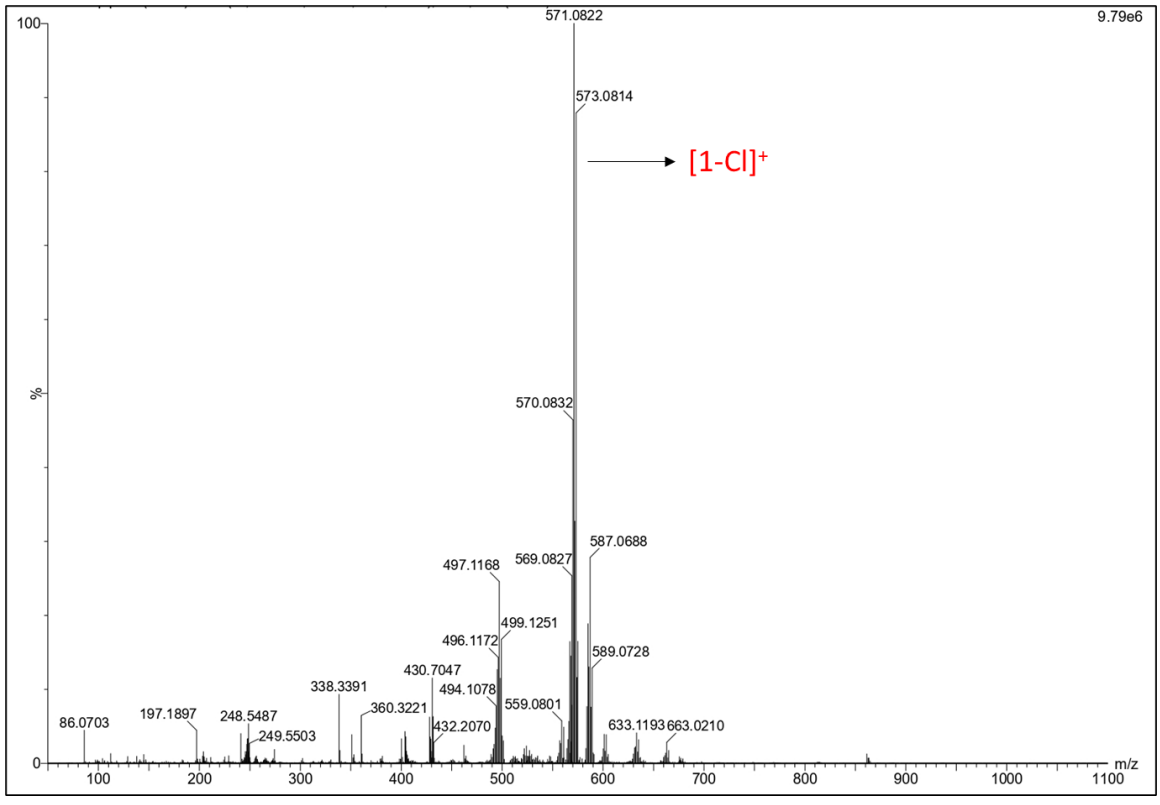


**Figure S34.** HRMS of complex **1**

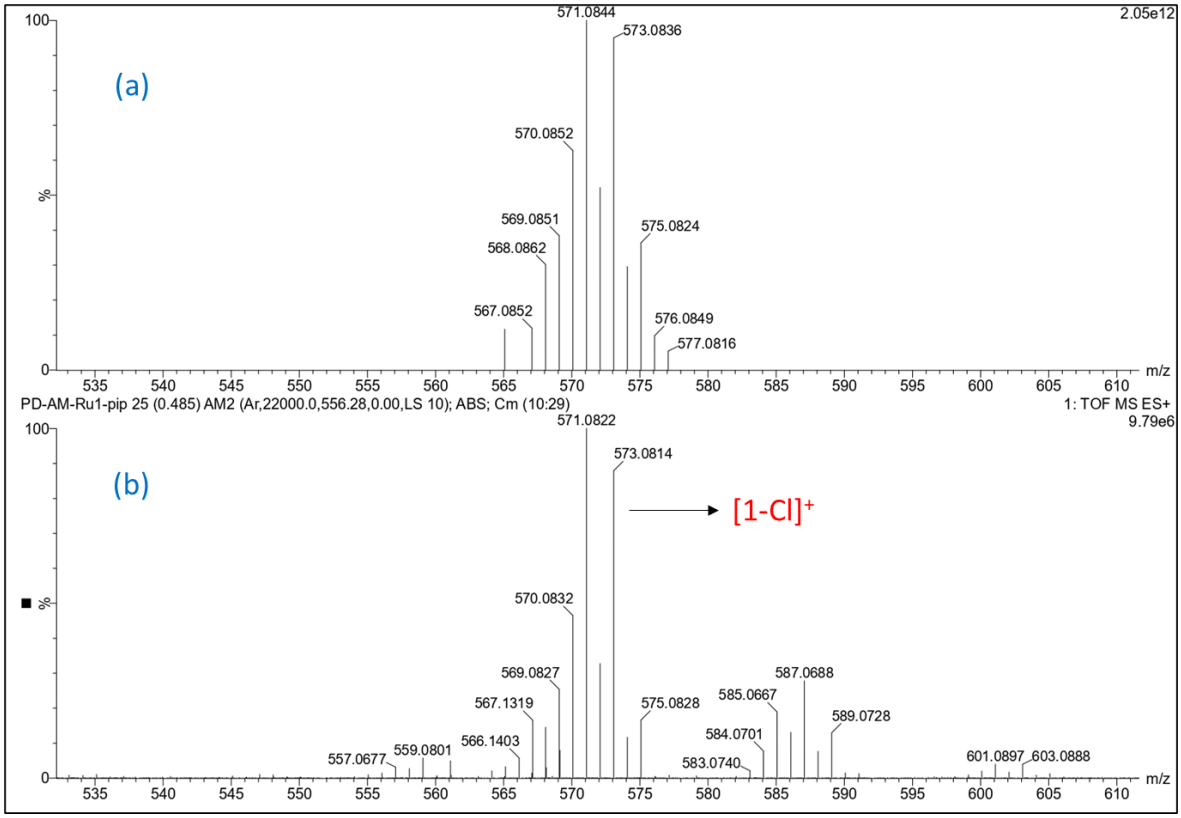


**Figure S35.** Isotopic mass distribution analysis of complex **1**. Simulated (a) and Experimental (b).

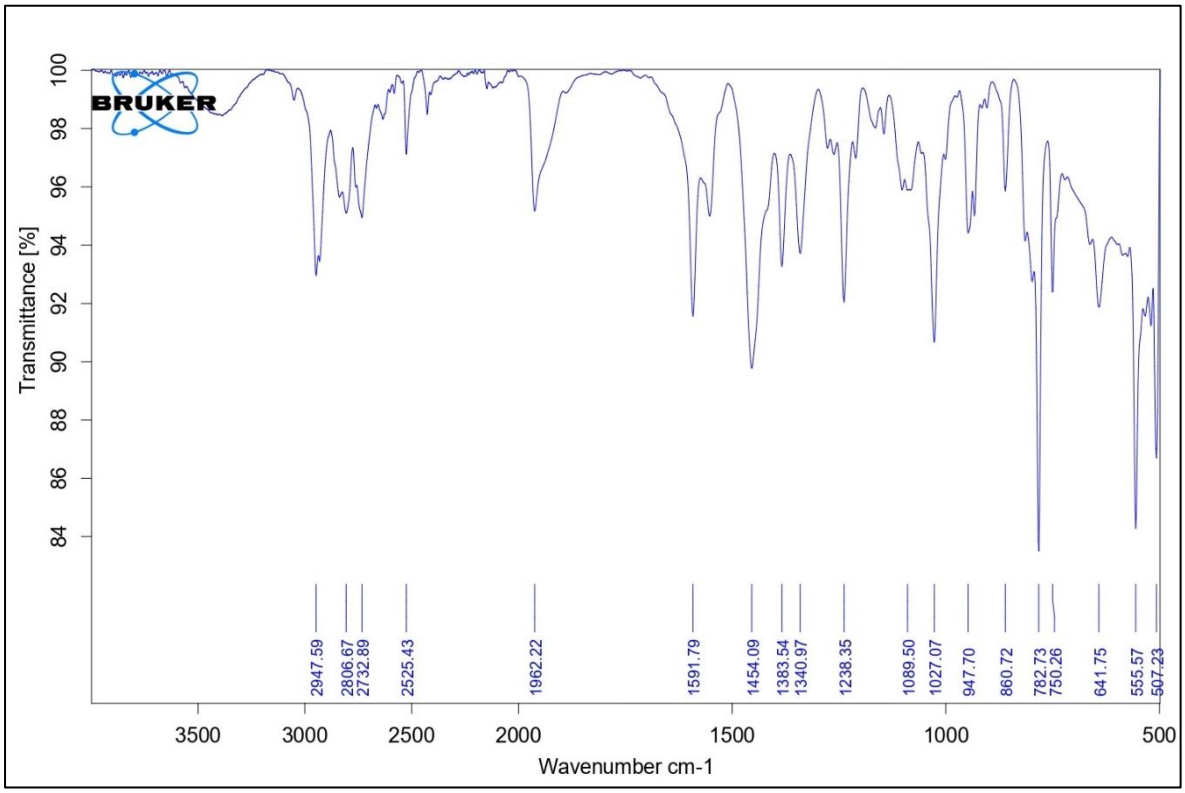


**Figure S36.** FTIR Spectrum of Complex **1**

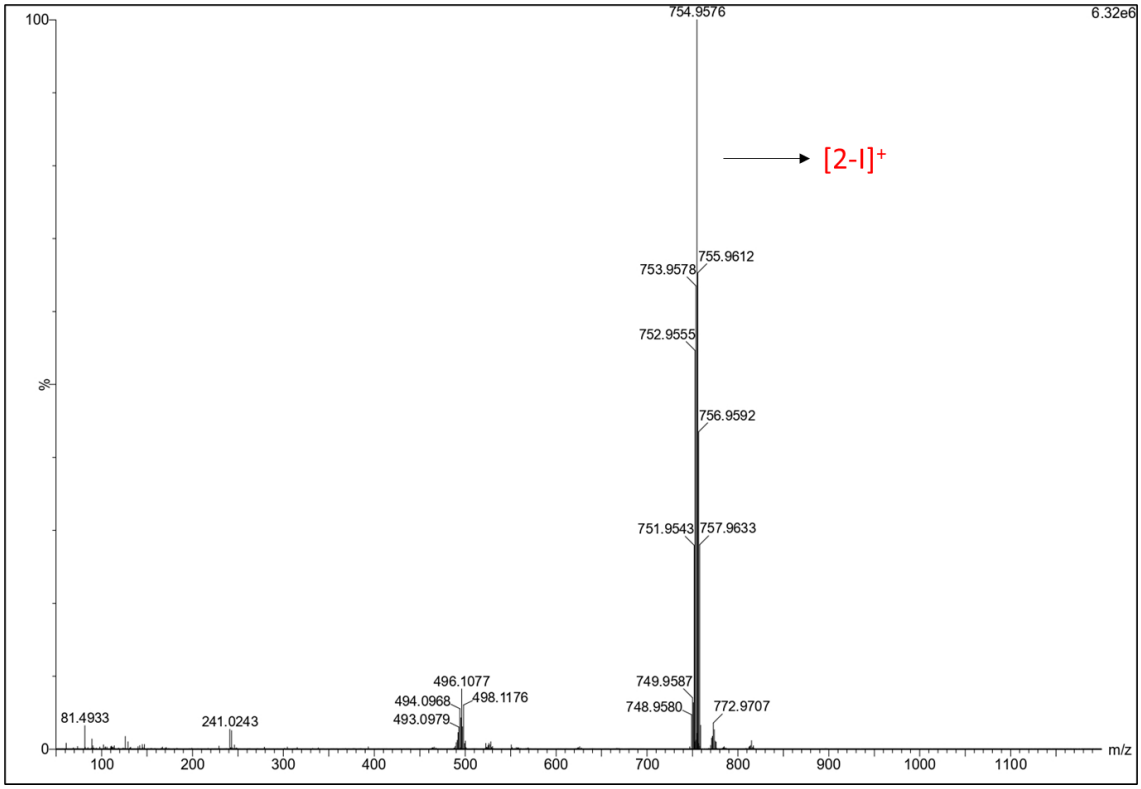


**Figure S37.** HRMS of complex **2**

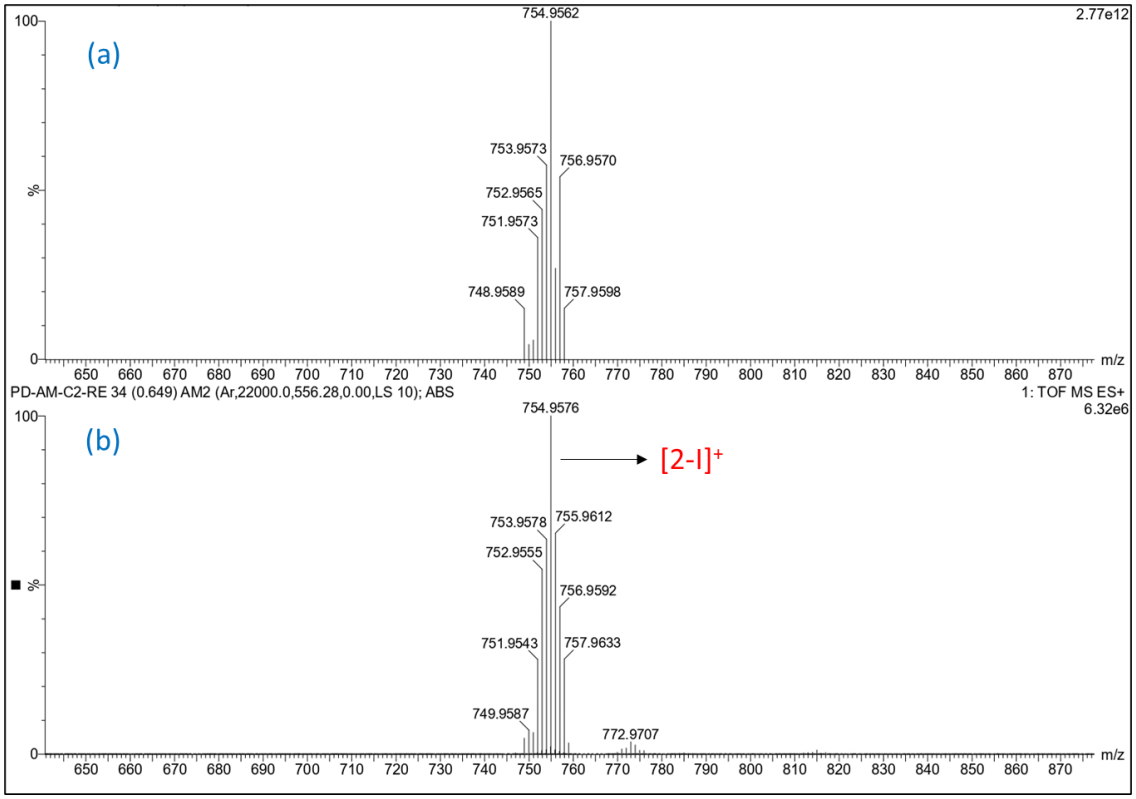


**Figure S38.** Isotopic mass distribution analysis of complex **2**. Simulated (a) and Experimental (b).

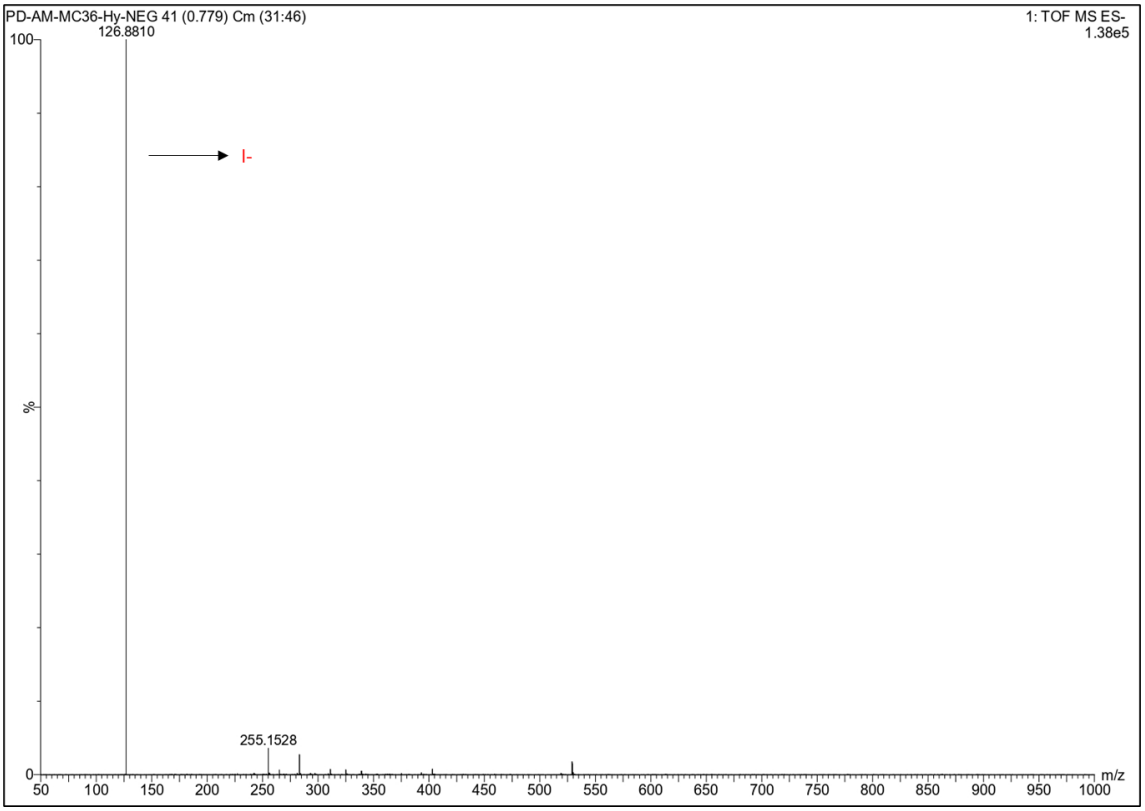


**Figure S39.** Negative range HRMS of Iodide ion of complex **2**

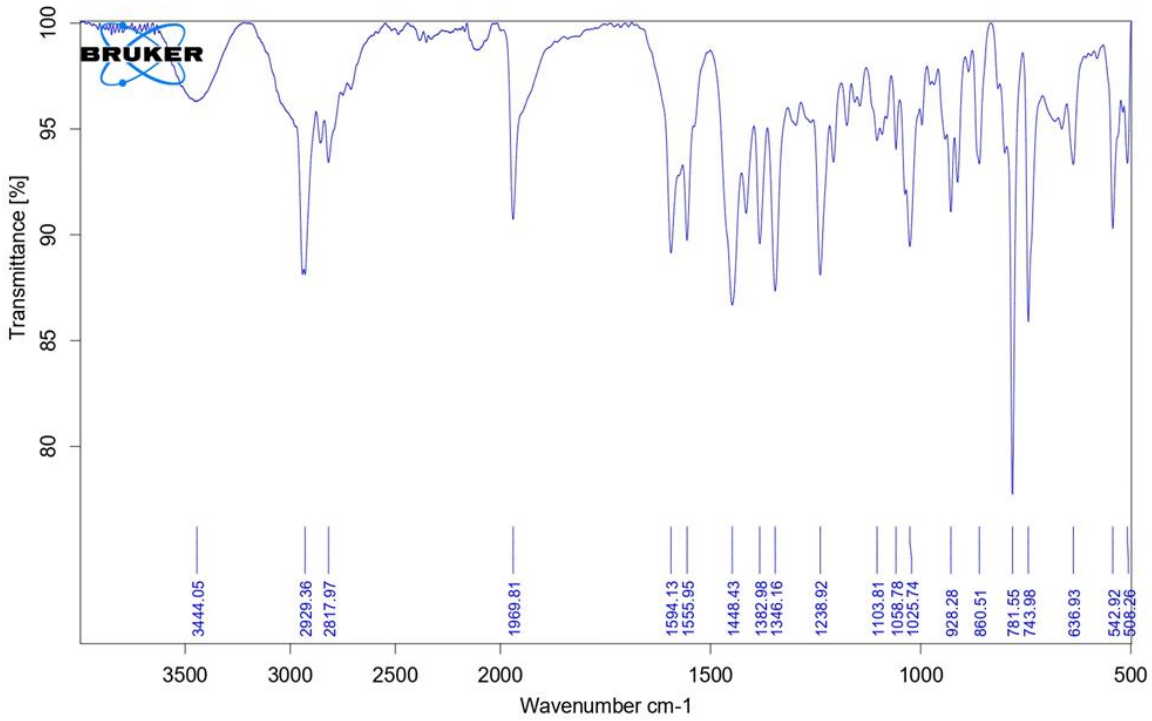


**Figure S40.** FTIR Spectrum of Complex **2**

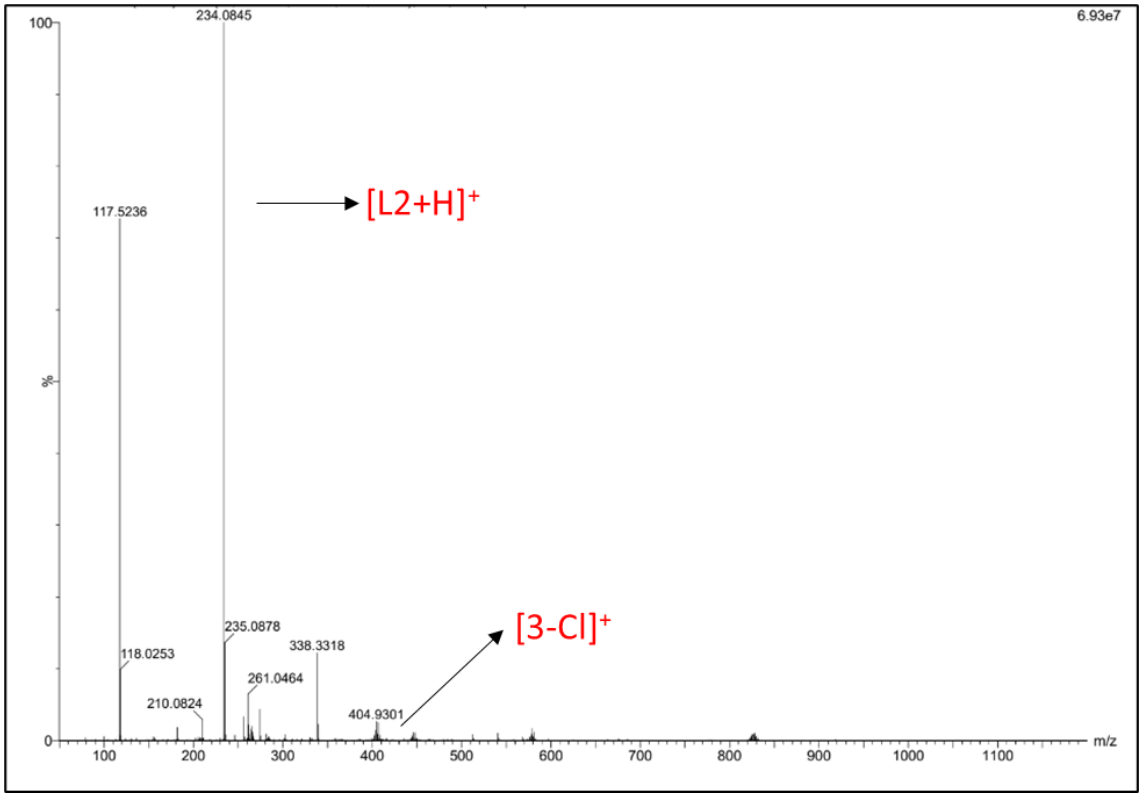


**Figure S41.** HRMS of complex **3**

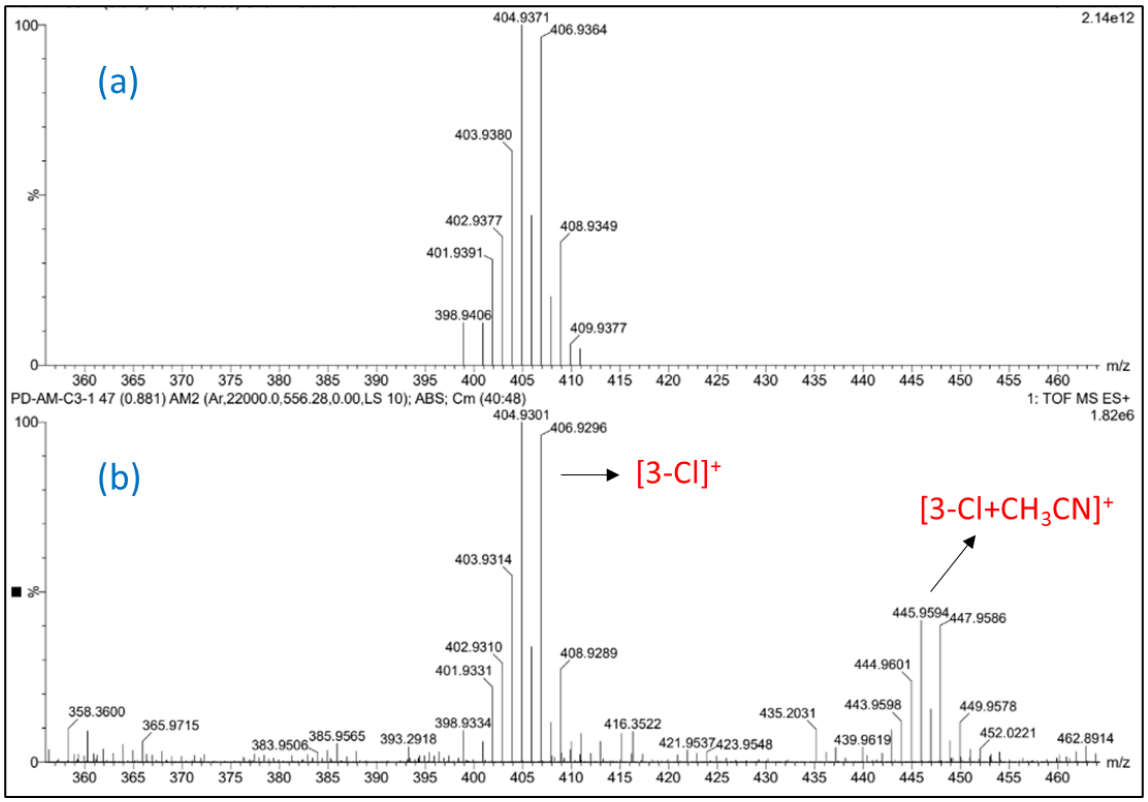


**Figure S42.** Isotopic mass distribution analysis of complex **3**. Simulated (a) and Experimental (b).

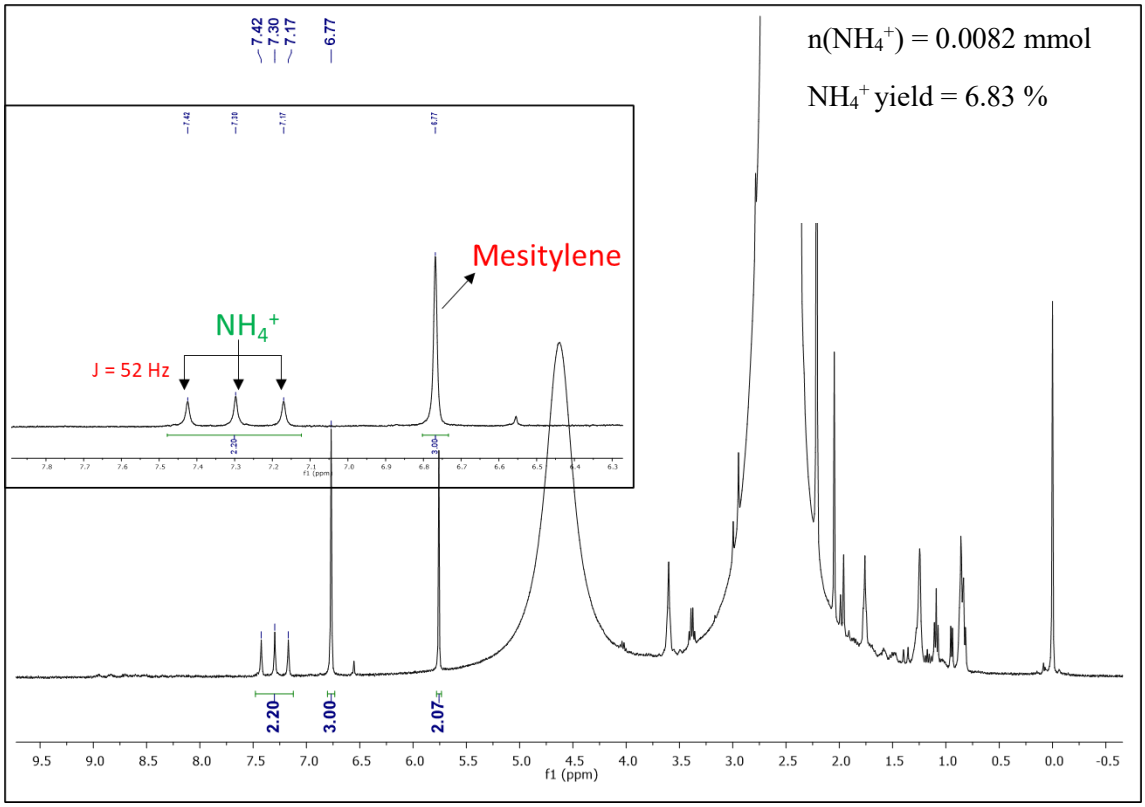


**Figure S43.** $^{1}$H NMR spectrum of Entry 1 Run1 (Table S1)

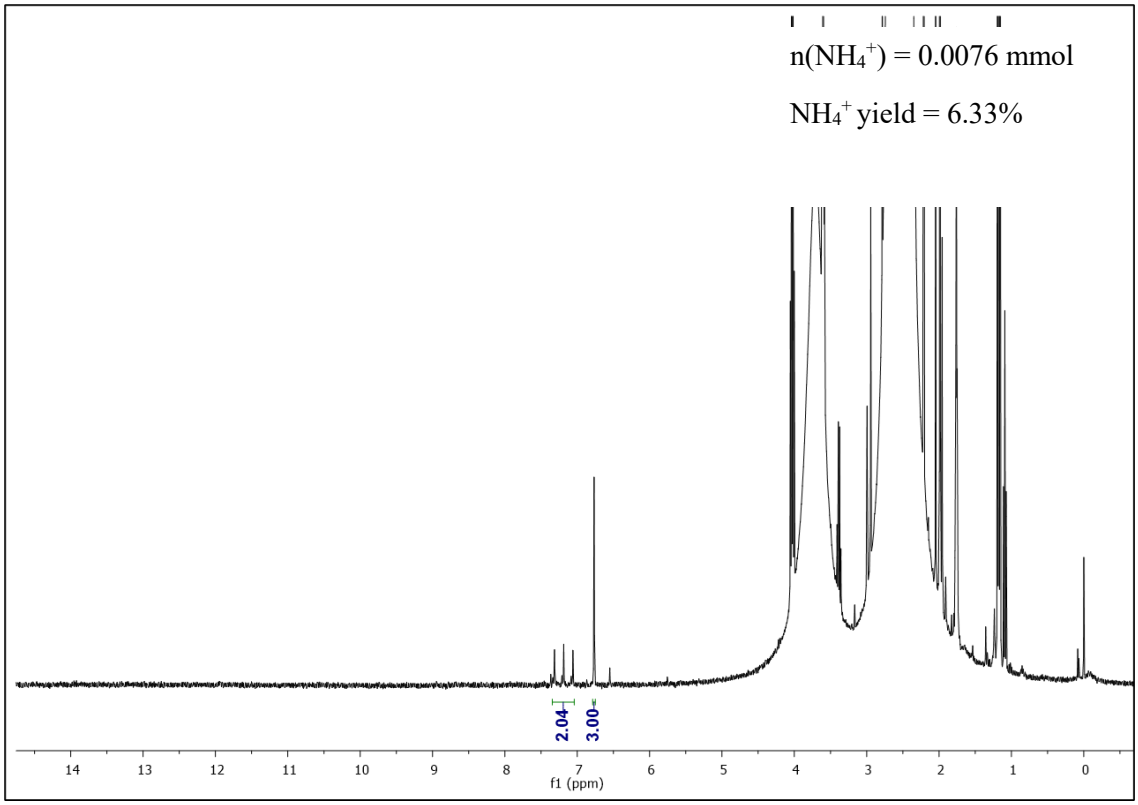


**Figure S44.** $^{1}$H NMR spectrum of Entry 1 Run2 (Table S1)

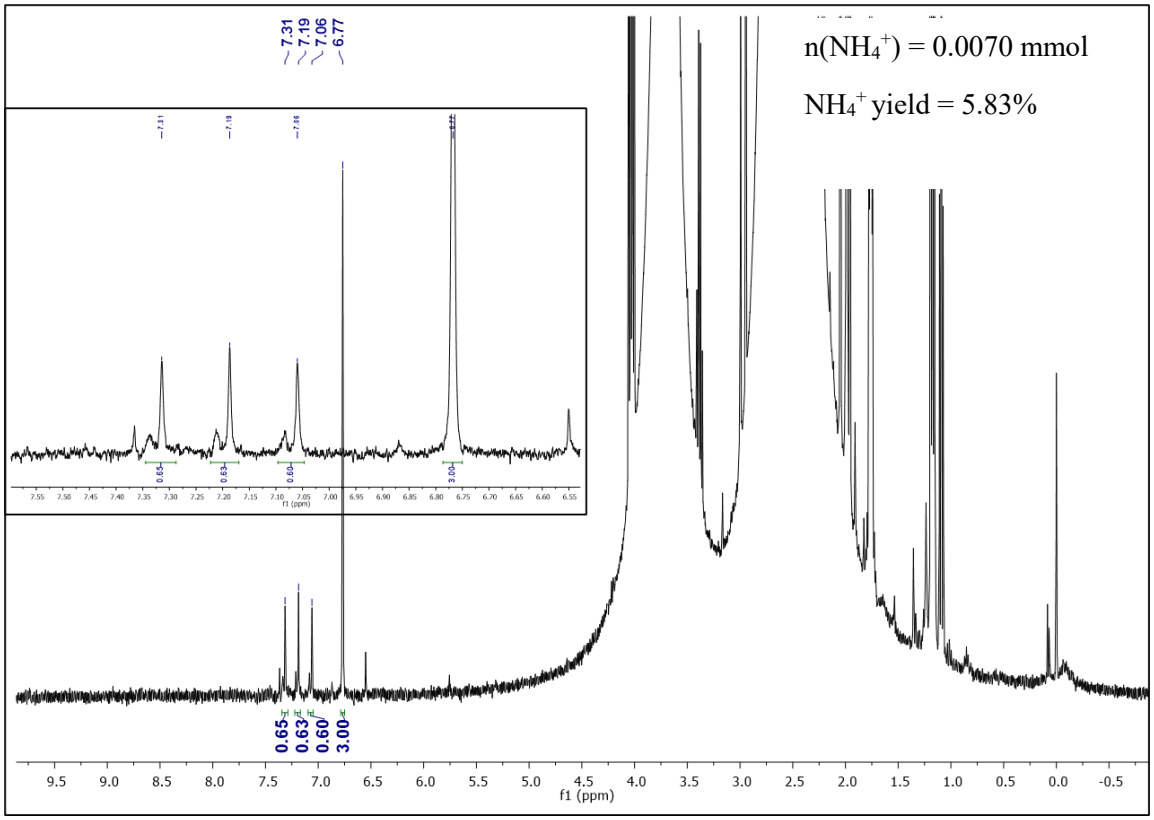


**Figure S45.** $^{1}$H NMR spectrum of Entry 2 Run1 (Table S1)

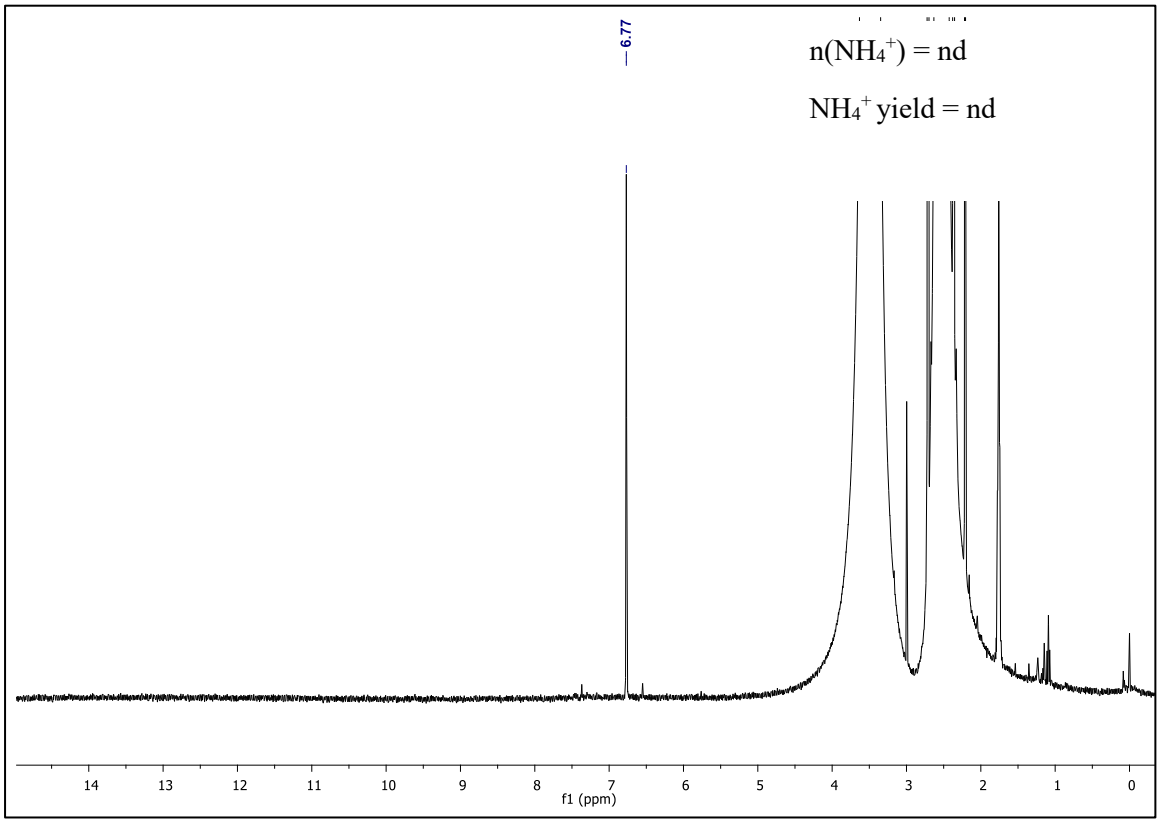


**Figure S46.** $^{1}$H NMR spectrum of Entry 3 Run1 (Table S1)

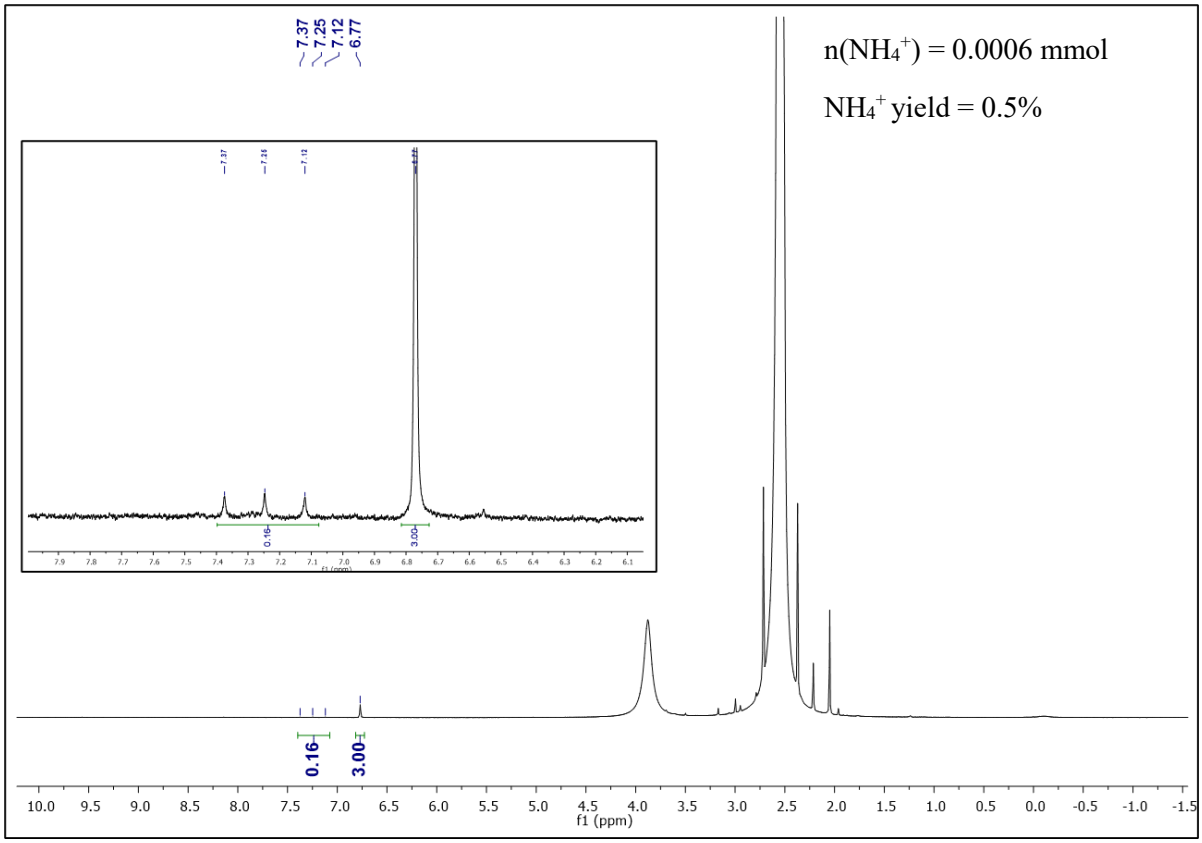


**Figure S47.** $^{1}$H NMR spectrum of Entry 3 Run2 (Table S1)

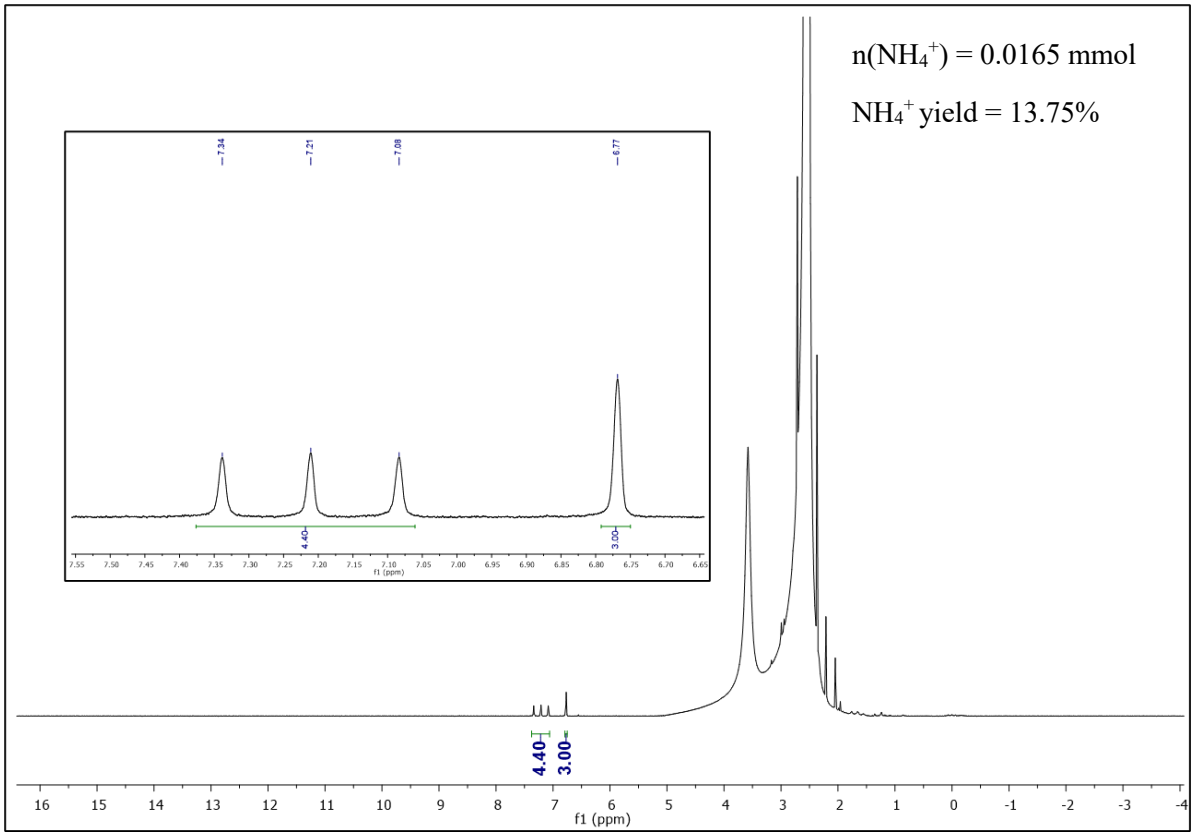


**Figure S48.** $^{1}$H NMR spectrum of Entry 4 Run1 (Table S1)

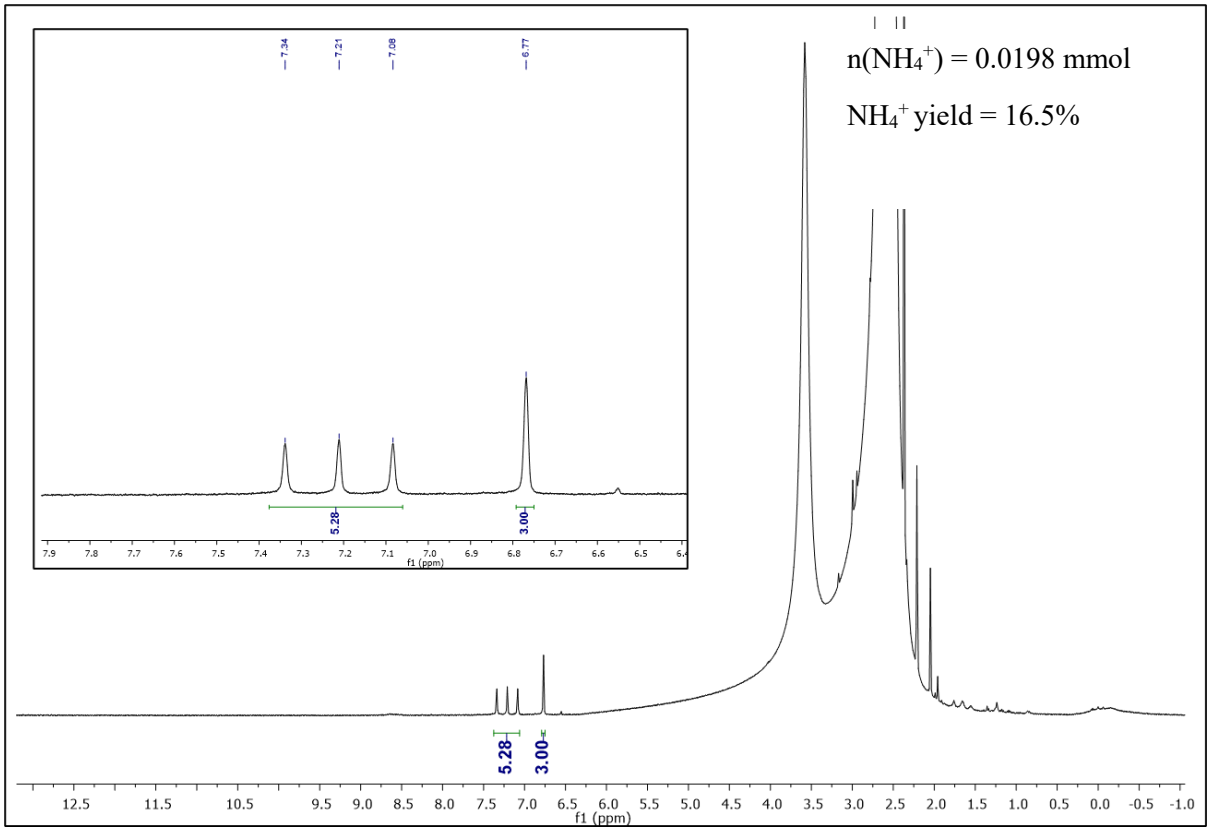


**Figure S49.** $^{1}$H NMR spectrum of Entry 4 Run 2 (Table S1)

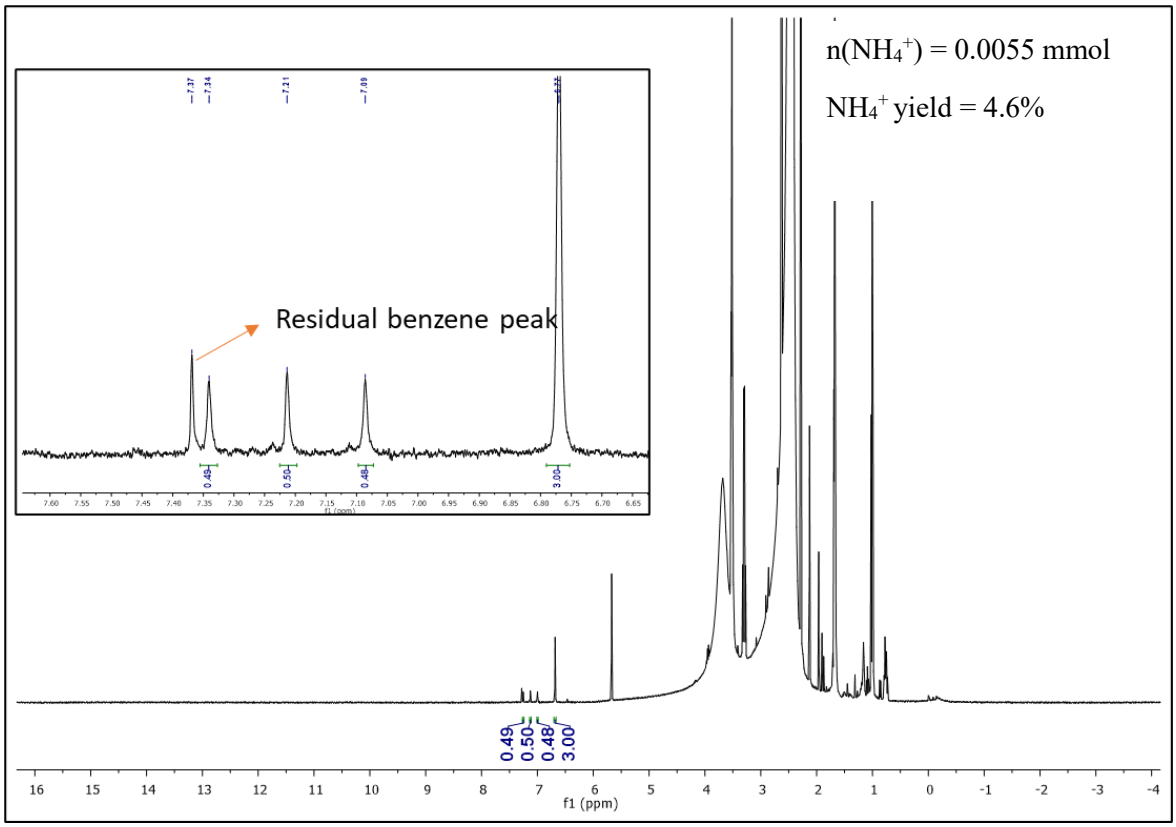


**Figure S50.** $^{1}$H NMR spectrum of Entry 5 (Table S1)

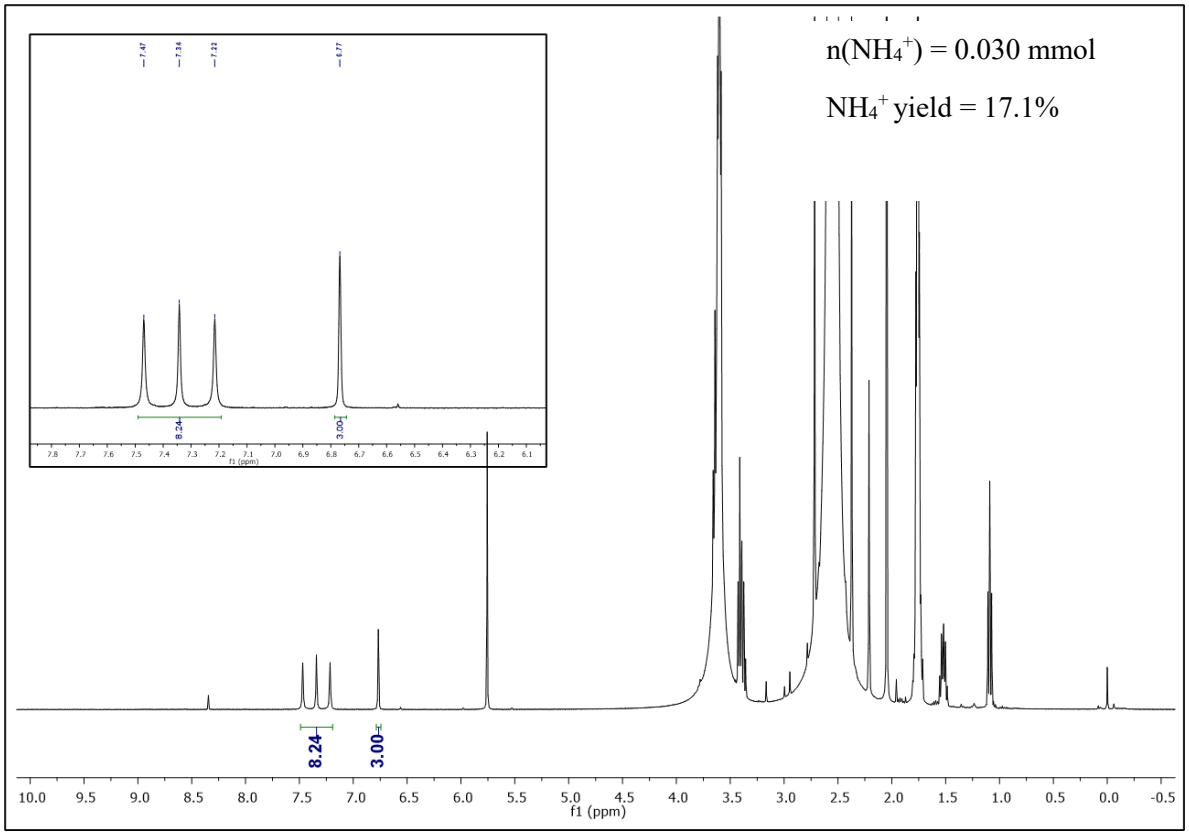


**Figure S51.** $^{1}$H NMR spectrum of Entry 1 (Table S2)

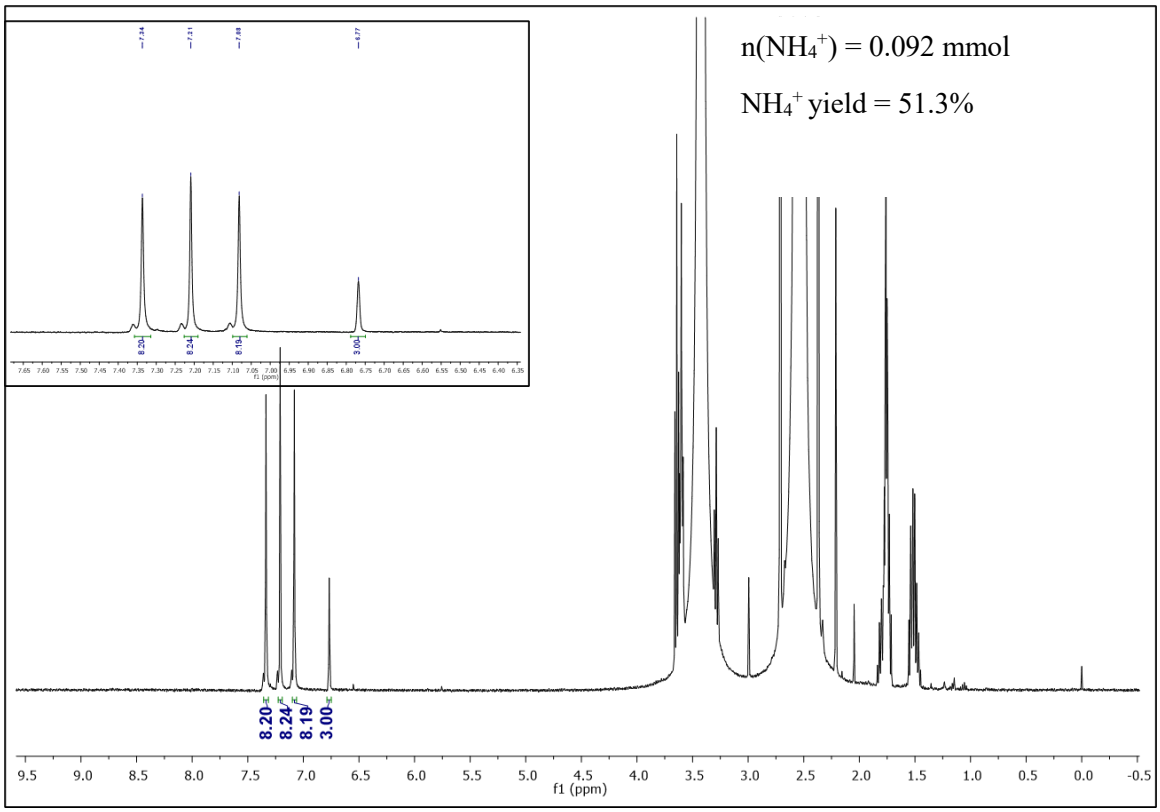


**Figure S52.** $^{1}$H NMR spectrum of Entry 2 Run 1 (Table S2)

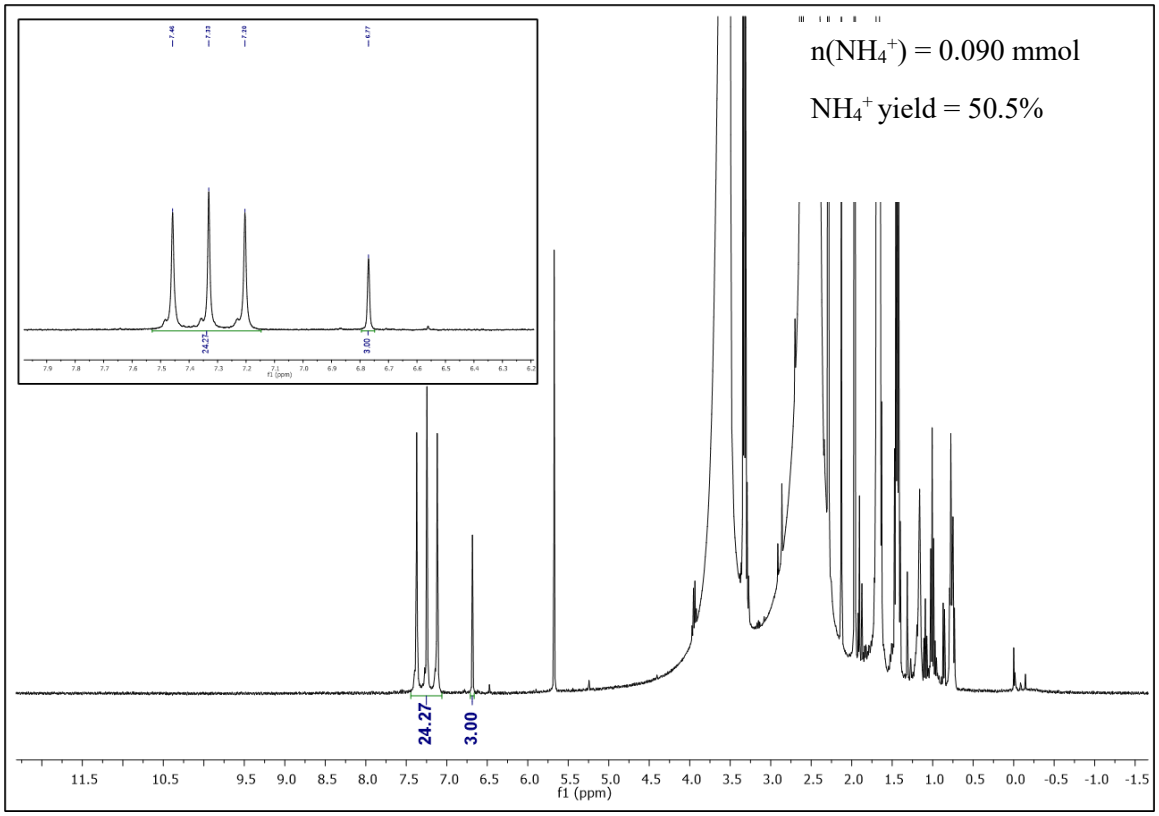


**Figure S53.** $^{1}$H NMR spectrum of Entry 2 Run 2 (Table S2)

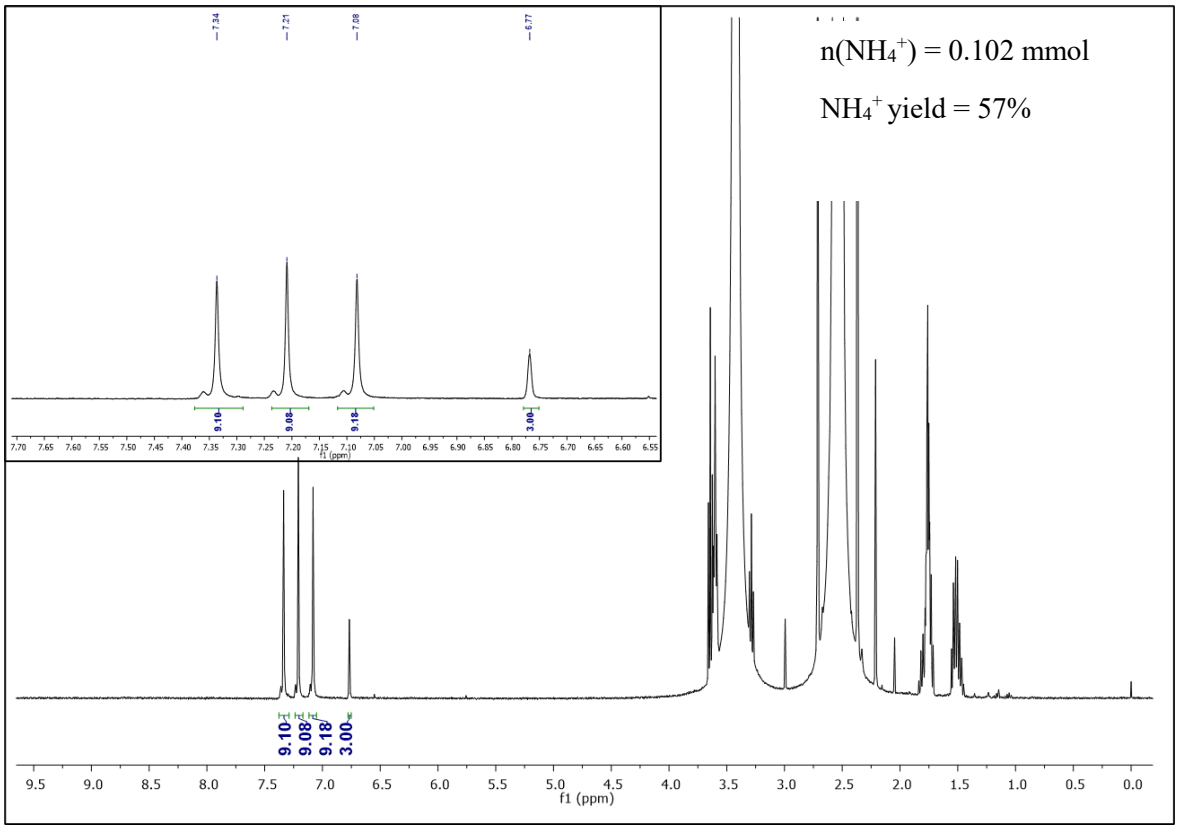


**Figure S54.** $^{1}$H NMR spectrum of Entry 3 (Table S2)

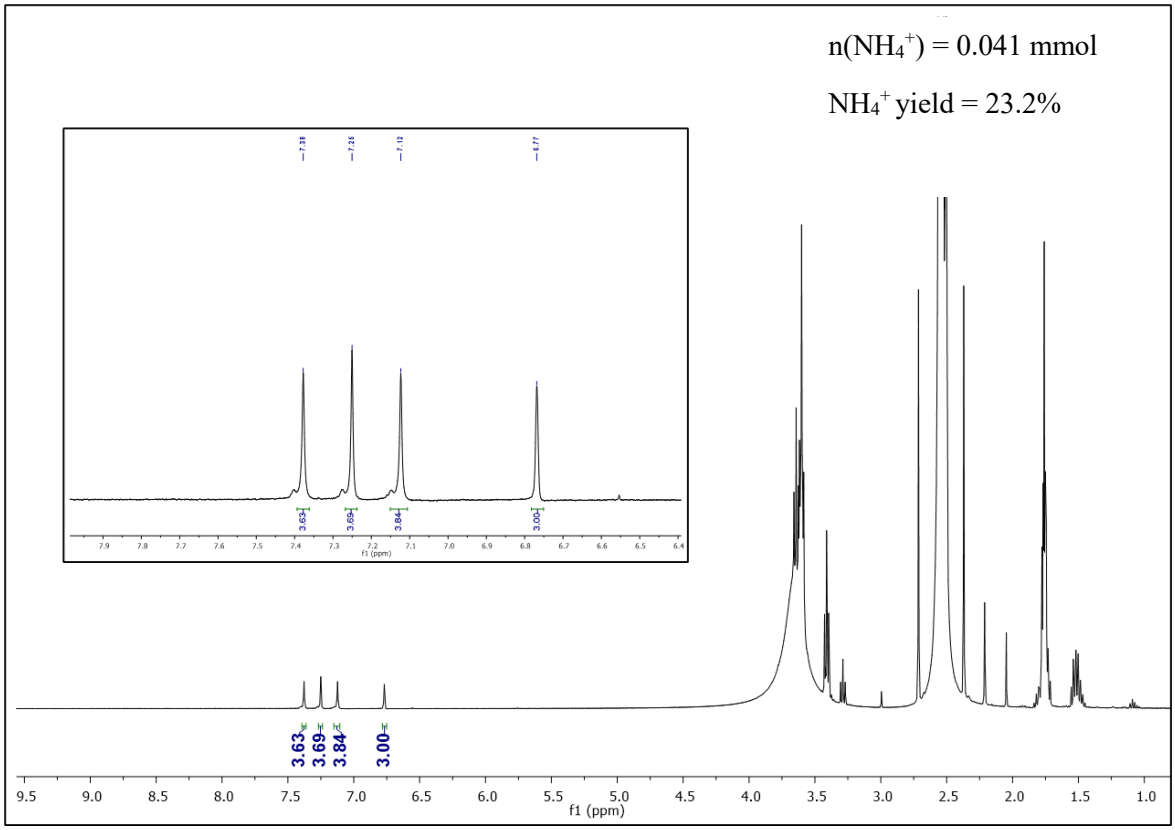


**Figure S55.** $^{1}$H NMR spectrum of Entry4 Run1(Table S2)

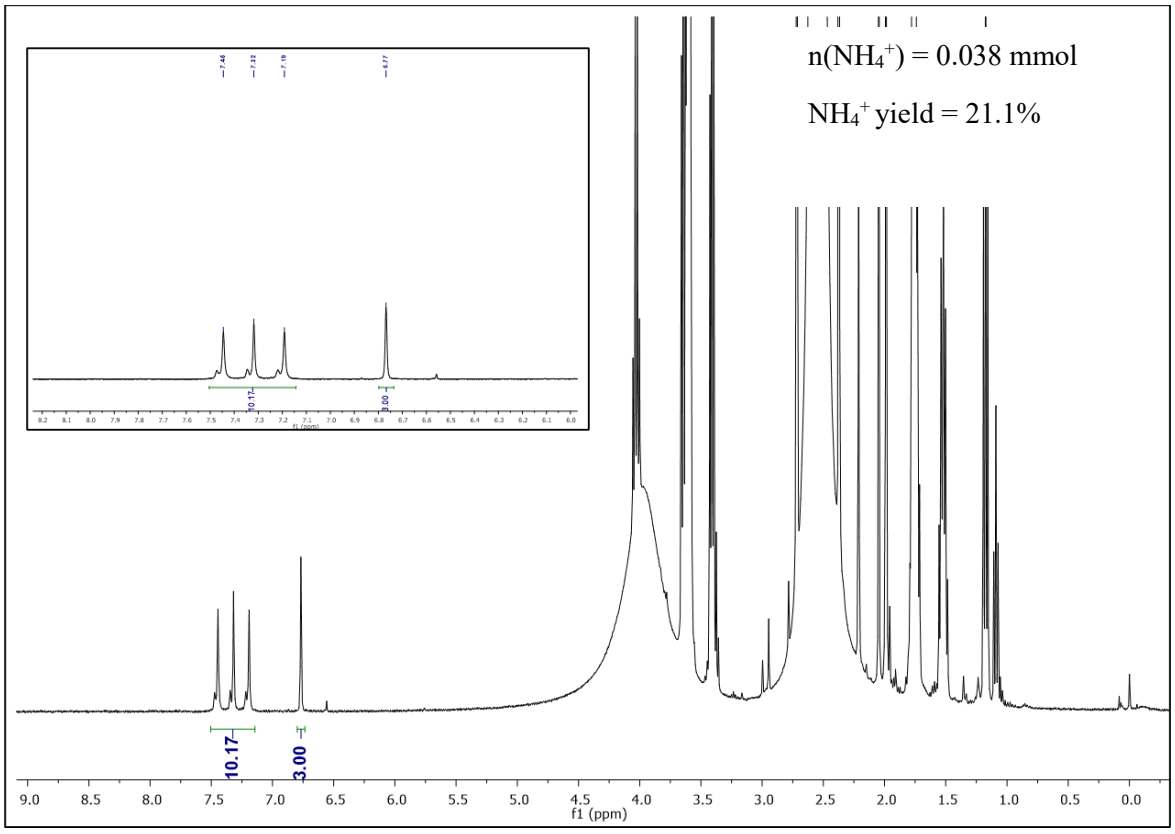


**Figure S56.** $^{1}$H NMR spectrum of Entry 4 Run 2 (Table S2)

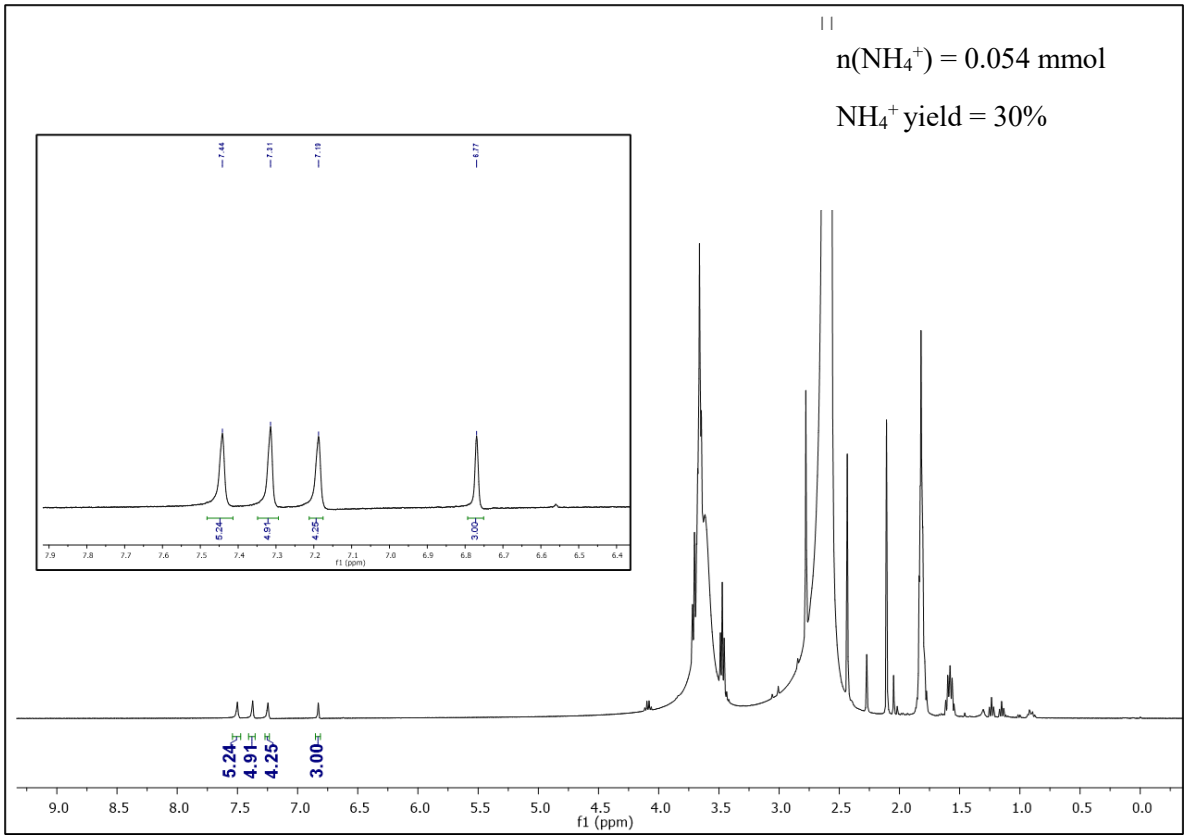


**Figure S57.** $^{1}$H NMR spectrum of Entry 5 Run 1 (Table S2)

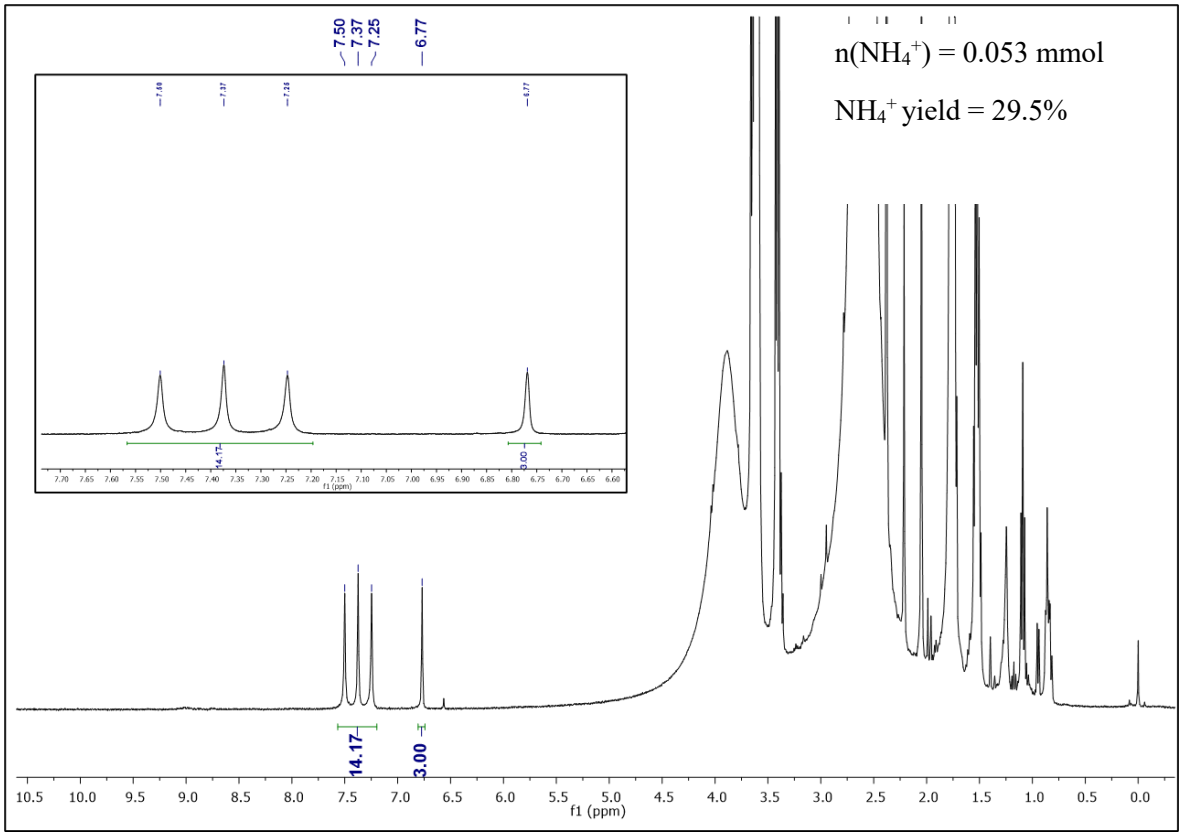


**Figure S58.** $^{1}$H NMR spectrum of Entry 5 Run 2 (Table S2)

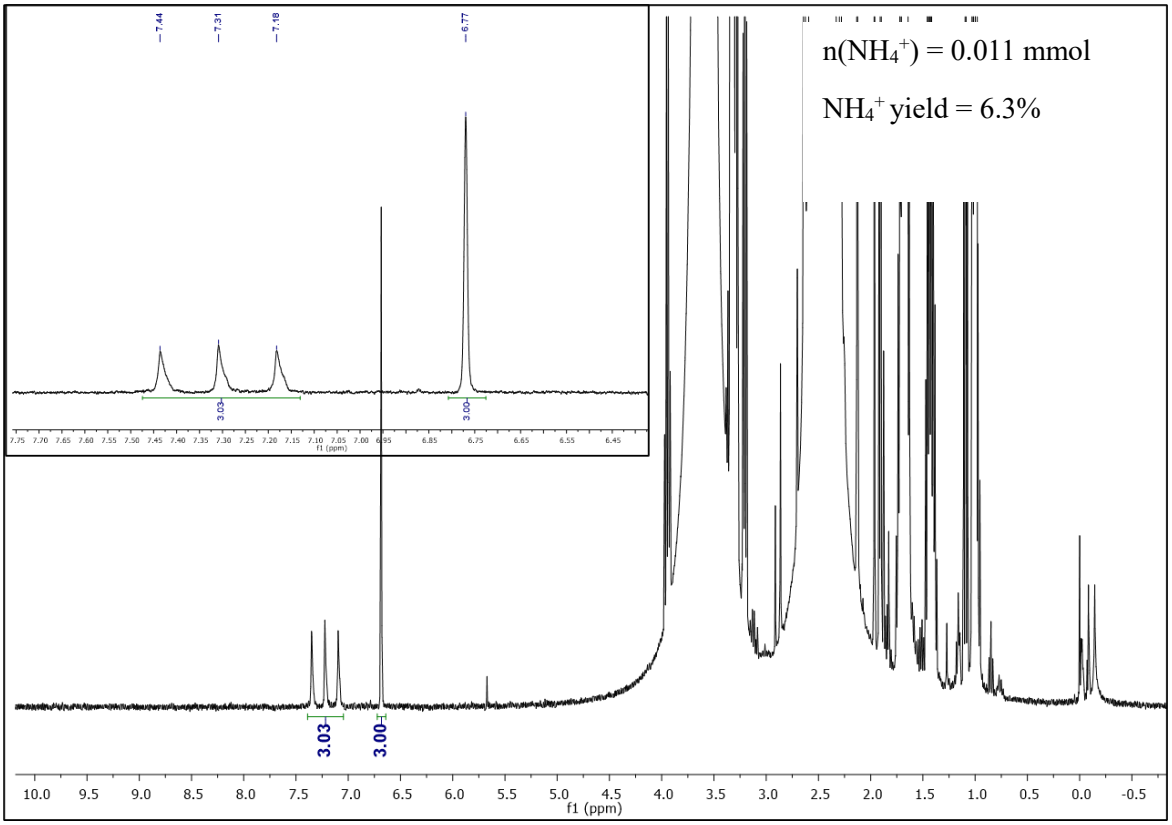


**Figure S59.** $^{1}$H NMR spectrum of Entry 6 Run 1 (Table S2)

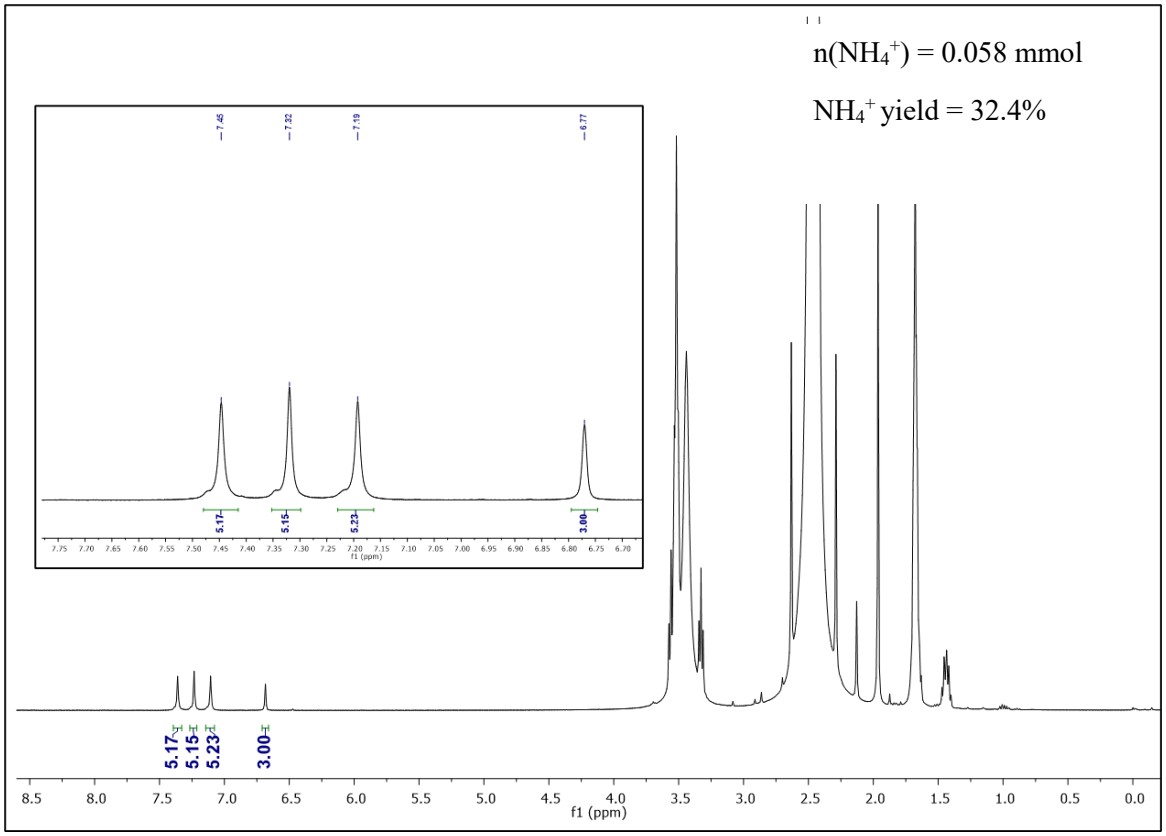


**Figure S60.** $^{1}$H NMR spectrum of Entry 7 Run 1 (Table S2)

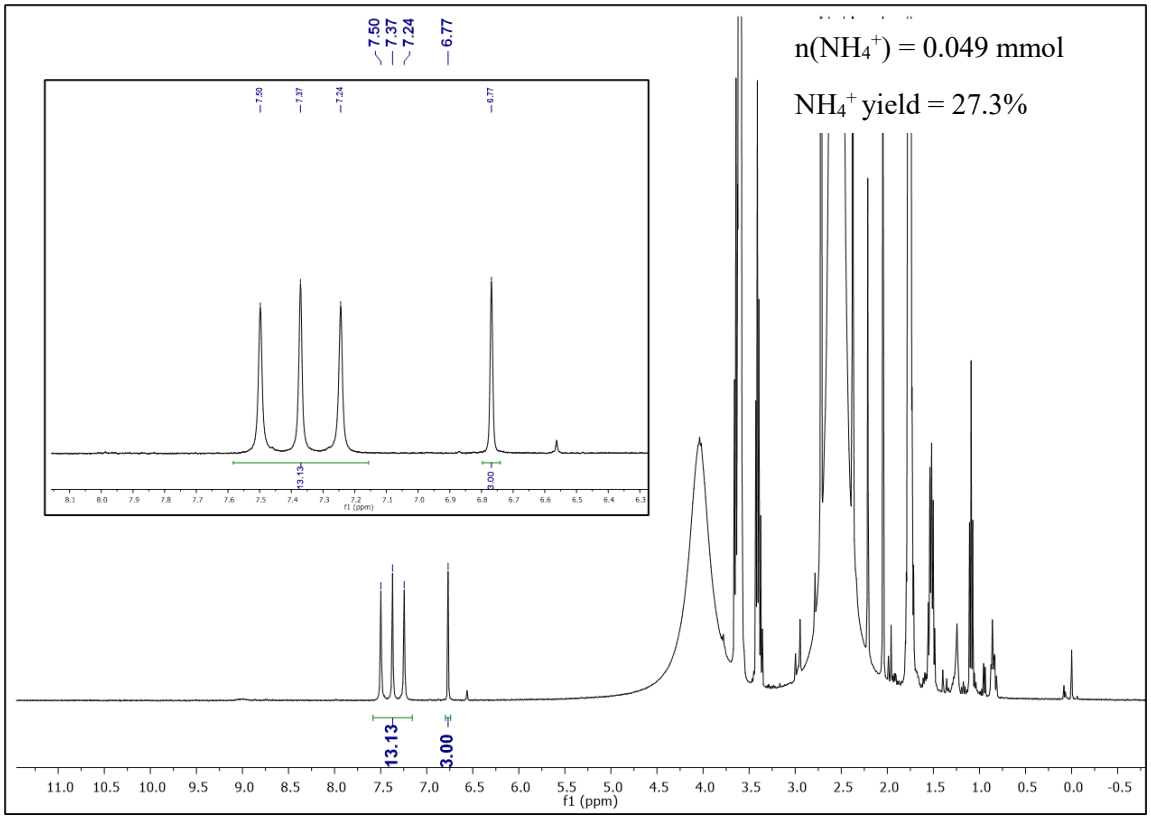


**Figure S61.** $^{1}$H NMR spectrum of Entry 7 Run 2 (Table S2)

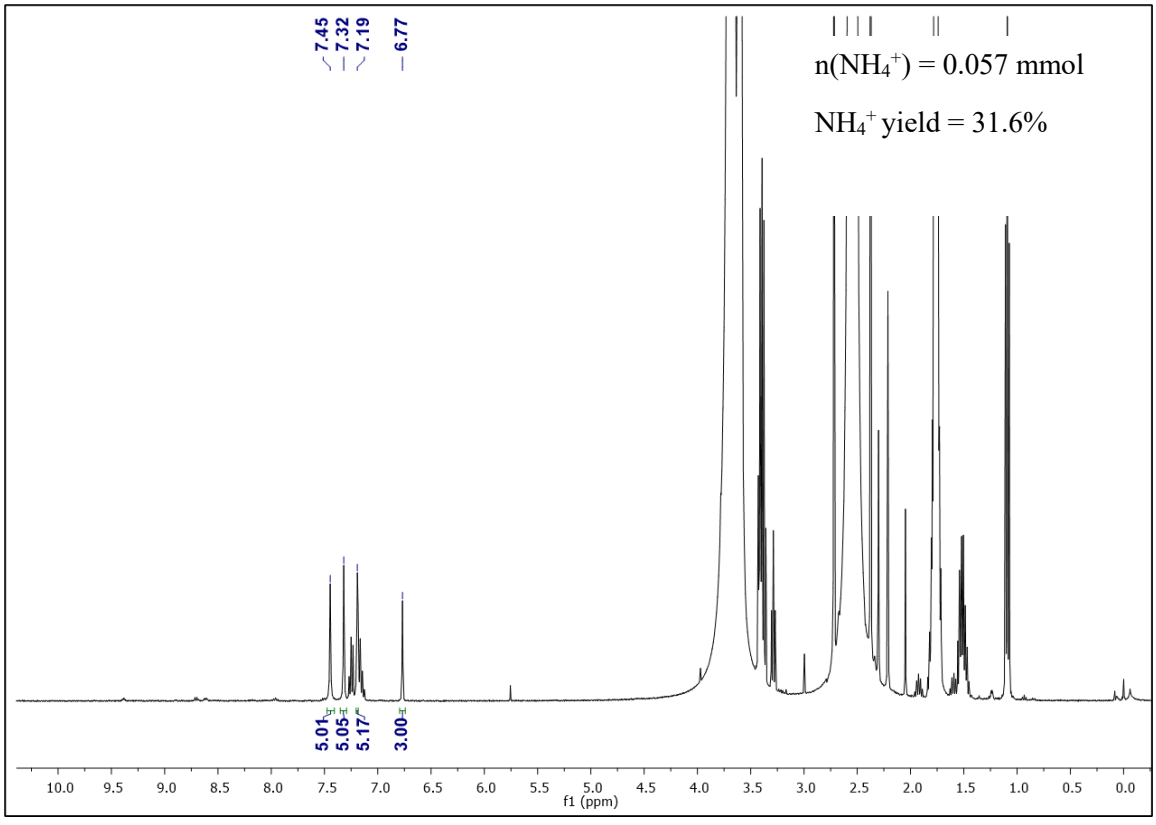


**Figure S62.** $^{1}$H NMR spectrum of Entry 8 Run 1 (Table S2)

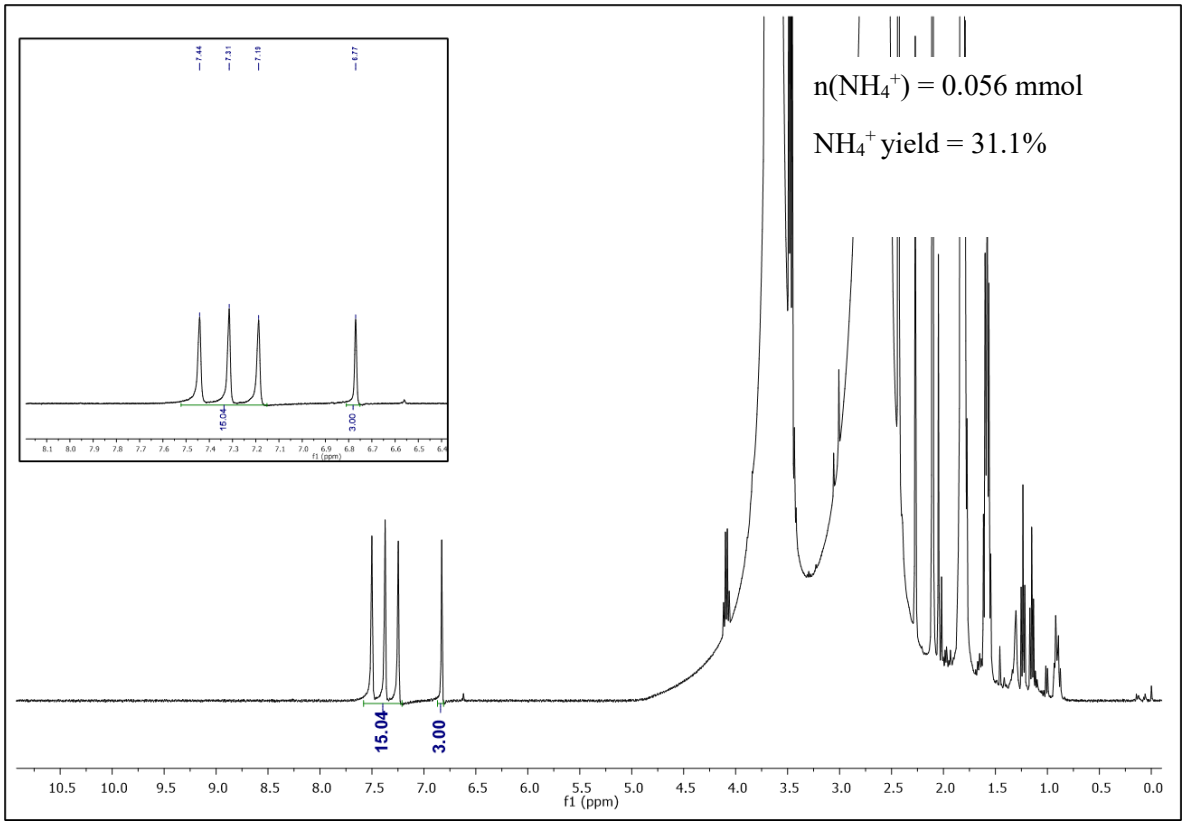


**Figure S63.** $^{1}$H NMR spectrum of Entry 8 Run 2(Table S2)

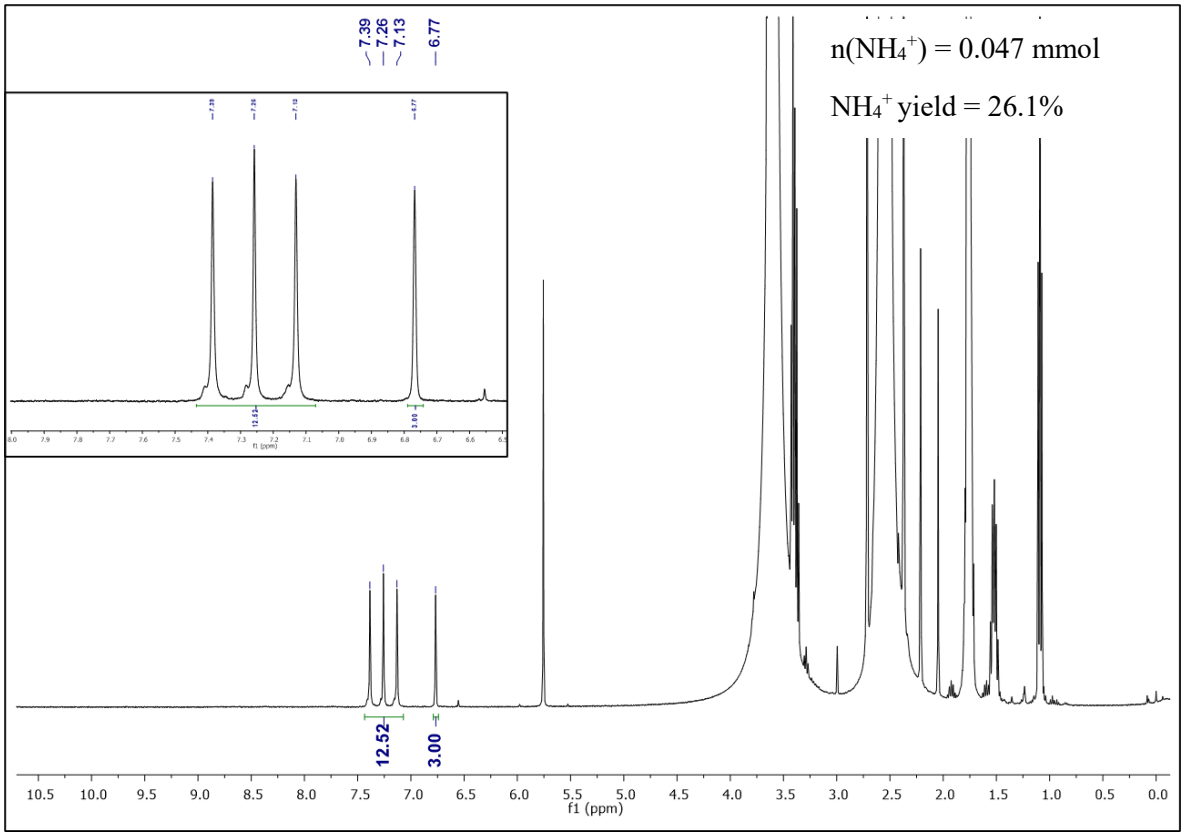


**Figure S64.** $^{1}$H NMR spectrum of Entry 9 Run 1(Table S2)

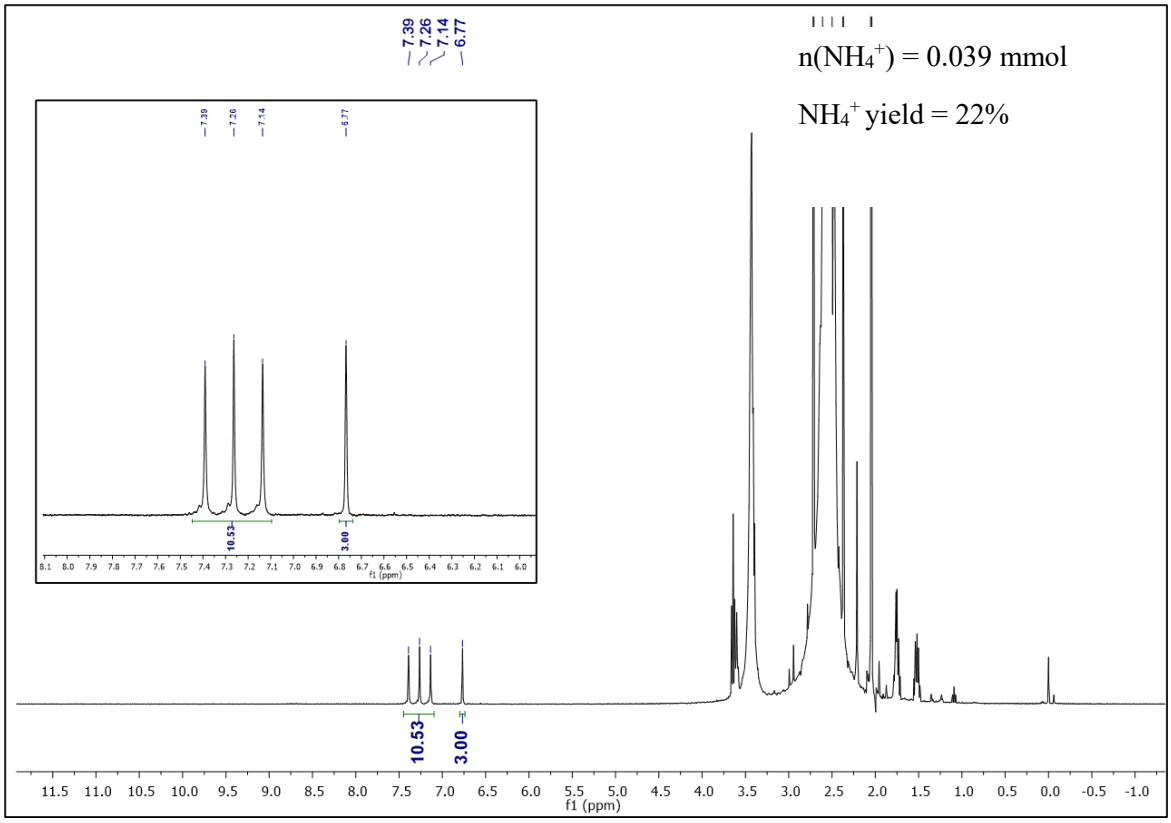


**Figure S65.** $^{1}$H NMR spectrum of Entry 9 Run 2 (Table S2)

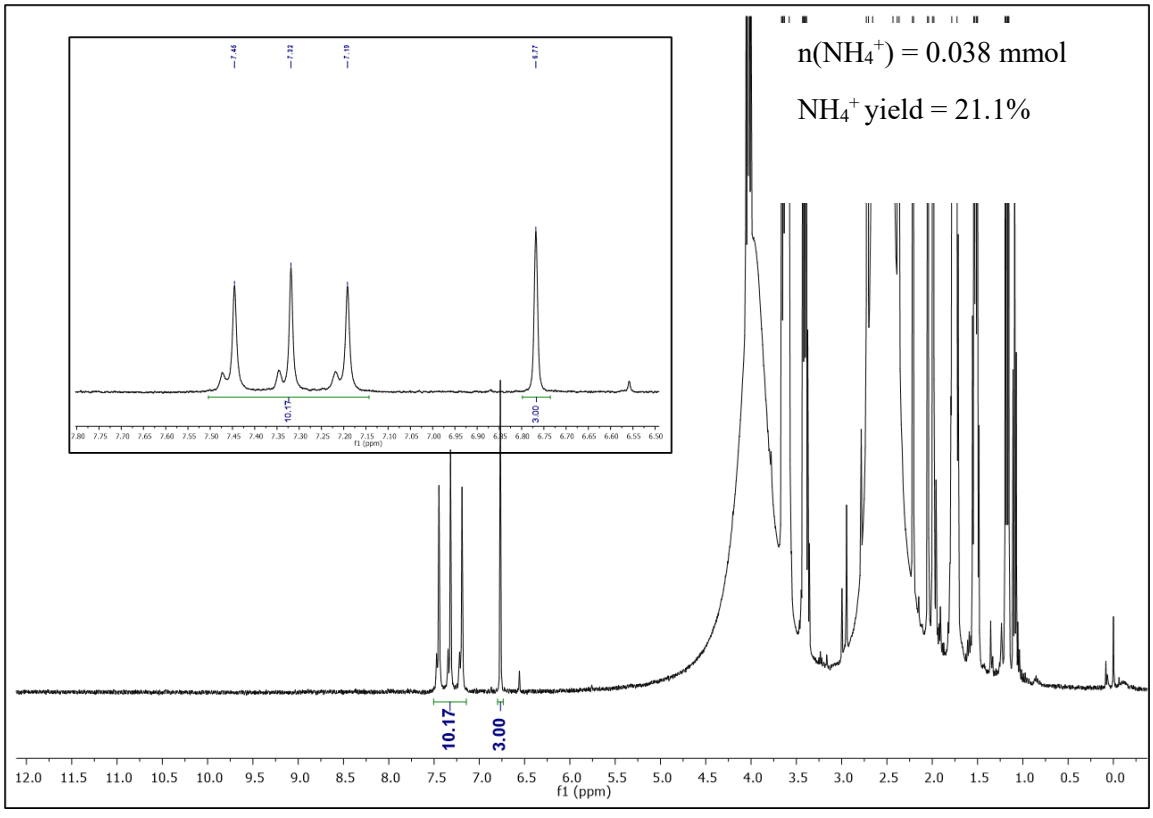


**Figure S66.** $^{1}$H NMR spectrum of Entry 10 Run 1 (Table S2)

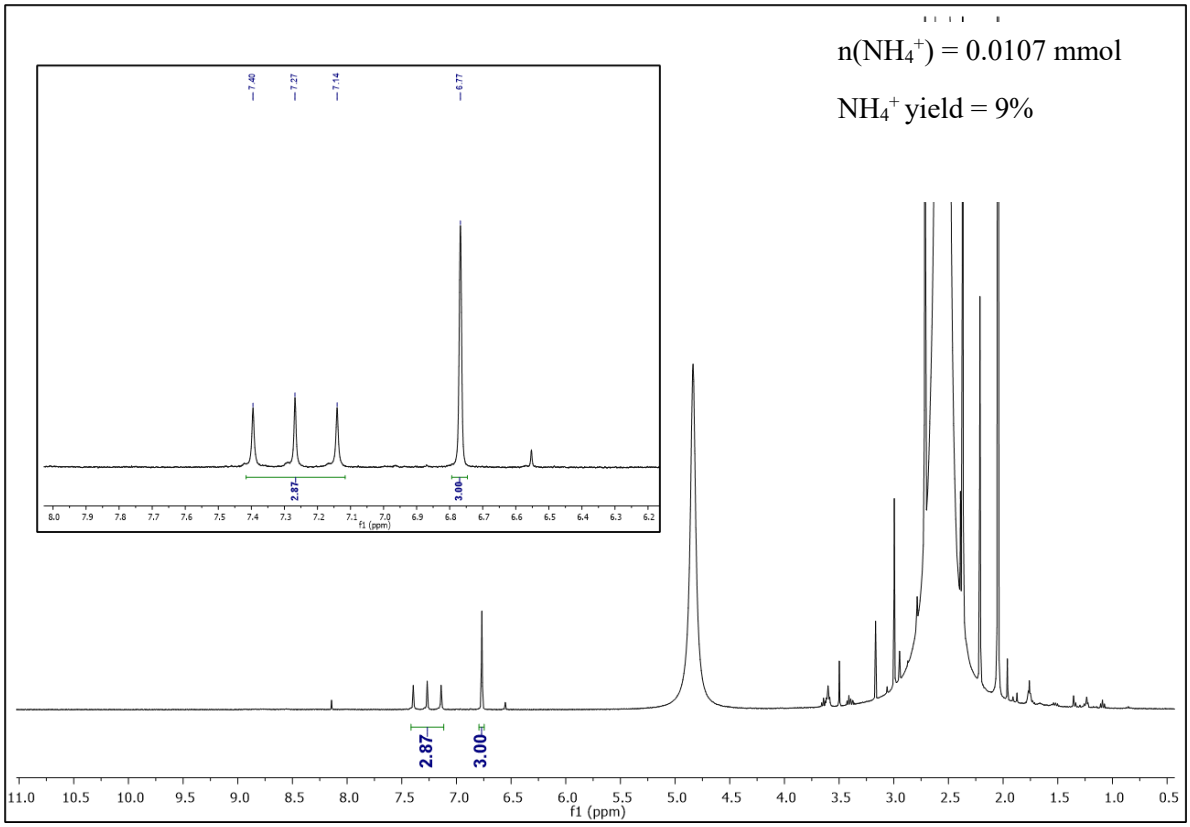


**Figure S67.** $^{1}$H NMR spectrum of Entry 11 Run 1 (Table S2)

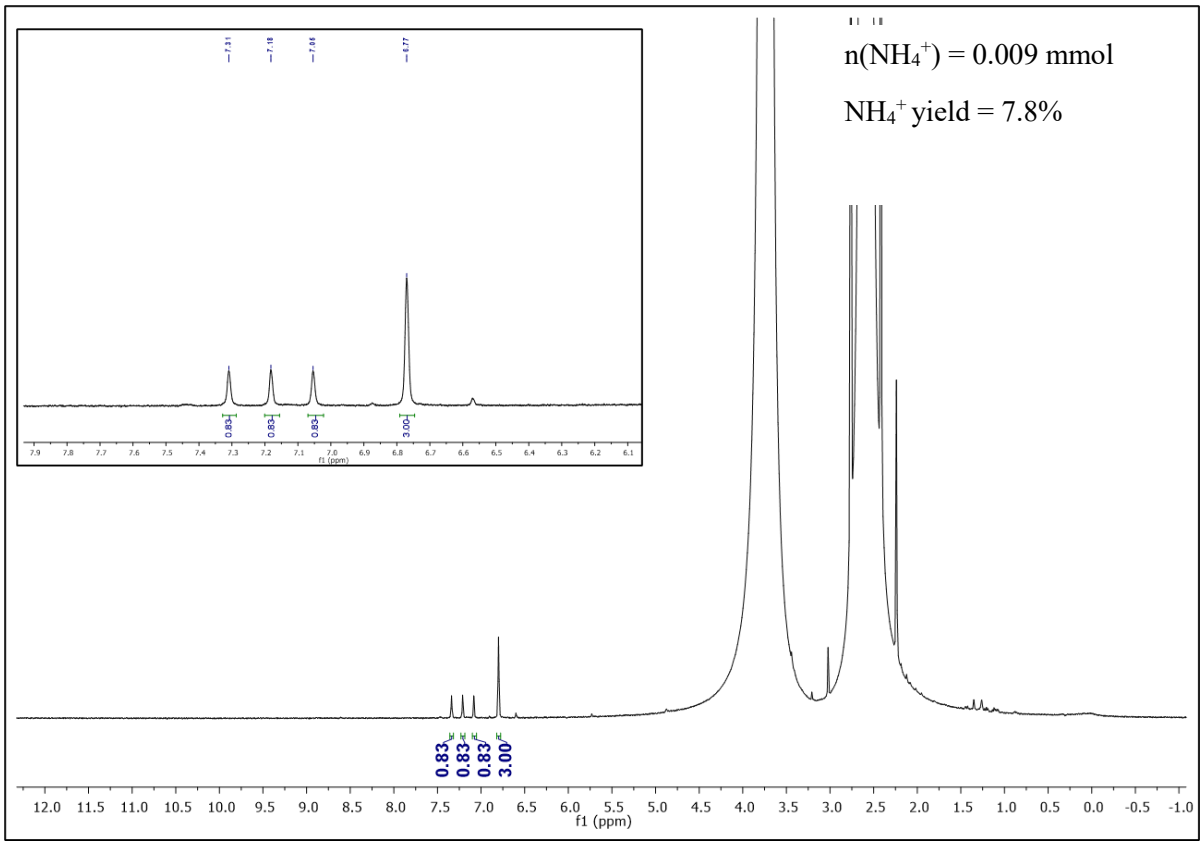


**Figure S68.** $^{1}$H NMR spectrum of Entry 11 Run 2 (Table S2)

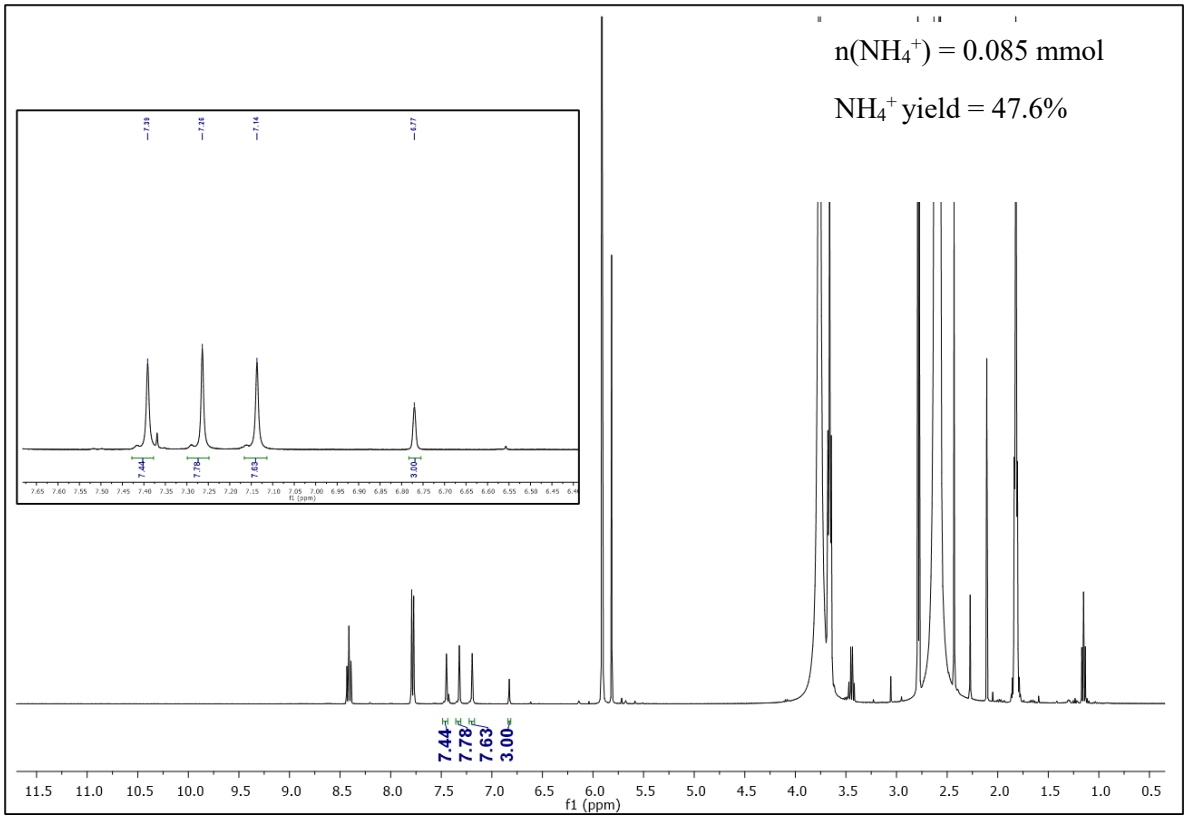


**Figure S69.** $^{1}$H NMR spectrum of Entry 12 Run 1 (Table S2)

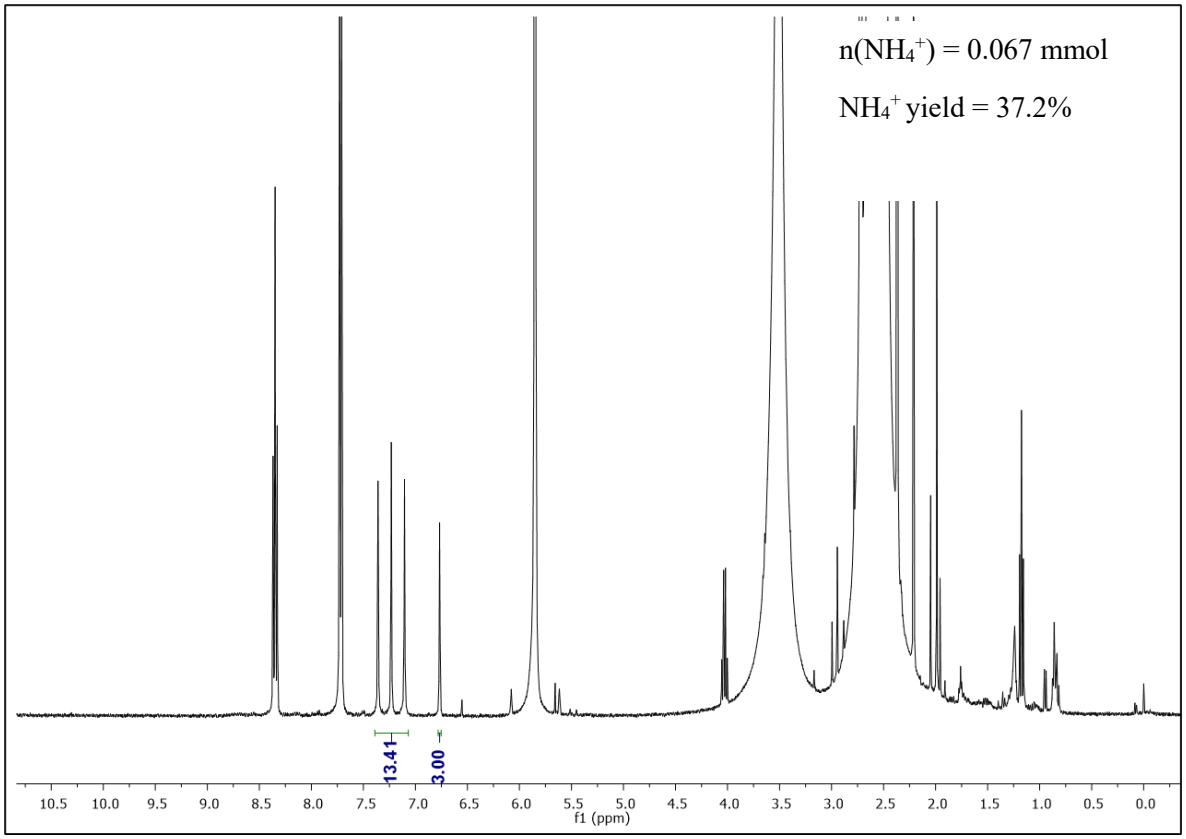


**Figure S70.** $^{1}$H NMR spectrum of Entry 12 Run 2 (Table S2) Mesitylene = 0.020 mmol

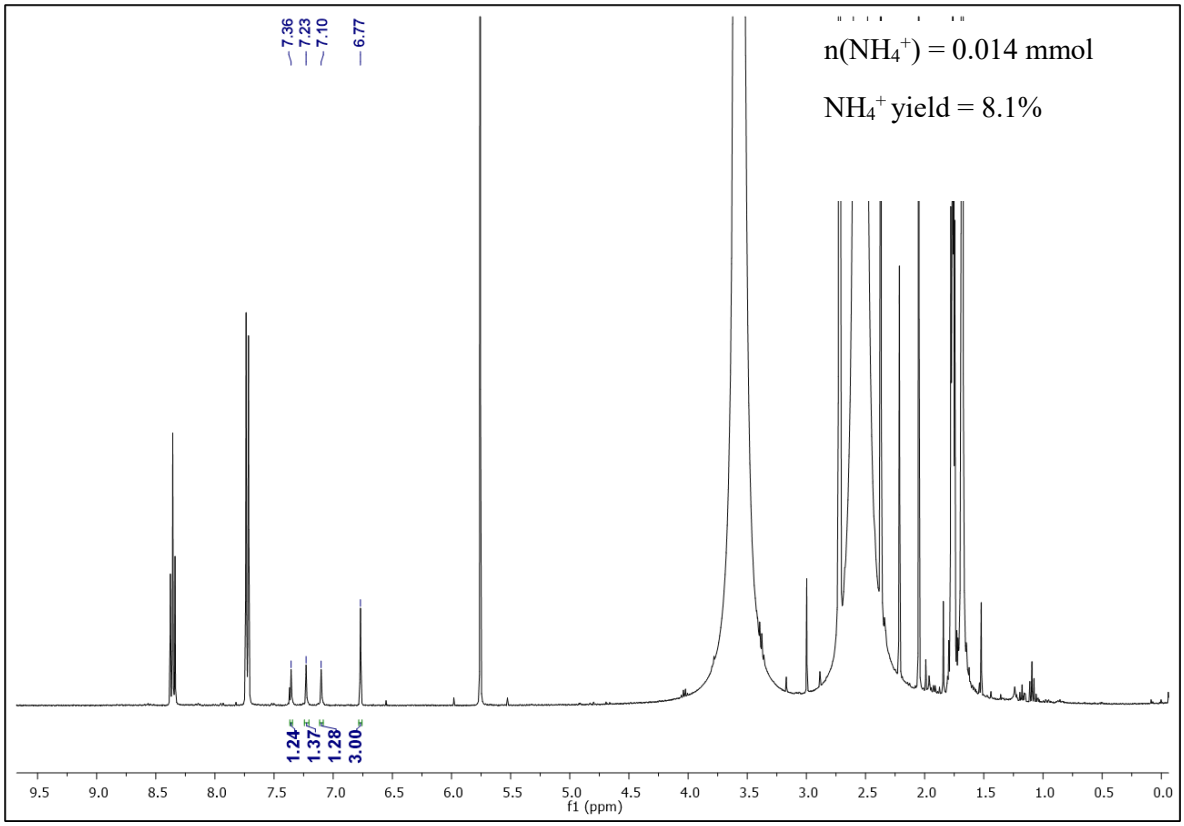


**Figure S71.** $^{1}$H NMR spectrum of Entry 13 Run 1 (Table S2)

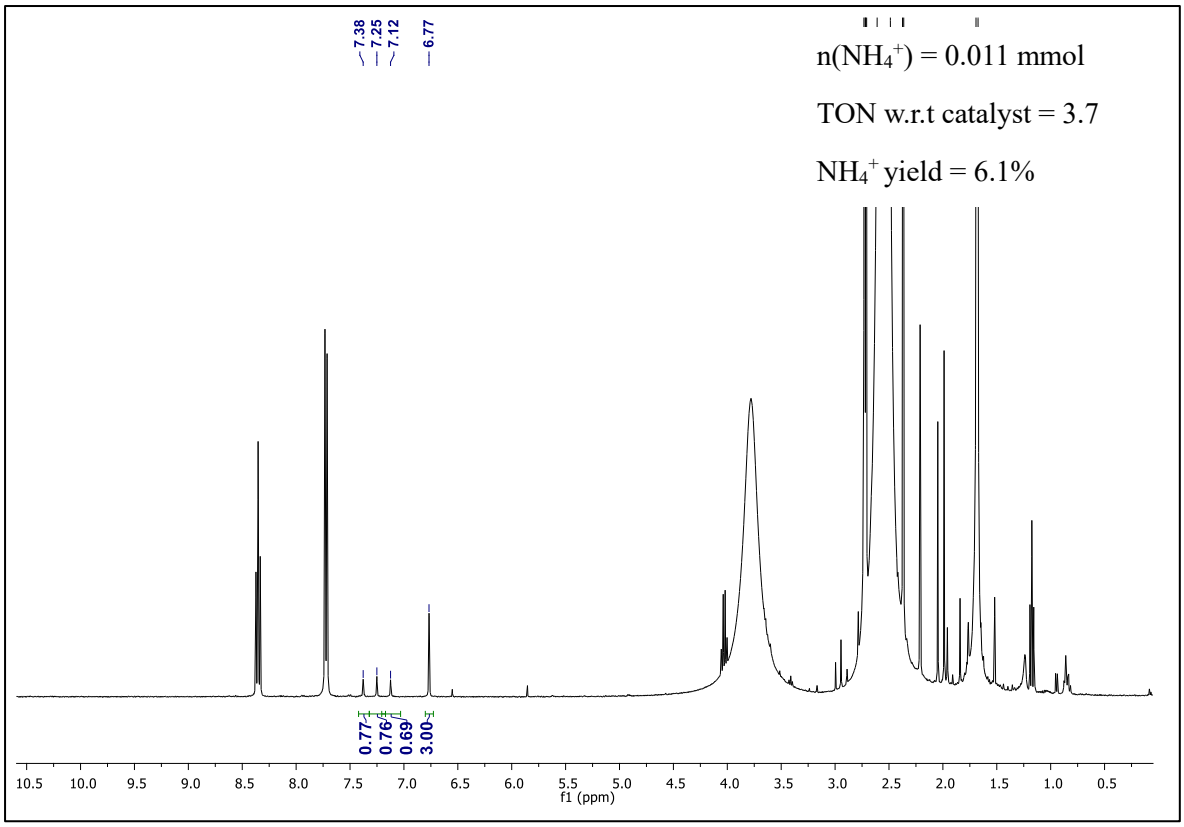


**Figure S72.** $^{1}$H NMR spectrum of Entry 13 Run 2 (Table S2) Mesitylene = 0.020 mmol

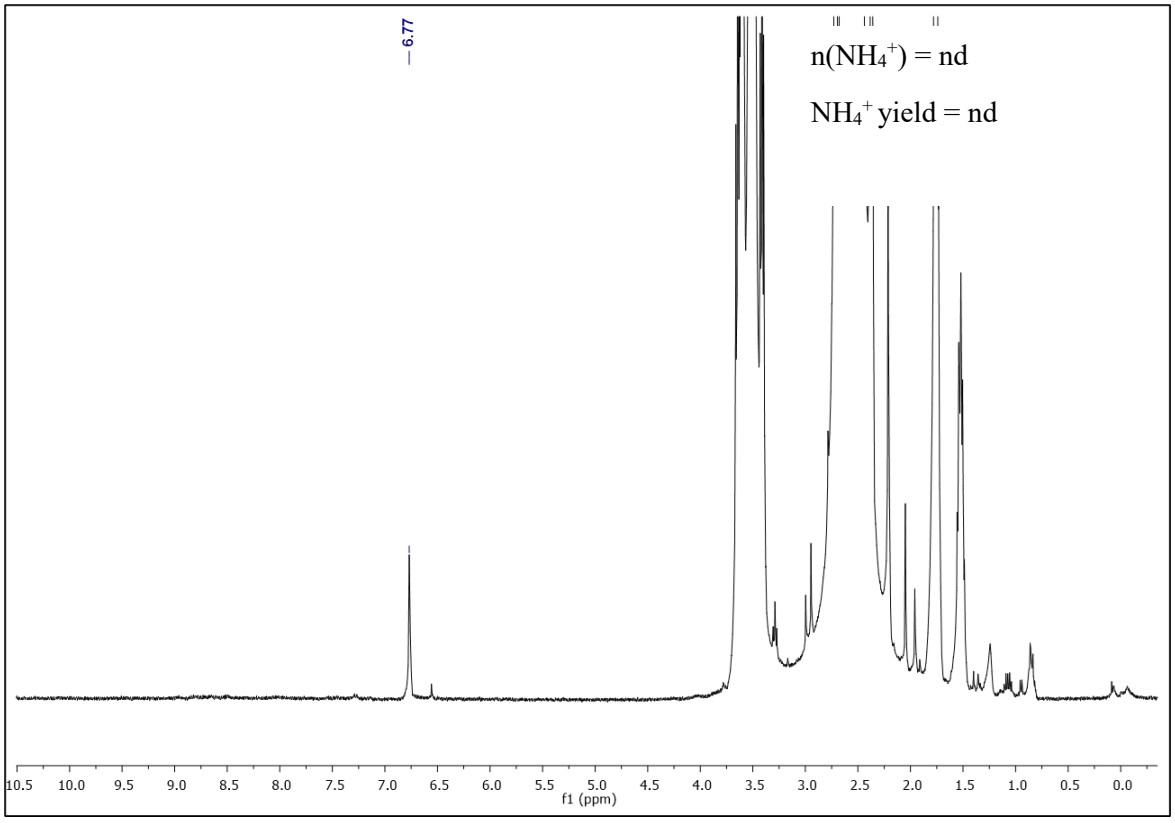


**Figure S73.** $^{1}$H NMR spectrum of Entry 14 (Table S2)

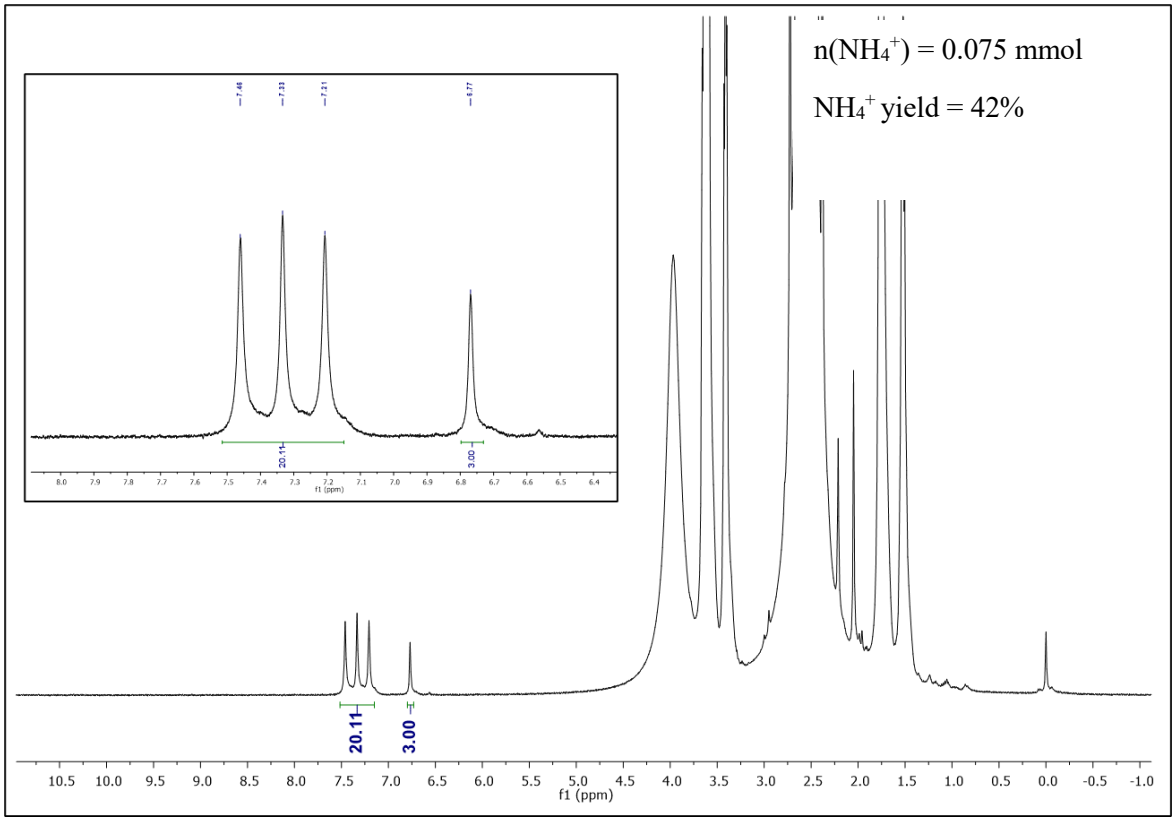


**Figure S74.** $^{1}$H NMR spectrum of Entry 15 (Table S2)

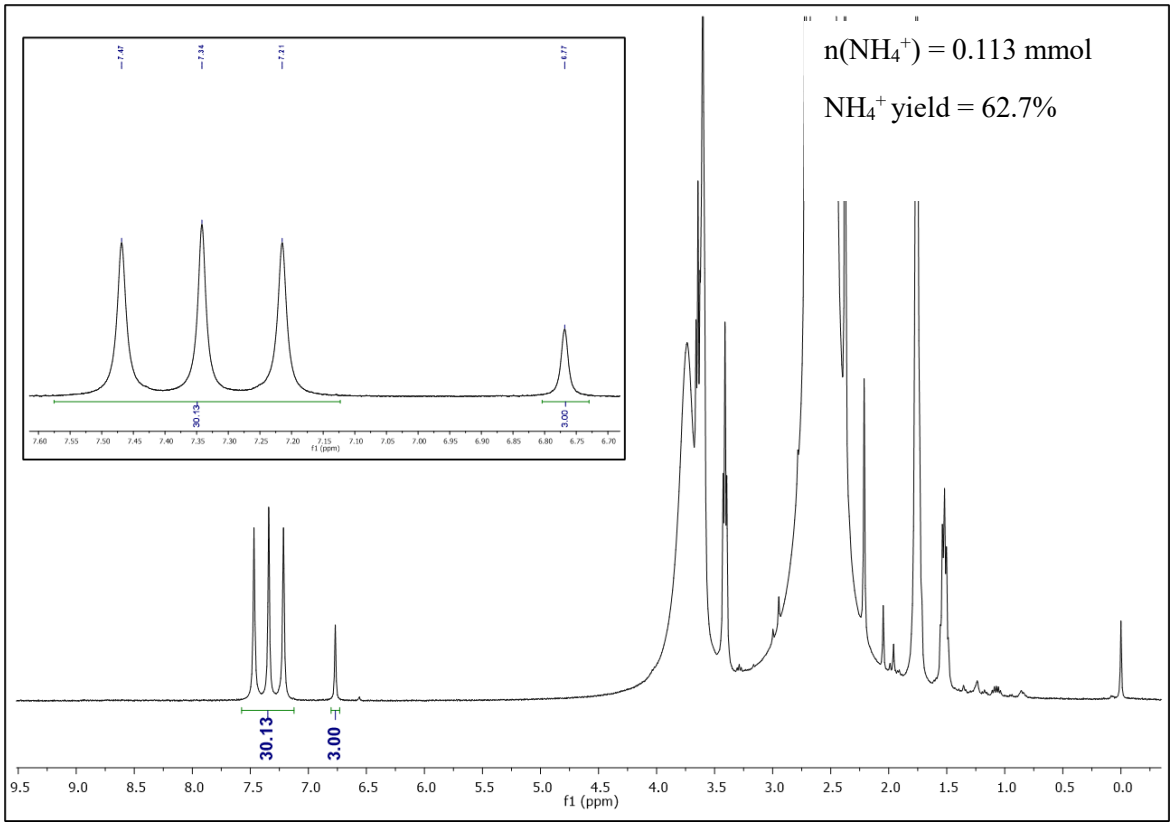


**Figure S75.** $^{1}$H NMR spectrum of Entry 16 (Table S2)

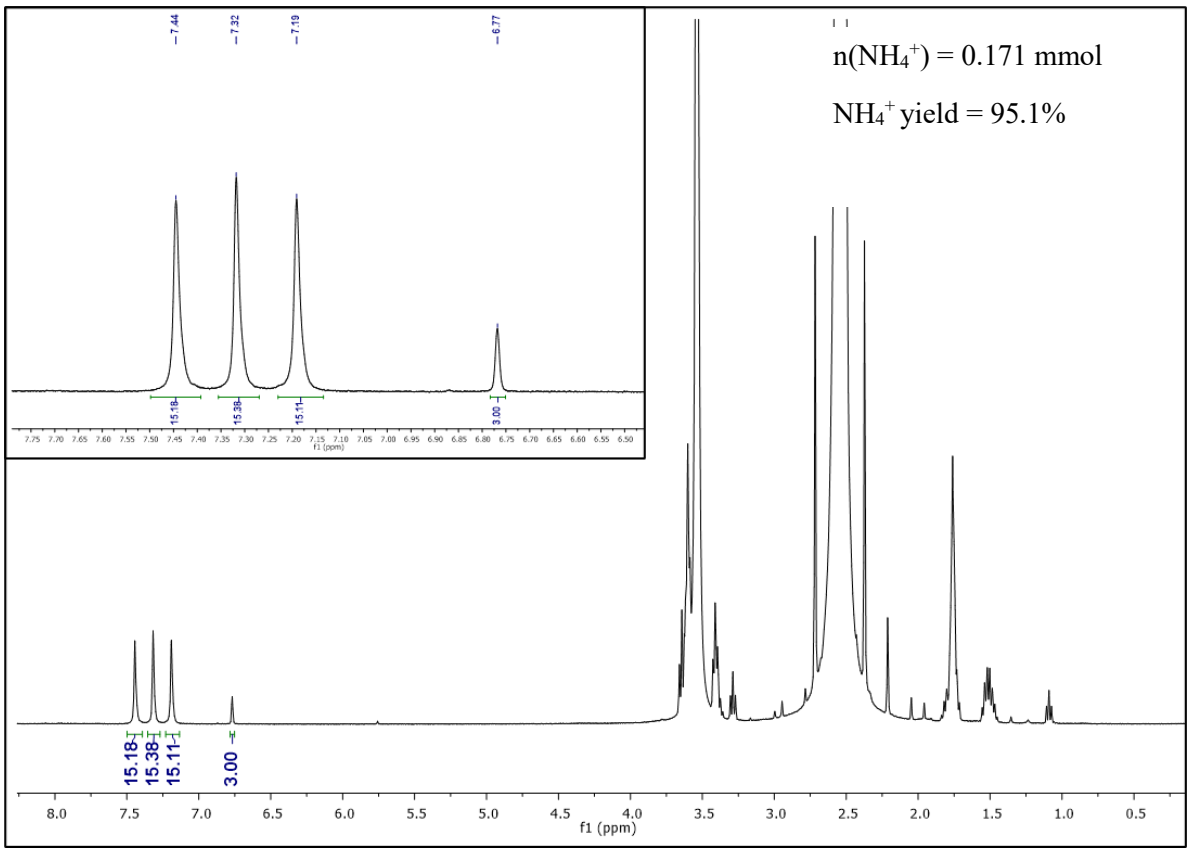


**Figure S76.** $^{1}$H NMR spectrum of Entry 17 Run 1 (Table S2)

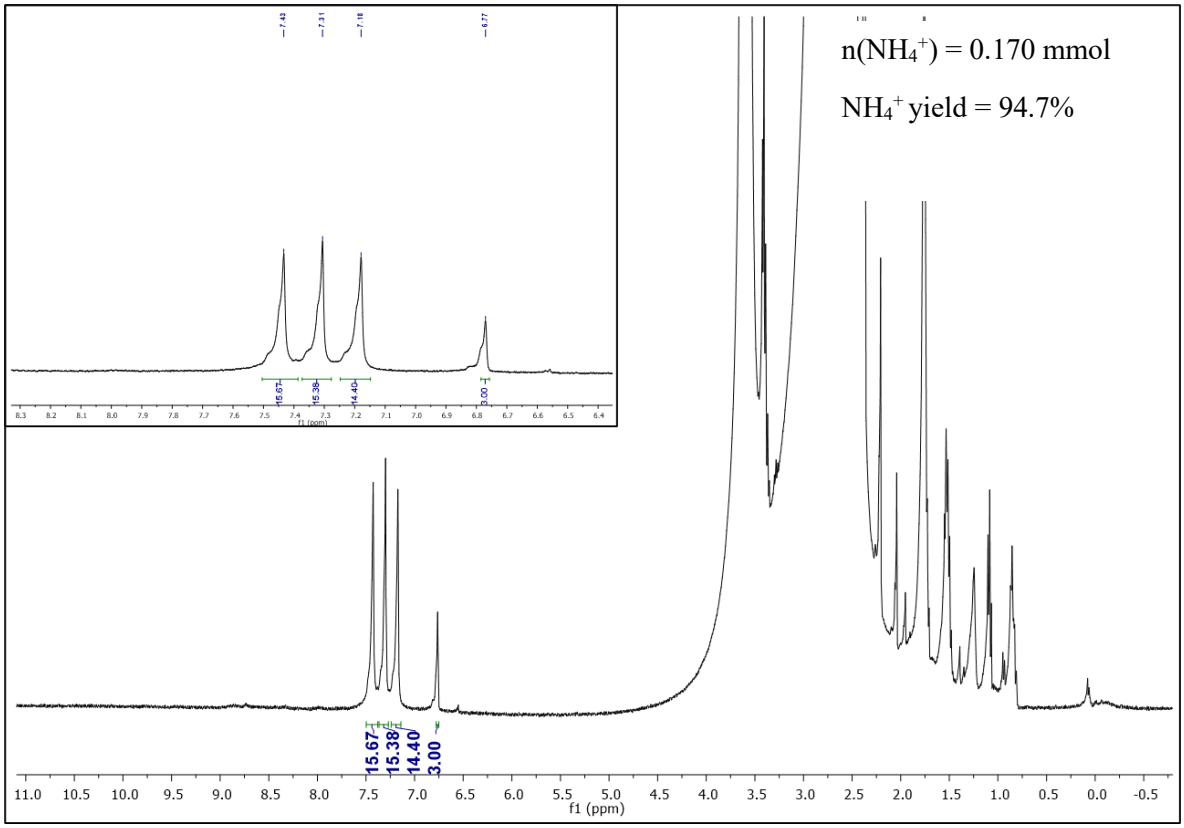


**Figure S77.** $^{1}$H NMR spectrum of Entry 17 Run 2 (Table S2)

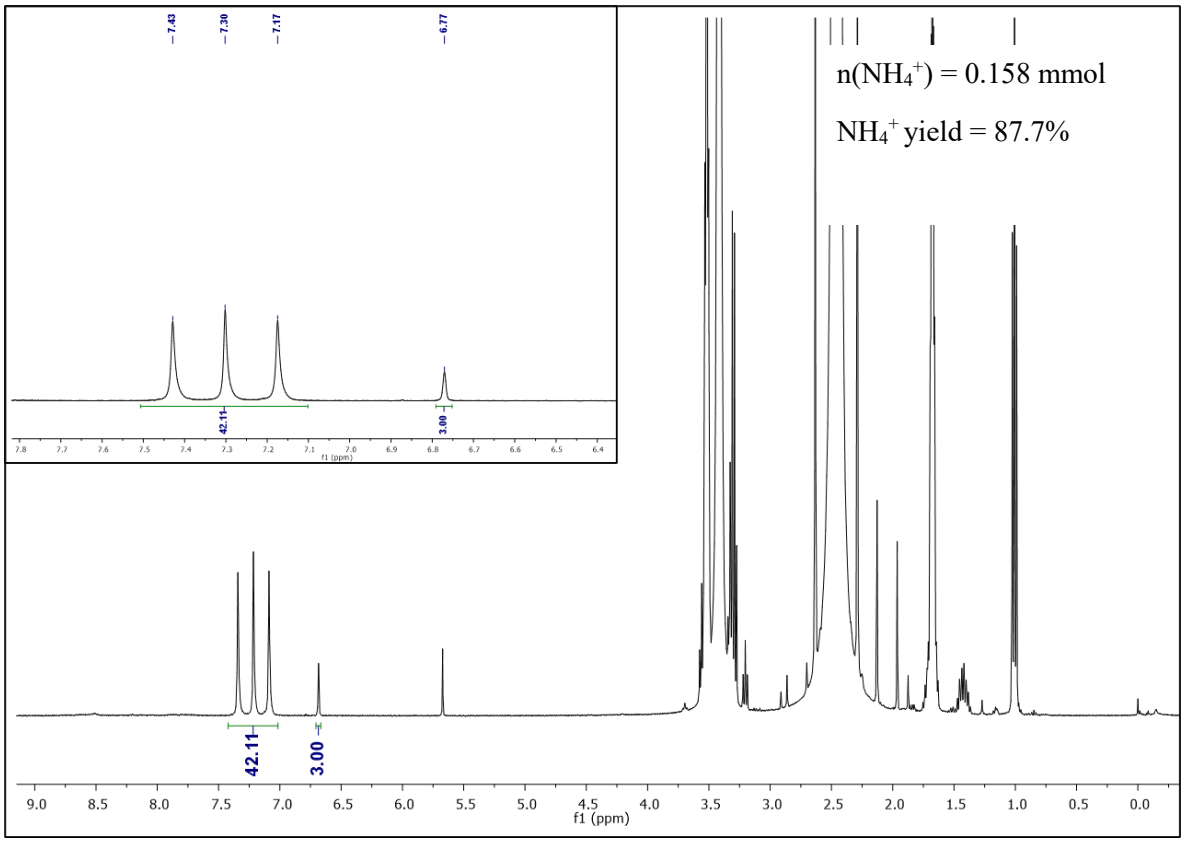


**Figure S78.** $^{1}$H NMR spectrum of Entry 17 Run 3 (Table S2)

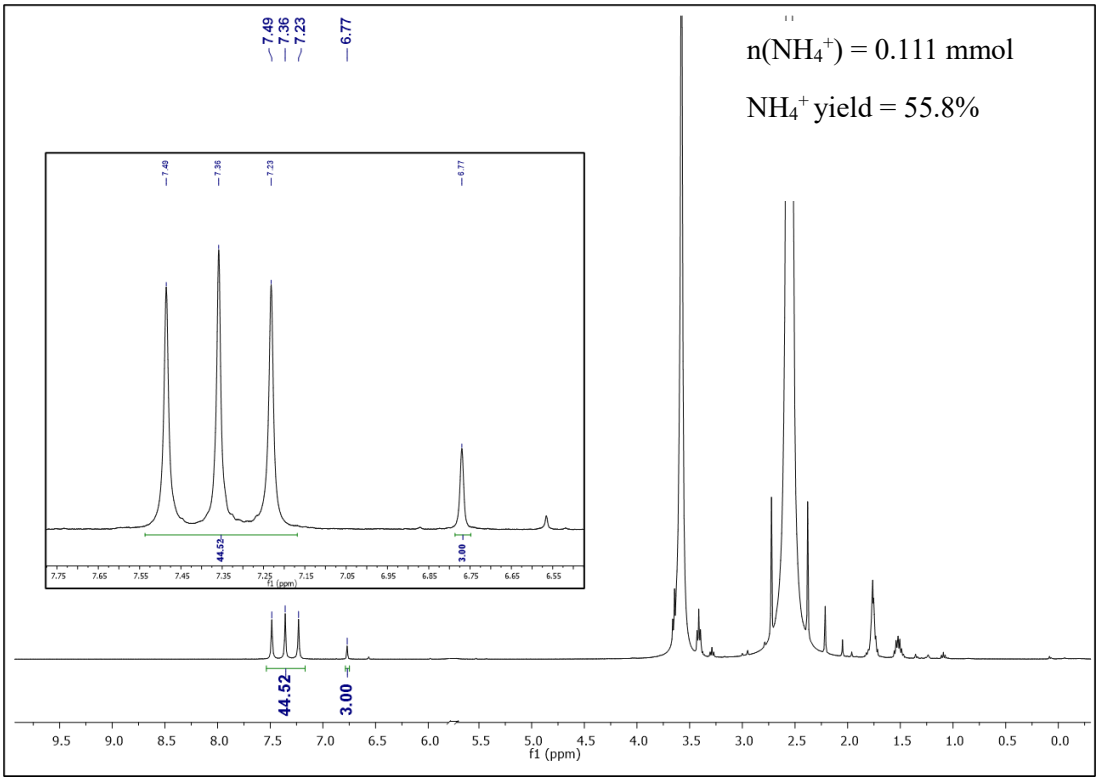


**Figure S79.** $^{1}$H NMR spectrum of ammonium peak when intermediate **A** used as a catalyst (section 10.6)

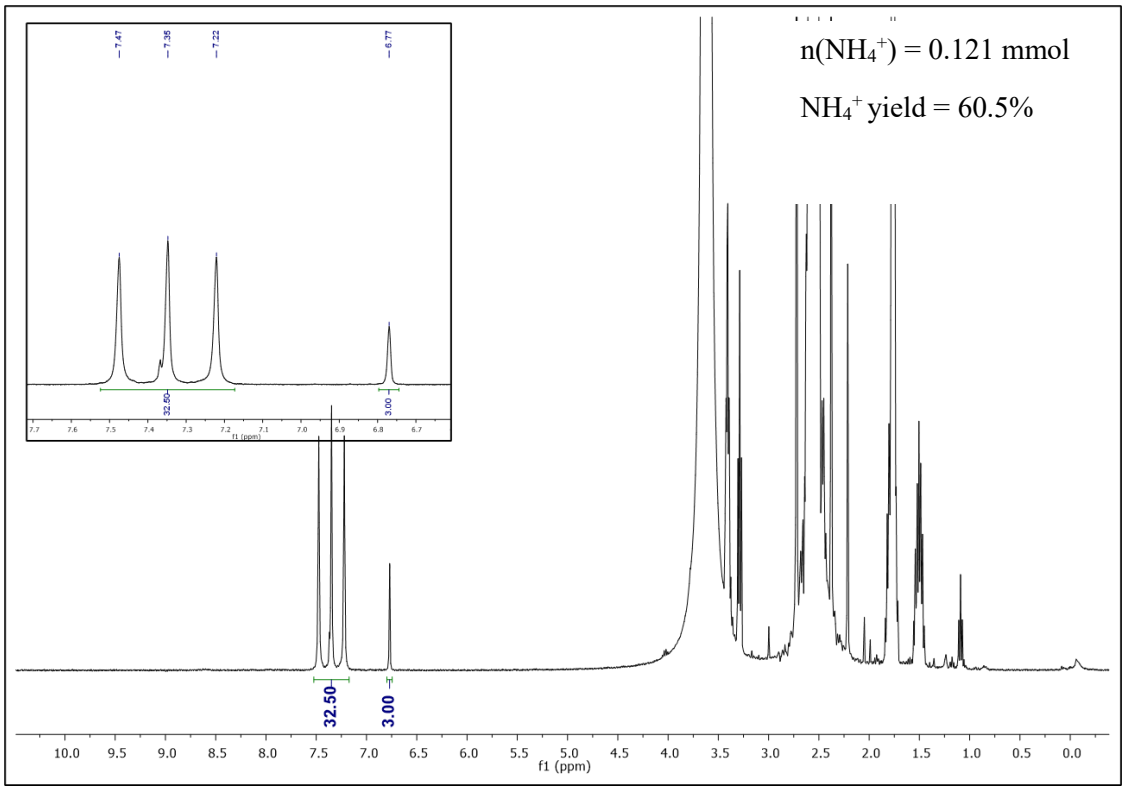


**Figure S80.** $^{1}$H NMR spectrum of ammonium peak when intermediate **B** used as a catalyst (section 10.7)

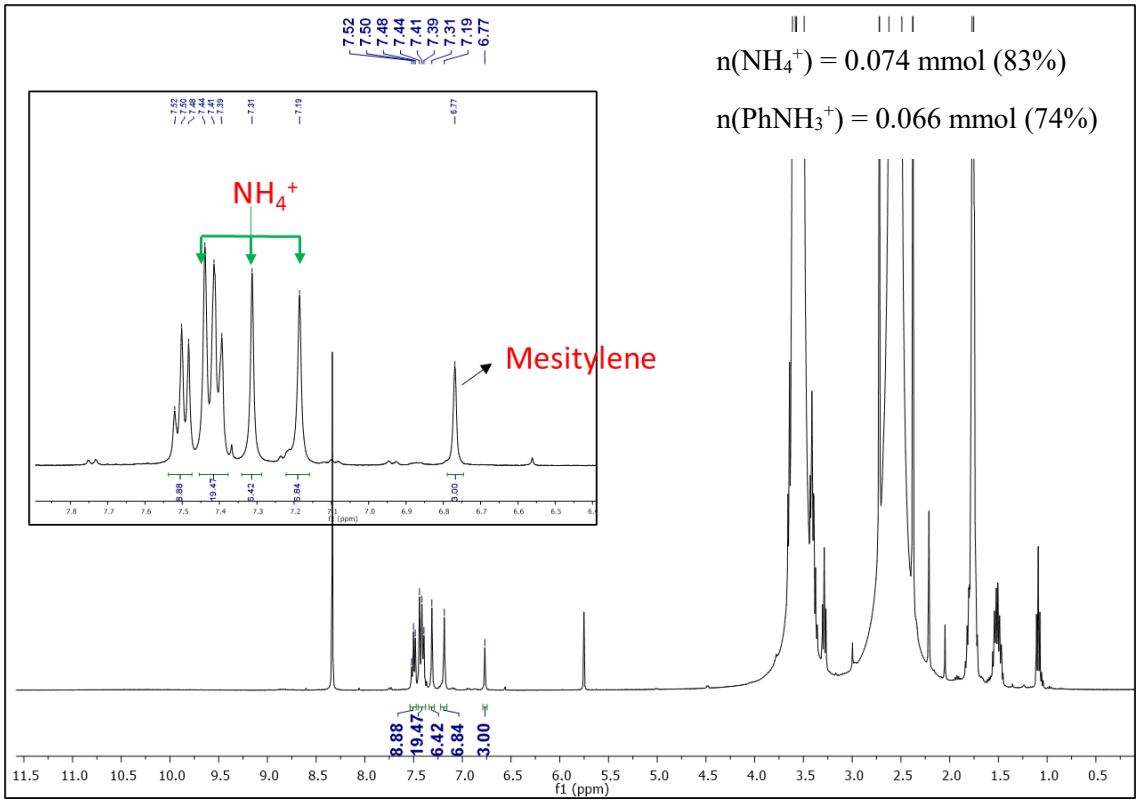


**Figure S81.** $^{1}$H NMR spectrum of Entry 1 (Table S9)

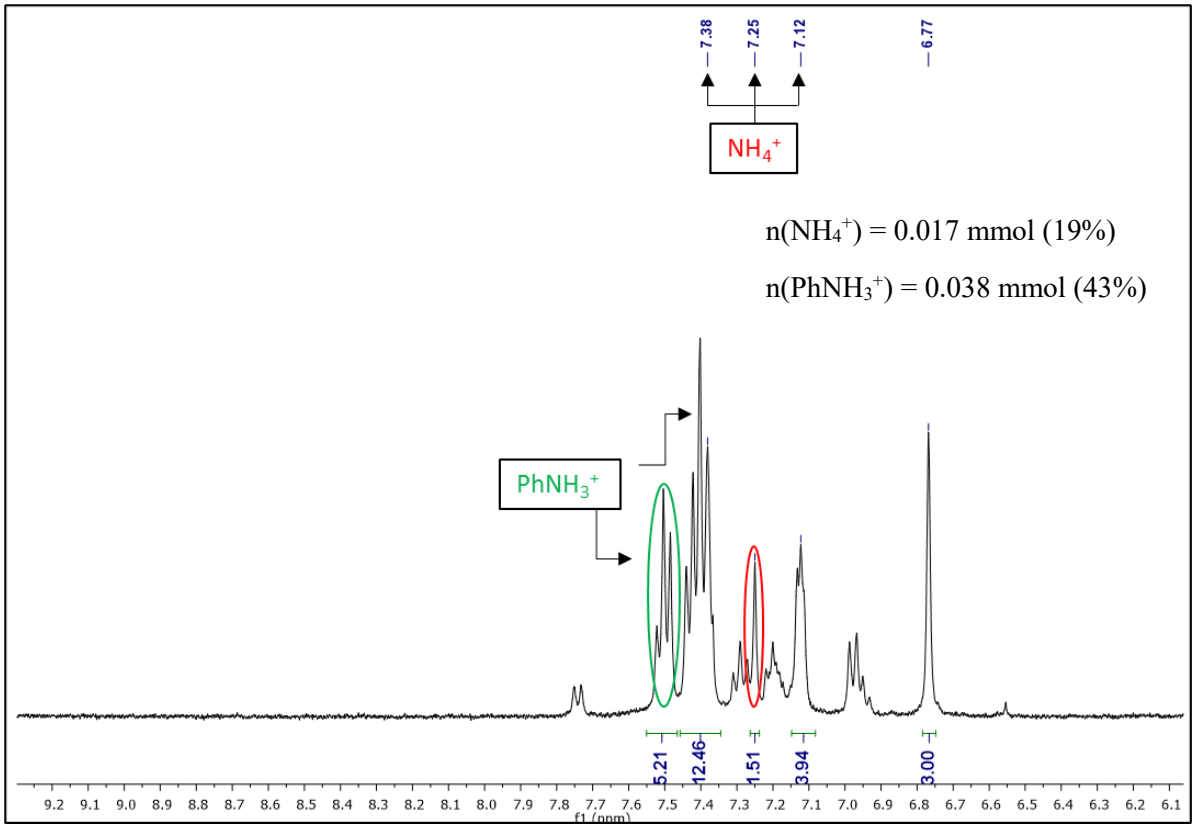


**Figure S82.** $^{1}$H NMR spectrum of Entry 2 (Table S9)

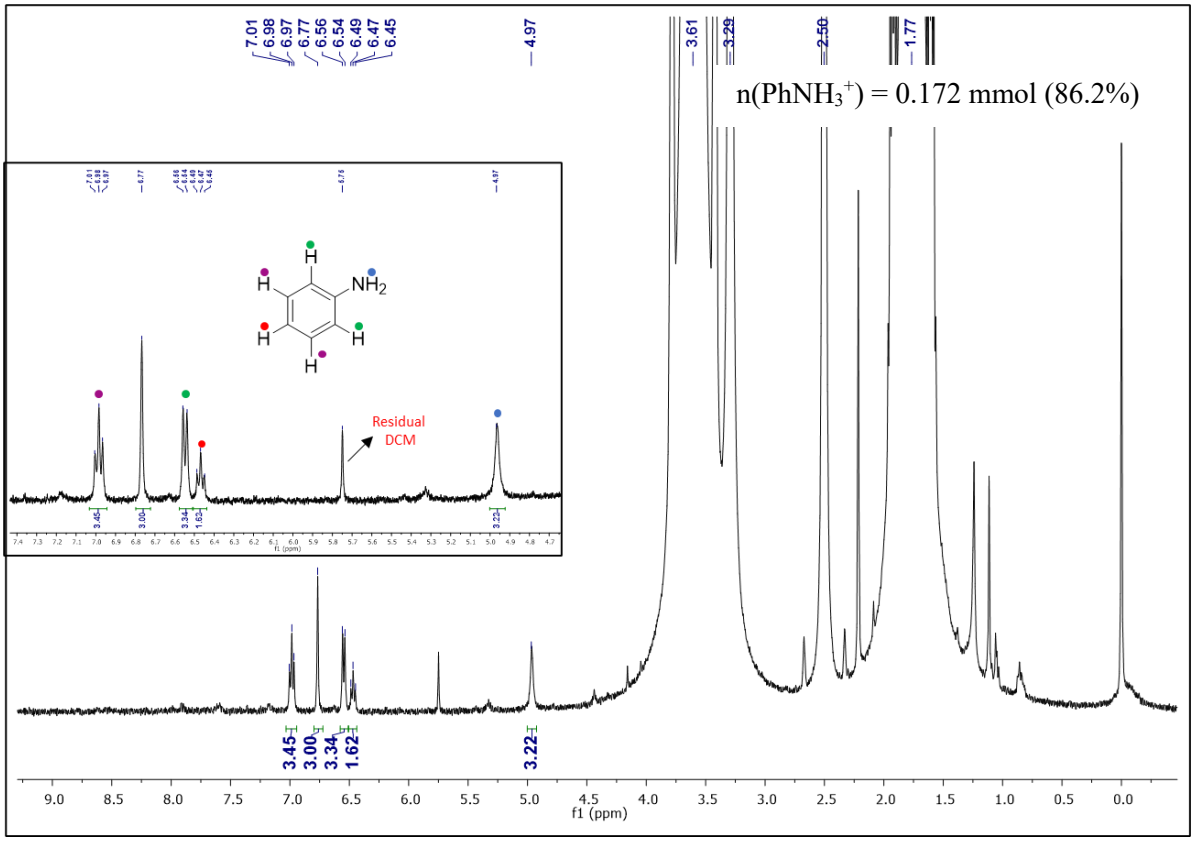


**Figure S83.** $^{1}$H NMR spectrum of Aniline reduced from hydrazobenzene

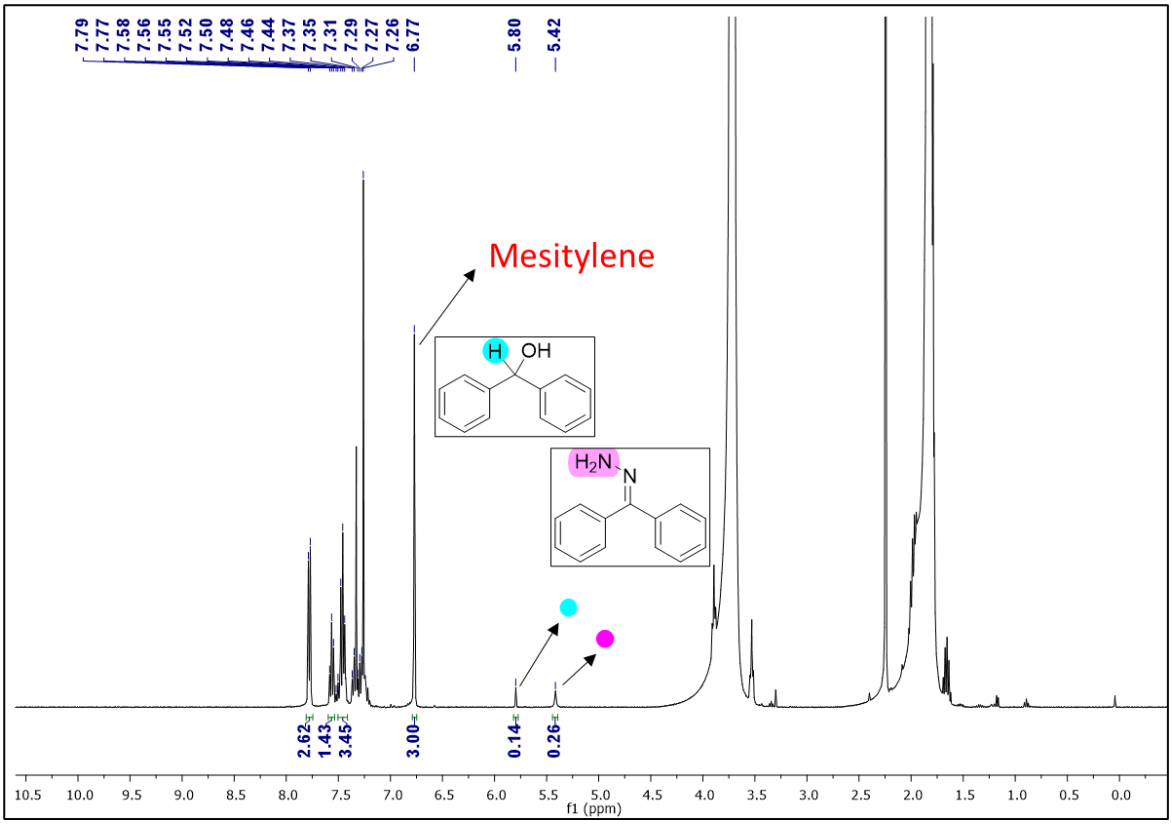


**Figure S84.** $^{1}$H NMR spectrum of the reaction mixture (section 12.1)

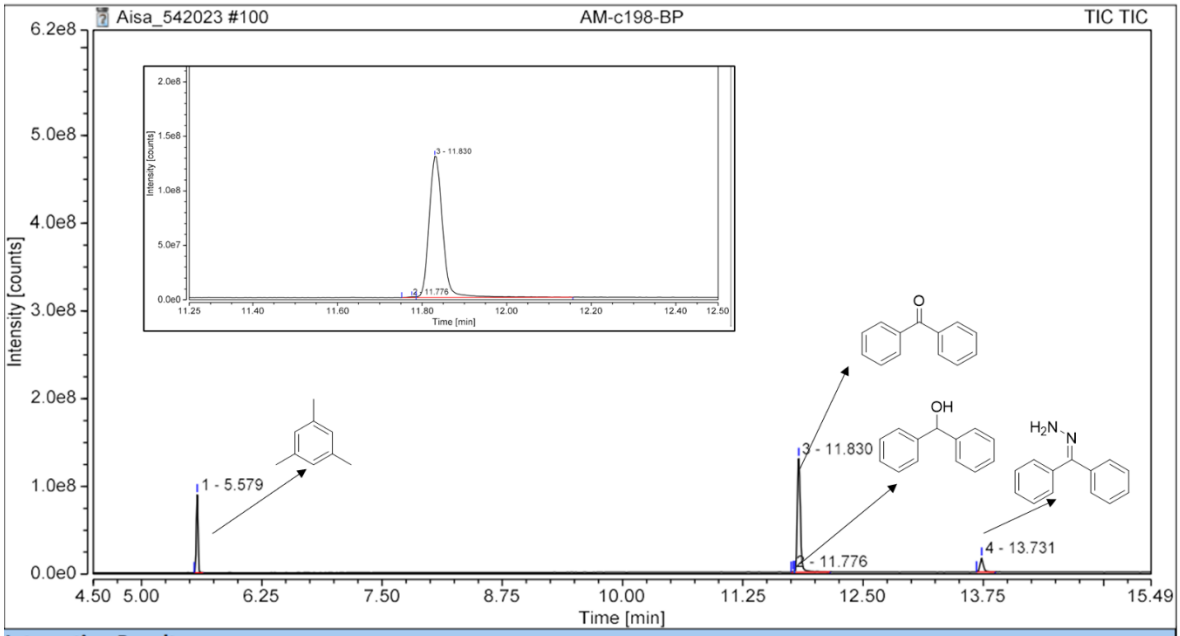


**Integration Results**

| No. | Peak Name | Retention Time min | Area counts*min | Height counts | Relative Area % | Relative Height % | Amount n.a. |
|---|---|---|---|---|---|---|---|
| 1 | | 5.579 | 1799754.075 | 88758753.765 | 24.76 | 37.80 | n.a. |
| 2 | | 11.776 | 13508.936 | 662406.024 | 0.19 | 0.28 | n.a. |
| 3 | | 11.830 | 4800808.588 | 129626140.575 | 66.05 | 55.20 | n.a. |
| 4 | | 13.731 | 653900.275 | 15763698.646 | 9.00 | 6.71 | n.a. |
| **Total:** | | | **7267971.874** | **234810999.010** | **100.00** | **100.00** | |

**Figure S85A.** GC-MS spectrum of the reaction mixture (section 12.1)

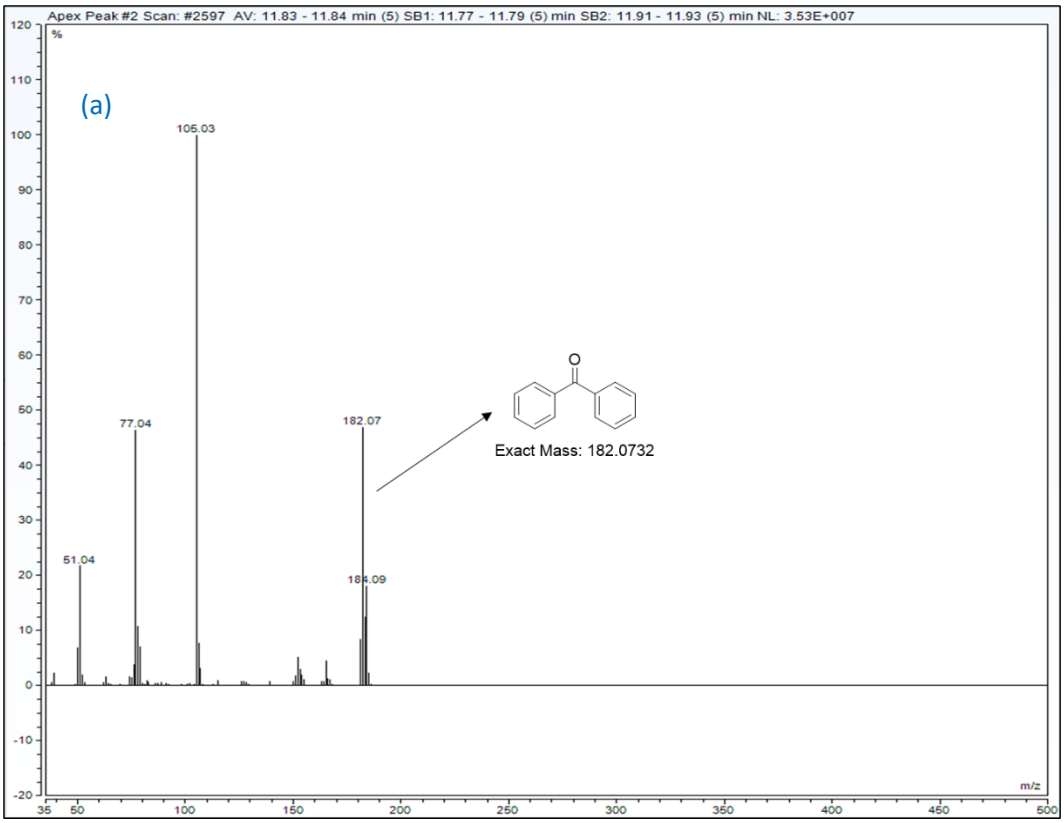

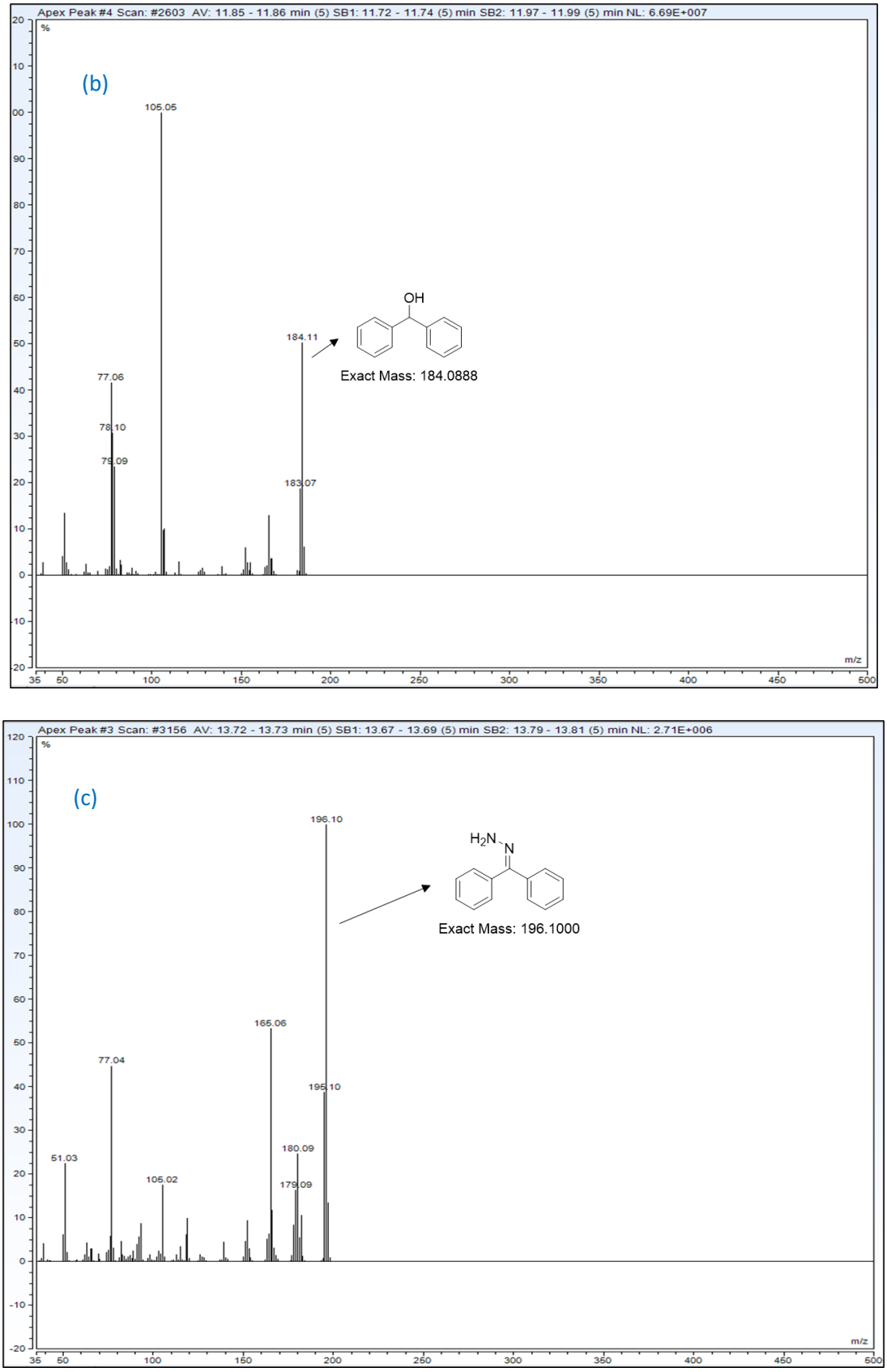


**Figure S85B.** Mass pattern of GC-MS spectrum Figure S85 A (a) Benzophenone (b) Diphenylmethanol (c) benzophenone-hydrazone

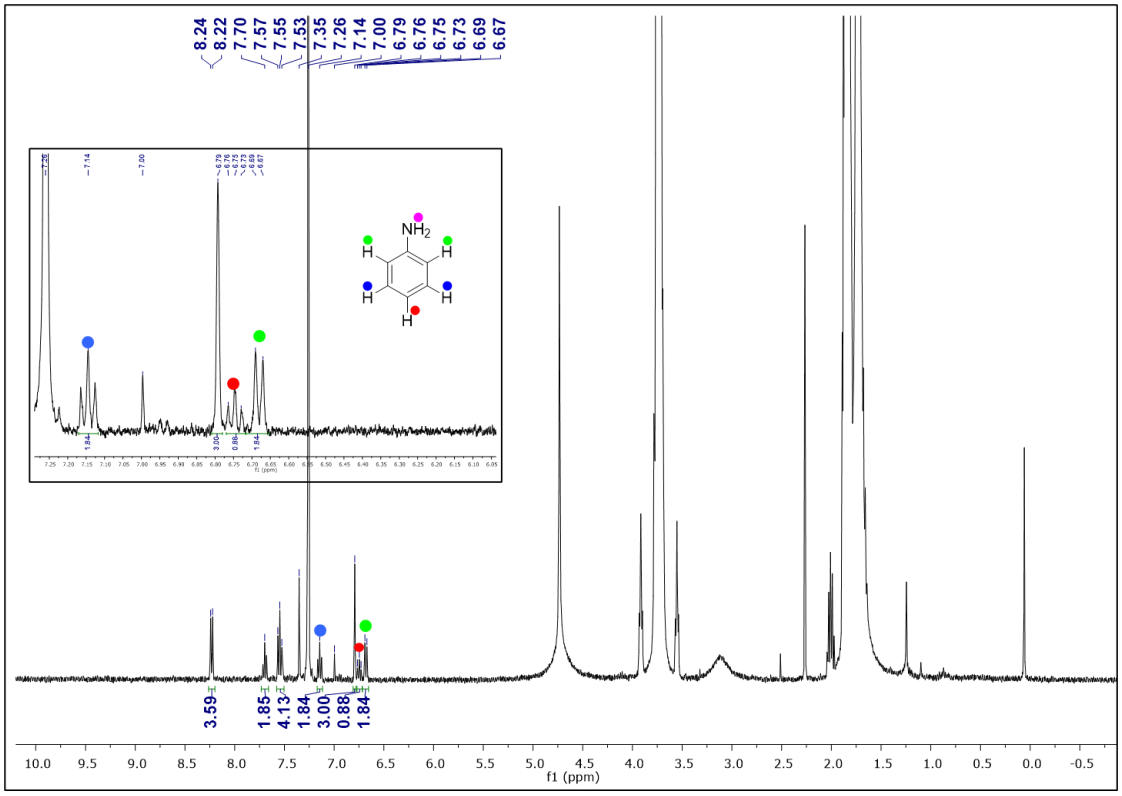


**Figure S86.** $^{1}$H NMR spectrum of the reaction mixture (section 12.2)

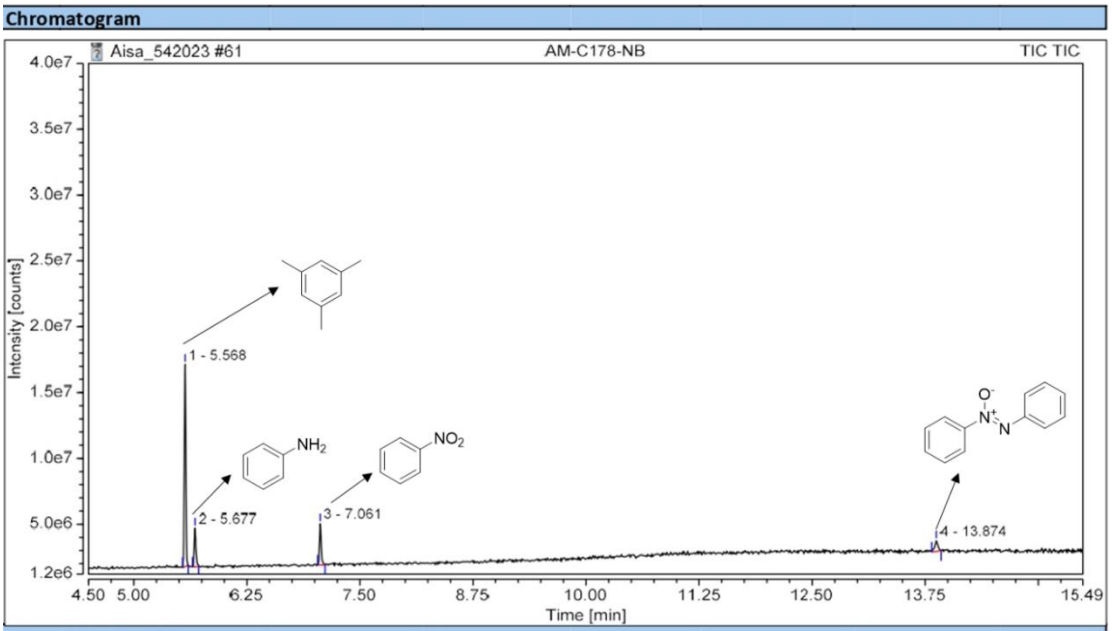


**Integration Results**

| No. | Peak Name | Retention Time min | Area counts*min | Height counts | Relative Area % | Relative Height % | Amount n.a. |
|---|---|---|---|---|---|---|---|
| 1 | | 5.568 | 303213.466 | 15356412.788 | 64.34 | 69.07 | n.a. |
| 2 | | 5.677 | 63788.120 | 2942616.914 | 13.54 | 13.24 | n.a. |
| 3 | | 7.061 | 69053.455 | 3133634.498 | 14.65 | 14.09 | n.a. |
| 4 | | 13.874 | 35186.362 | 800743.114 | 7.47 | 3.60 | n.a. |
| **Total:** | | | **471241.404** | **22233407.315** | **100.00** | **100.00** | |

**Figure S87A.** GC-MS spectrum of the reaction mixture (section 12.2)

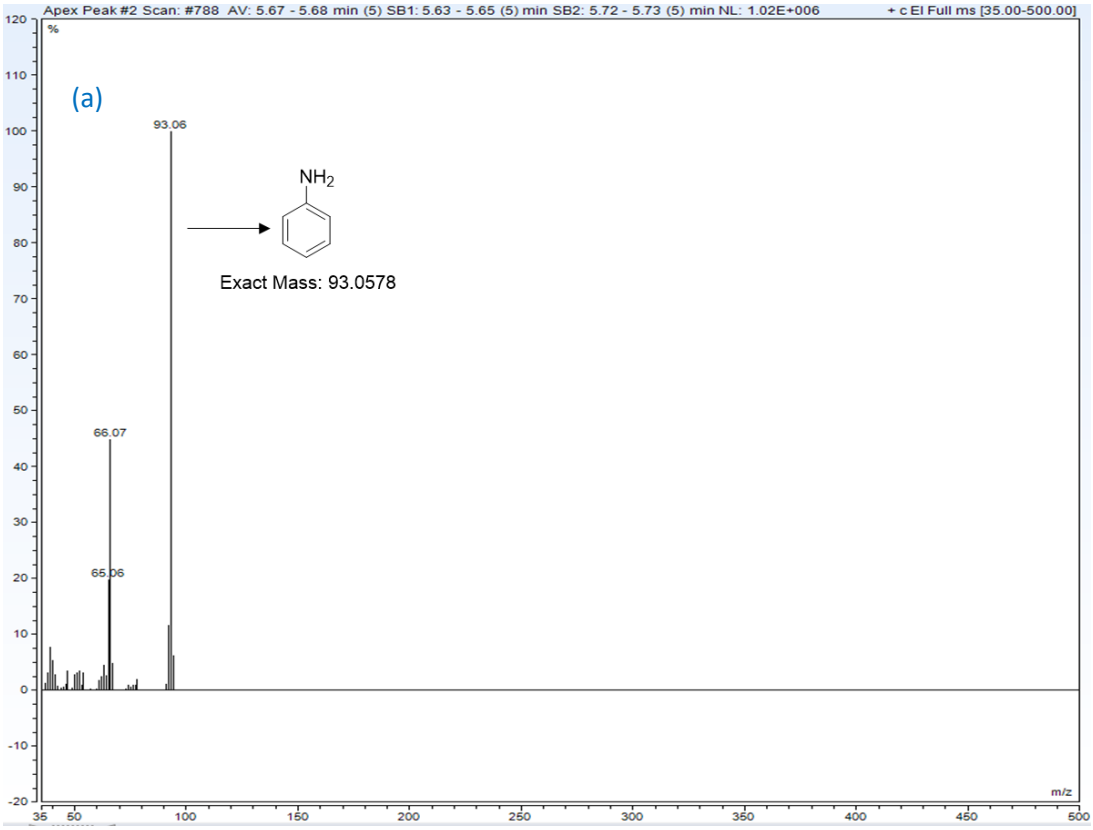
Apex Peak #2 Scan: #788 AV: 5.67 - 5.68 min (5) SB1: 5.63 - 5.65 (5) min SB2: 5.72 - 5.73 (5) min NL: 1.02E+006
+ c EI Full ms [35.00-500.00]
%
(a)
93.06
66.07
65.06
NH2
Exact Mass: 93.0578
m/z

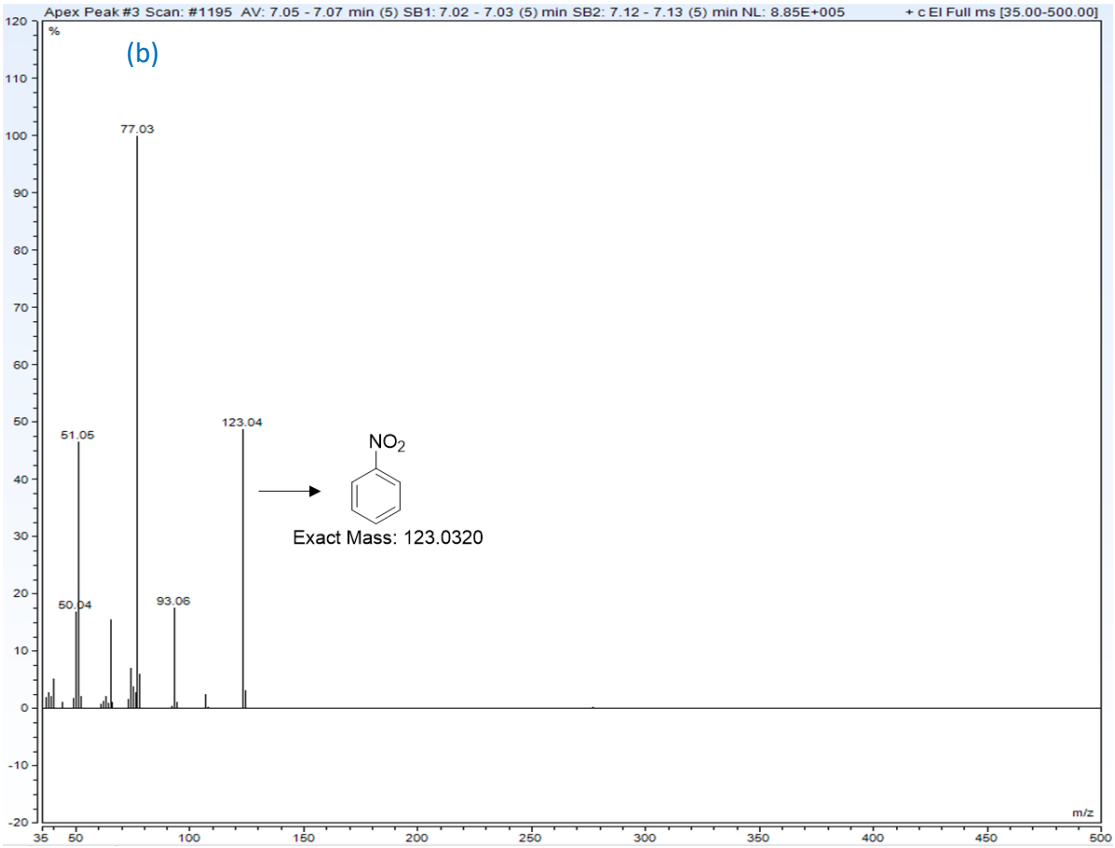
Apex Peak #3 Scan: #1195 AV: 7.05 - 7.07 min (5) SB1: 7.02 - 7.03 (5) min SB2: 7.12 - 7.13 (5) min NL: 8.85E+005
+ c EI Full ms [35.00-500.00]
%
(b)
77.03
123.04
51.05
50.04
93.06
NO2
Exact Mass: 123.0320
m/z

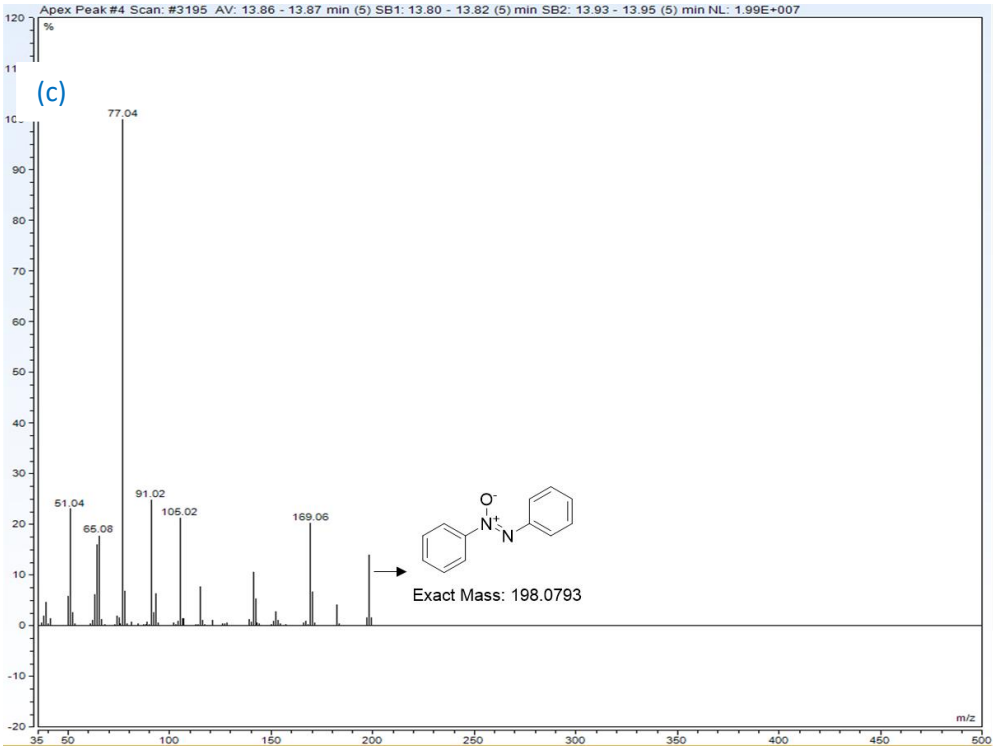


**Figure S87B.** Mass pattern of GC-MS spectrum Figure S87A (a) Aniline (b) Nitrobenzene(c) Azoxybenzene

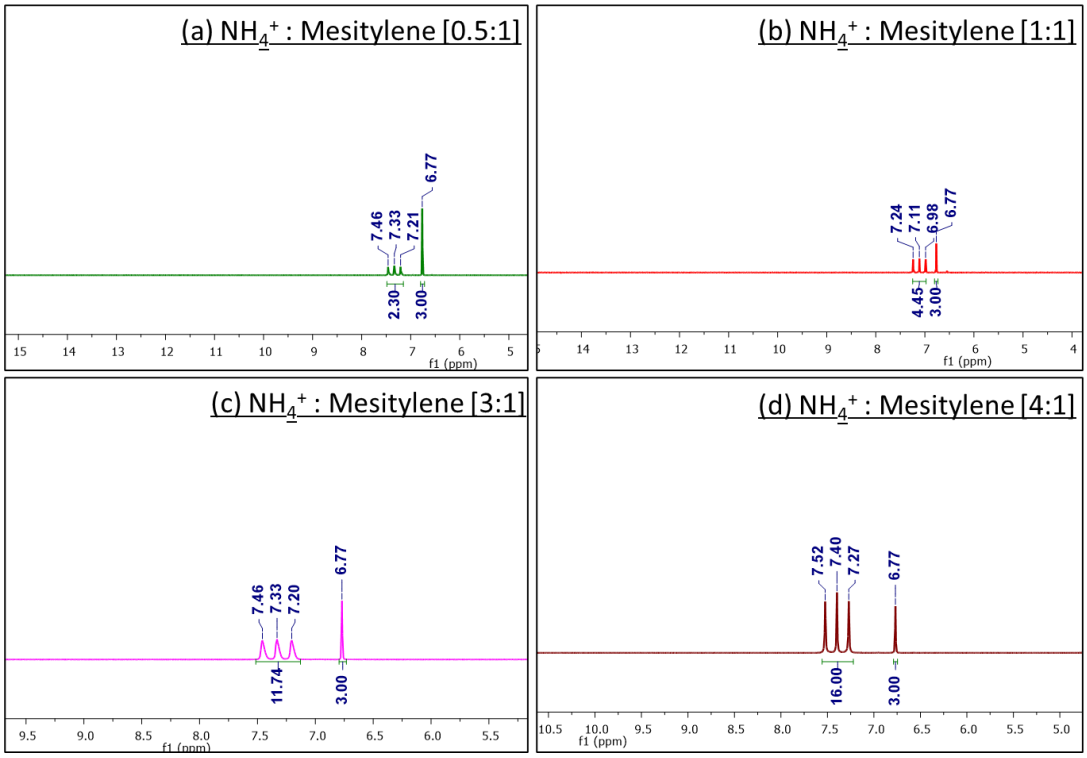


**Figure S88.** $^{1}$H NMR spectra of $NH_4Cl$ with Mesitylene in different concentration under acidified reaction condition (a) 0.5:1 (b) 1:1 (c) 3:1 (d) 4:1.

## 15. References


1 D. L. Jameson and L. E. Guise, *Tetrahedron Lett.*, 1991, **32**, 1999–2002.

2 A. M. W. Cargill Thompson, *Coord. Chem. Rev.*, 1997, **160**, 1–52.

3 P. L. Derivatives, *Inorg. Synth.*, 1998, **32**, 186–198.

4 R. Lakshmanan, N. C. Shivaprakash and S. Sindhu, *J. Fluoresc.*, 2018, **28**, 173–182.

5 A. Breivogel, K. Hempel and K. Heinze, *Inorg. Chim. Acta*, 2011, **374**, 152–162.

6 G. W. Watt and J. D. Chrisp, *Anal. Chem.*, 1952, **24**, 2006–2008.

7 D. B. Adam, M. C. Tsai, Y. A. Awoke, W. H. Huang, Y. W. Yang, C. W. Pao, W. N. Su and B. J. Hwang, *ACS Sustain. Chem. Eng.*, 2021, **9**, 8803–8812.

8 A. Reynal and E. Palomares, *Eur. J. Inorg. Chem.*, 2011, **2011**, 4509–4526.

9 G. Kerenskaya, I. U. Goldschleger, V. A. Apkarian, E. Fleischer and K. C. Janda, *J. Phys. Chem. A*, 2007, **111**, 10969–10976.